

St. John's University

St. John's Scholar

Theses and Dissertations

2021

**DESIGN, SYNTHESIS AND PHARMACOLOGICAL EVALUATION OF
QUINAZOLINAMINE DERIVATIVES AS BCRP AND P-GP
INHIBITORS WITH IMPROVED METABOLIC STABILITY**

Chao-Yun Cai

Follow this and additional works at: https://scholar.stjohns.edu/theses_dissertations

 Part of the [Pharmacology Commons](#)

**DESIGN, SYNTHESIS AND PHARMACOLOGICAL EVALUATION OF
QUINAZOLINAMINE DERIVATIVES AS BCRP AND P-GP INHIBITORS
WITH IMPROVED METABOLIC STABILITY**

A dissertation submitted in partial fulfillment

of the requirements for the degree of

DOCTOR OF PHILOSOPHY

to the faculty of the

DEPARTMENT OF GRADUATE DIVISION

of

COLLEGE OF PHARMACY AND HEALTH SCIENCES

at

ST. JOHN'S UNIVERSITY

New York

by

Chao-Yun Cai

Date Submitted: _____

Chao-Yun Cai

Date Approved: _____

Dr. Vijaya L. Korlipara

© Copyright by Chao-Yun Cai 2021
All Rights Reserved

ABSTRACT

DESIGN, SYNTHESIS AND PHARMACOLOGICAL EVALUATION OF QUINAZOLINAMINE DERIVATIVES AS BCRP AND P-GP INHIBITORS WITH IMPROVED METABOLIC STABILITY

Chao-Yun Cai

A series of twenty-two quinazolinamine derivatives showing potent inhibitory activities on BCRP and P-gp was synthesized. The reversal study showed that when combined with the potent dual BCRP and P-gp inhibitors **7-8**, **29-31**, and **34**, the IC₅₀ value of mitoxantrone was decreased from 6.50 μM to the range of 0.24 - 0.35 μM for BCRP, and IC₅₀ value of colchicine was decreased from 7.34 μM to the range of 0.12 - 0.29 μM for P-gp. Cyclopropyl quinazolinamine **29** (VKCY-1), which was a dual BCRP and P-gp inhibitor, and azide quinazolinamine **40** (VKCY-2), which was a BCRP inhibitor, were selected for mechanistic studies. The results revealed that target compound **29** (VKCY-1) changed the localization of BCRP in H460/MX20 cells and P-gp in KB-C2 cells rather than altering the expression level of BCRP or P-gp proteins, thus inhibiting the efflux of the anticancer drugs, which is different from the mechanisms of other reported ABC transporter inhibitors. Azide quinazolinamine **40** (VKCY-2), on the other hand, did not change the expression level or the localization

of BCRP protein. In addition, compounds **29 (VKCY-1)** and **40 (VKCY-2)** significantly stimulated the ATP hydrolysis of BCRP transporter indicating that they can be competitive substrates of BCRP transporter, and thereby significantly increasing the accumulation of mitoxantrone in BCRP-overexpressing H460/MX20 cells. Azide quinazolinamine **40 (VKCY-2)** with photoaffinity label can be a valuable probe for investigating the interactions of quinazolinamine derivatives with BCRP. After activation by the UV light, azide quinazolinamine **40 (VKCY-2)** showed greater inhibitory effect on BCRP. Overall, this study indicated that quinazolinamine analogues can significantly reverse both BCRP- and P-gp-mediated MDR by blocking the efflux of anticancer drugs. Target compounds have the potential to be useful as BCRP and P-gp modulators to overcome MDR. The target quinazolinamine derivatives **7-8, 29-32, and 34** exhibited potency similar to that of the known BCRP inhibitor, Ko143. In addition, the P-gp inhibitory activities of quinazolinamine derivatives **7-8, 29-31, and 34** were greater than that of verapamil. Notably, the selected dual BCRP and P-gp inhibitors **7-8, 29-31, 34, and 40** showed improved metabolic stability than the standard pharmacologic tool Ko143.

ACKNOWLEDGEMENT

I would like to express my gratitude to many individuals who have made my professional and personal life in America so wonderful. Firstly, I would like to thank Dr. Vijaya L. Korlipara, and Dr. Zhe-Sheng Chen for their mentorship. Dr. Vijaya L. Korlipara continuously supported my doctoral study and research, and guided me in all the time of research and writing of this thesis. I would like to thank Dr. Zhe-Sheng Chen for his supervision, advice, and guidance. He is always willing to help students in many aspects. With the help of my mentors, I have grown a lot as a student and future researcher. I also would like to thank my master's mentor Dr. Bo Wang who supported me not only as a mentor but also as a friend and encouraged me to pursue doctoral studies in the United States. Without her encouragement and guidance, I would not have studied in America. I would like to thank my committee members Dr. Sandra E. Reznik, Dr. Tanaji T. Talele and Dr. John N. D. Wurpel for serving as members of my doctoral thesis committee. I am grateful for their valuable suggestions and critical comments that helped enhance my project and thesis. I am thankful to the PHS department for the support of my research and providing me the opportunities to work as a GA/TF. I would like to thank Dean's office for the support during my studies and for providing me the Doctoral Research Fellowship. I am truly thankful to my friends and colleagues for their help and support in the laboratory during my research. And last but not the least, I would like to express my deepest regard for my parents and brother for their unwavering love and support.

TABLE OF CONTENTS

ACKNOWLEDGEMENT.....	ii
LIST OF FIGURES.....	vi
LIST OF ABBREVIATIONS	x
Chapter 1. Introduction	1
1.1. ABC Transporters	1
1.1.1. The Structure and Function of BCRP Transporter.....	1
1.1.2. BCRP Substrates	2
1.1.3. The Structure and Function of P-gp Transporter	4
1.1.4. P-gp Substrates.....	5
1.2. The Co-expression of BCRP and P-gp in Cancers.....	8
1.3. Mechanisms of Reversing ABC Transporters-mediated MDR	9
1.4. BCRP and P-gp Inhibitors.....	10
1.4.1. Representative BCRP and/or P-gp inhibitors	10
1.4.2. Gefitinib as a BCRP and P-gp Dual Inhibitor	14
1.5. Electrophilic and Photoaffinity Probes	15
Chapter 2. Design Rationale.....	17
Chapter 3. Experimental Section	22
3.1. Chemistry.....	22
2-(Pyridin-4-yl)quinazolin-4(3 <i>H</i>)-one (4)	23
4-Chloro-2-(pyridin-4-yl)quinazolinamine (5).....	23
General Procedure for the Preparation of the Substituted 4-Anilinoquinazolinamines 6-8.....	24
2-(Pyridin-4-yl)- <i>N</i> -(<i>p</i> -tolyl)quinazolin-4-amine (6).....	24
<i>N</i> -(4-Ethylphenyl)-2-(pyridin-4-yl)quinazolin-4-amine (7).....	25
<i>N</i> -(4-Propylphenyl)-2-(pyridin-4-yl)quinazolin-4-amine (8)	26
2-(<i>p</i> -Tolyl)-2,3-dihydroquinazolin-4(1 <i>H</i>)-one (9).....	26
General Procedure for the Preparation of the Quinazolinamine Derivatives 13-15.	27
2-(<i>p</i> -Tolyl)quinazolin-4(3 <i>H</i>)-one (13).....	27
2-(4-Ethylphenyl)quinazolin-4(3 <i>H</i>)-one (14).....	28
2-(4-Propylphenyl)quinazolin-4(3 <i>H</i>)-one (15).....	28
General Procedure for the Preparation of the 4-Chloro-quinazolinamine Derivatives 16-18.....	28
4-Chloro-2-(<i>p</i> -tolyl)quinazolinamine (16)	29

4-Chloro-2-(4-ethylphenyl)quinazolinamine (17)	29
4-Chloro-2-(4-propylphenyl)quinazolinamine (18)	30
General Procedure for the Preparation of the Substituted 4-Anilinoquinazolinamines 19-21.	30
<i>N</i> -(Pyridin-4-yl)-2-(<i>p</i> -tolyl)quinazolin-4-amine (19).....	30
2-(4-Ethylphenyl)- <i>N</i> -(pyridin-4-yl)quinazolin-4-amine (20).....	31
2-(4-Propylphenyl)- <i>N</i> -(pyridin-4-yl)quinazolin-4-amine (21)	32
Methyl 3-benzamidopicolinate (22)	32
2-Phenylpyrido[3,2- <i>d</i>]pyrimidin-4(3 <i>H</i>)-one (23)	33
4-Chloro-2-phenylpyrido[3,2- <i>d</i>]pyrimidine (24)	33
General Procedure for the Preparation of the Substituted 4-Anilinoquinazolinamines 25-36.	34
2-Phenyl- <i>N</i> -(<i>p</i> -tolyl)pyrido[3,2- <i>d</i>]pyrimidin-4-amine (25).....	35
<i>N</i> -(4-Ethylphenyl)-2-phenylpyrido[3,2- <i>d</i>]pyrimidin-4-amine (26).....	35
2-Phenyl- <i>N</i> -(4-propylphenyl)pyrido[3,2- <i>d</i>]pyrimidin-4-amine (27)	36
<i>N</i> -Phenyl-2-(pyridin-4-yl)quinazolin-4-amine (28).....	36
<i>N</i> -(4-Cyclopropylphenyl)-2-(pyridin-4-yl)quinazolin-4-amine (29).....	37
<i>N</i> -(4-Isopropylphenyl)-2-(pyridin-4-yl)quinazolin-4-amine (30).....	38
<i>N</i> -(3-Ethylphenyl)-2-(pyridin-4-yl)quinazolin-4-amine (31).....	38
<i>N</i> -(3-Propylphenyl)-2-(pyridin-4-yl)quinazolin-4-amine (32)	39
2-Nitro-4-((2-(pyridin-4-yl)quinazolin-4-yl)amino)phenol (33).....	40
<i>N</i> -(4-Methoxyphenyl)-2-(pyridin-4-yl)quinazolin-4-amine (34).....	40
<i>N</i> ^{<i>l</i>} -(2-(Pyridin-4-yl)quinazolin-4-yl)benzene-1,4-diamine (35).....	41
<i>N</i> ,2-Di(pyridin-4-yl)quinazolin-4-amine (36).....	41
<i>N</i> -(4-Isothiocyanatophenyl)-2-(pyridin-4-yl)quinazolin-4-amine (37).....	42
2-Bromo- <i>N</i> -(4-((2-(pyridin-4-yl)quinazolin-4-yl)amino)phenyl)acetamide (38).....	43
<i>N</i> -(4-((2-(Pyridin-4-yl)quinazolin-4-yl)amino)phenyl)acetamide (39).....	43
<i>N</i> -(4-Azidophenyl)-2-(pyridin-4-yl)quinazolin-4-amine (40).....	44
3.2. Cell Lines and Cell Culture	45
3.3. MTT Assay	45
3.4. Metabolic Stability Study	46
3.5. Drug Accumulation Assay	46
3.6. Western Blot Analysis	47
3.7. Immunofluorescence Assay	48

3.8. ATPase Assay	48
3.9. Molecular Modeling	49
Chapter 4. Results and Discussion	50
4.1. Chemistry	50
4.2. Cytotoxicity and Reversal Study on BCRP	59
4.3. Cytotoxicities and Reversal Effects on P-gp	63
4.4. Metabolic Stability Study	65
4.5 The Reversal Study of 29 (VKCY-1) and 40 (VKCY-2) in Combination with Anticancer Drugs	67
4.6. Drug Accumulation Assay	69
4.7. Western Blot Assay	70
4.8. Immunofluorescence Assay	71
4.9. The effect of compound 29 on BCRP and P-gp expression levels on membrane and cytoplasm.	74
4.10. ATPase Assay	75
4.11. Docking Analysis.....	77
Chapter 5. Conclusions	81
References	83

LIST OF FIGURES

Figure 1. Topology of BCRP Transporter.	2
Figure 2. The substrates of BCRP.....	3
Figure 3. Topology of P-gp Transporter.....	5
Figure 4. The substrates of P-gp	6
Figure 5. Structures of representative BCRP inhibitors.....	12
Figure 6. Structures of representative P-gp inhibitors.	13
Figure 7. Structures of BCRP and P-gp dual inhibitors	14
Figure 8. Quinazolinamine analogues as BCRP and P-gp inhibitors.....	15
Figure 9. Design Rationale.....	19
Figure 10. ¹ H NMR (400 MHz, <i>d</i> ₆ -DMSO) of 9	52
Figure 11. ¹ H NMR (400 MHz, <i>d</i> ₆ -DMSO) of 13	53
Figure 12. IR spectrum of 37	57
Figure 13. IR spectrum of 38	58
Figure 14. IR spectrum of 39	58
Figure 15. IR spectrum of 40	58
Figure 16. The reversal effects of quinazolinamine derivatives 6-8 , 19-21 , and 25-40 on P-gp-mediated MDR cell line KB-C2.....	65
Figure 17. The reversal effects of quinazolinamine derivatives on P-gp-mediated MDR cell line KB-C2.	65
Figure 18. The reversal study of compounds 29 and 40 in combination with anticancer drugs.....	68

Figure 19. The effect of 29 and 40 on the accumulation of mitoxantrone on H460/MX20 or paclitaxel on KB-C2 cells.	70
Figure 20. The effect of 29 on BCRP and P-gp expression level in drug resistant cell lines.	71
Figure 21. The effect of 40 on BCRP expression level in H460/MX20 cells.	71
Figure 22. The effect of compound 29 on BCRP localization in H460 and H460/MX20 cells.	72
Figure 23. The effect of compound 29 on P-gp localization in KB-C2 cells.	73
Figure 24. The effect of compound 40 on BCRP localization in H460/MX20 cells. .	73
Figure 25. The effect of 29 on BCRP expression level on membrane and cytoplasm.	75
Figure 26. The effect of compound 29 on P-gp expression level on membrane and cytoplasm.	75
Figure 27. The effect of compound 29 on orthovanadate (Vi)-sensitive BCRP ATPase activity.	76
Figure 28. The effect of compound 40 on orthovanadate (Vi)-sensitive BCRP ATPase activity.	77
Figure 29. The effect of compound 29 on orthovanadate (Vi)-sensitive P-gp ATPase activity.	77
Figure 30. The docking analysis of compound 29 , 40 , and Ko143 binding with BCRP (PDB 6FFC).	79
Figure 31. The docking analysis of compound 29 and verapamil binding with human	

P-gp (PDB 6FN1).80

LIST OF SCHEMES

Scheme 1. The synthesis of 6-8	51
Scheme 2. The synthesis of 9	52
Scheme 3. Plausible pathway of synthesis of 2-aryl-4-quinazolinones.	53
Scheme 4. The synthesis of 19-21	54
Scheme 5. The synthesis of 25-27	55
Scheme 6. The synthesis of 28-36	56
Scheme 7. The synthesis of 37-40	57

LIST OF ABBREVIATIONS

Abbreviation	Definition
ABC	ATP-binding cassette
BBB	Blood brain barrier
BCRP	Breast cancer resistance protein
DMAP	4-Dimethylaminopyridine
DMF	Dimethylformamide
DMSO	Dimethyl sulfoxide
DOX	Doxorubicin
EGFR	Epidermal growth factor receptor
FBS	Fetal bovine serum
FTC	Fumitremorgin C
HPLC	High performance liquid chromatography
HRP	Horseradish peroxidase
IR	Infrared spectroscopy
MDR	Multidrug resistance
MTT	3-(4,5-dimethylthiazol-2-yl)-2,5-diphenyltetrazolium bromide
NADPH	Nicotinamide adenine dinucleotide phosphate
NBD	Nucleotide binding domains
NMR	Nuclear magnetic resonance
P-gp	P-glycoprotein
PKC	Protein kinase C
PTX	Paclitaxel
PVDF	Polyvinylidene fluoride
SDS	Sodium dodecyl sulfate
SDS-PAGE	Sodium dodecyl sulfate polyacrylamide gel electrophoresis
TFA	Trifluoroacetic acid
TKIs	Tyrosine kinase inhibitors
TLC	Thin-layer chromatography
TMD	Transmembrane domains

Chapter 1. Introduction

Cancer is a disease that causes cells to divide uncontrollably and spread into surrounding tissues. It is the second leading cause of death globally. In 2021, it is estimated that 1.9 million new cancer cases will be diagnosed and 608,570 will die from cancer in the United States.¹ In 2020, lung, colorectal, breast, and prostate cancers were the four leading cancers, with breast cancer causing more deaths than lung, prostate, and colorectal cancers.¹ The failure of chemotherapy is mainly caused by multidrug resistance (MDR), which involves a variety of cellular pathways. The factors that contribute to MDR in cancer include the reduction of the intracellular accumulation and increase of drug efflux,² enhanced DNA damage repair,³ cell death inhibition, epithelial-mesenchymal transition,⁴ drug target alteration,⁵ and the enhancement of drug inactivation.⁶

1.1. ABC Transporters

The overexpression of ATP-binding cassette (ABC) transporters is an important cause of drug efflux, resulting in MDR in cancers. ABC transporters, with seven subfamilies (ABCA–ABCG), are a superfamily of 48 transporters expressed in humans, of which ABCE and ABCF subfamilies have no membrane transport function.^{7,8}

1.1.1. The Structure and Function of BCRP Transporter

Breast cancer resistance protein (BCRP), the second member of the G subfamily of the ABC transporters, also named ABCG2, was identified in an MDR human breast cancer cell line MCF-7/AdrVp in 1998.⁹ Since then it has been found to be mainly overexpressed in drug-resistant tumors. BCRP is an approximately 75 kDa polytopic

plasma membrane protein with one cytoplasmic nucleotide binding domain (NBD) and one transmembrane domain (TMD) composed of a single polypeptide chain¹⁰ (**Figure 1**). BCRP is a half-transporter that dimerizes to become a functional homodimer with a molecular weight of approximately 144 kDa homodimer. High levels of BCRP are found in the BBB, placenta, liver, adrenal gland, prostate, testes, and uterus.¹¹ BCRP extrudes endogenous toxins or xenobiotics from the tissues and regulates endogenous compounds such as heme, porphyrins, and estrogens.^{12,13}

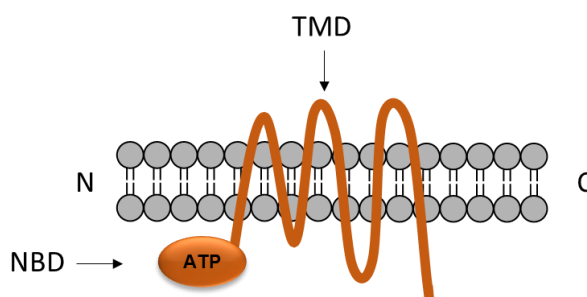


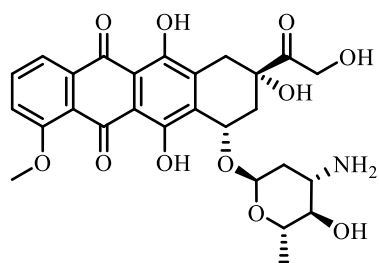
Figure 1. Topology of BCRP Transporter.

1.1.2. BCRP Substrates

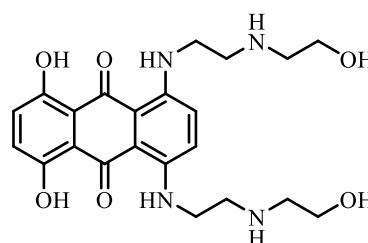
BCRP utilizes the energy generated from ATP hydrolysis to drive the efflux of a diverse array of chemicals across the cell membranes. A large number of anticancer drugs including doxorubicin, mitoxantrone, gefitinib, methotrexate, SN-38, and topotecan^{14,15} (**Figure 2**) are BCRP substrates that get pumped out of BCRP overexpressing cancer cells resulting in decrease in their efficacy. BCRP substrates also comprise antiviral drugs such as zidovudine and lamivudine¹⁶; non-chemotherapy drugs such as prazosin¹⁷ (antihypertensive drug), glyburide¹⁸ (anti-diabetic), nitrofurantoin¹⁹ (antibiotic), and dipyridamole²⁰ (vasodilator); photosensitizers²¹ such

as pheophorbide A and hematoporphyrin (**Figure 2**); nontherapeutic compounds such as the flavonoids²², porphyrins²³, and estrone 3-sulfate²⁴.

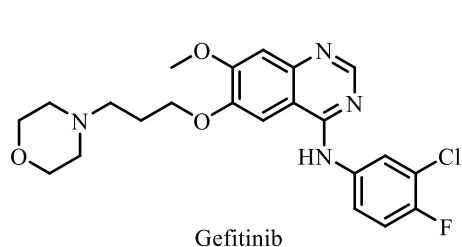
Anticancer drugs



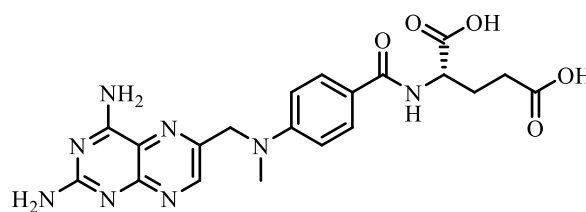
Doxorubicine



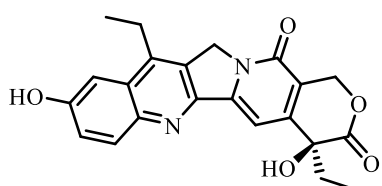
Mitoxantrone



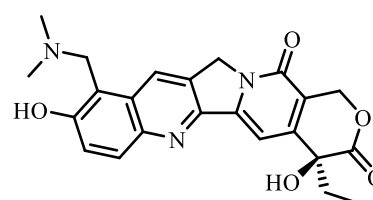
Gefitinib



Methotrexate

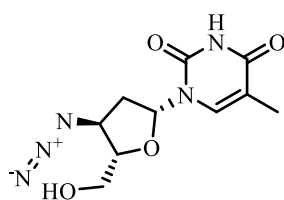


SN-38

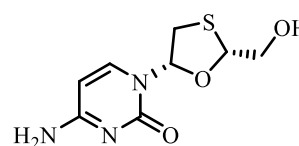


Topotecan

Antiviral drugs



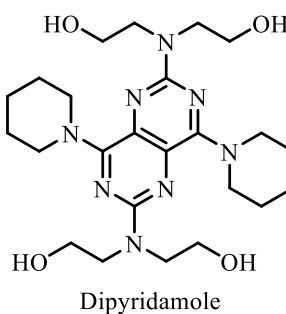
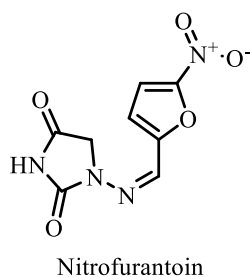
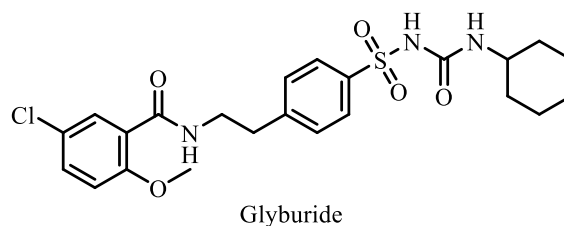
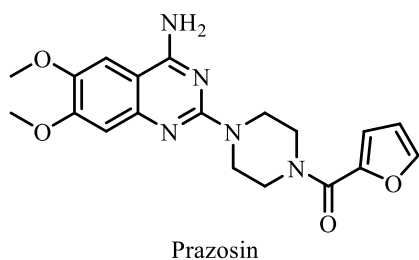
Zidovudine



Lamivudine

Figure 2. The substrates of BCRP (continued)

Non-chemotherapy drugs



Photosensitizers

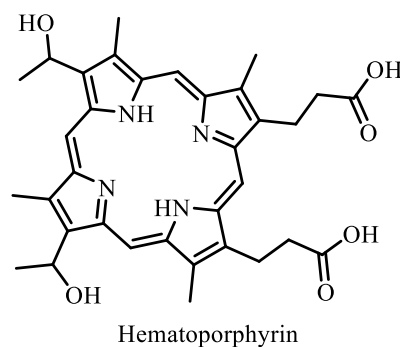
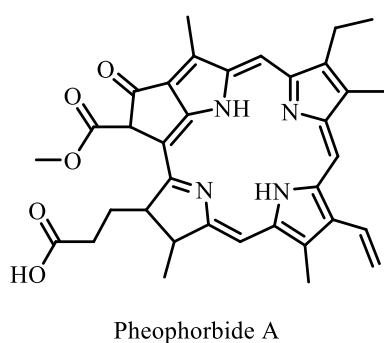


Figure 2. The substrates of BCRP

1.1.3. The Structure and Function of P-gp Transporter

P-gp, also known as ABCB1, contains two TMDs and two cytoplasmic NBDs²⁵ (**Figure 3**). P-gp is the first human ABC transporter to be identified through its ability to confer MDR in cancer cells. Drug resistance mediated by P-gp depends on ATP hydrolysis, with adenosine triphosphatase (ATPase) activity of P-gp being stimulated by the transported drugs. Vanadate (Vi) trapping and photocleavage experiments showed that P-gp contains two active ATPase sites, but only one ATP is hydrolyzed at

a time²⁶. P-gp translocates the substrates from the basolateral to the apical side of the epithelium.

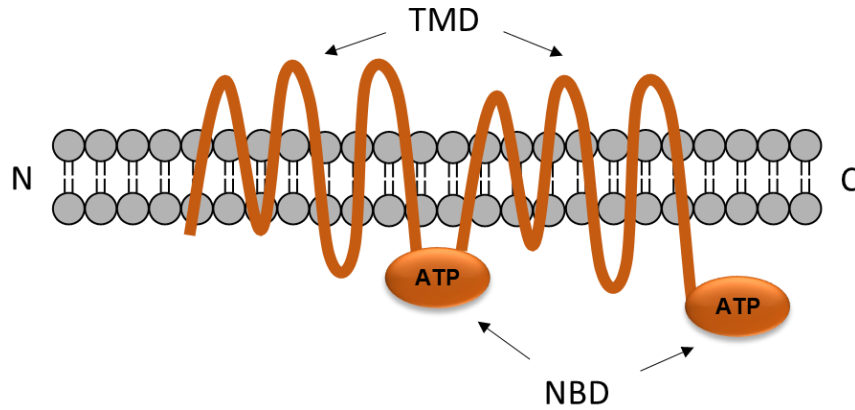


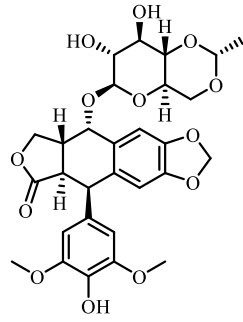
Figure 3. Topology of P-gp Transporter.

1.1.4. P-gp Substrates

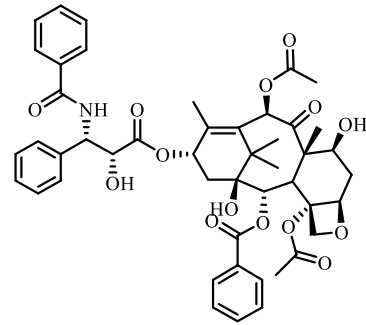
A variety of compounds have been identified as substrates of P-gp whose pharmacokinetic behaviors, efficacy, and toxicity are dramatically altered by P-gp²⁷.

P-gp substrates include anticancer drugs (etoposide, paclitaxel²⁸, 5-fluorouracil, gefitinib²⁹, vincristine³⁰, doxorubicin³¹); antibiotics²⁷ (ceftriaxone, clarithromycin, doxycycline, levofloxacin); antihistamines (cimetidine, fexofenadine³²); calcium channel blockers³³ (diltiazem, felodipine); HIV protease inhibitors³⁴ (ritonavir, nelfinavir); corticosteroids³⁵ (dexamethasone, hydrocortisone); diagnostic dyes (Hoechst 33342³⁶), and analgesics (morphine³⁷) (**Figure 4**).

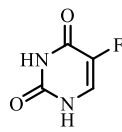
Anticancer drugs



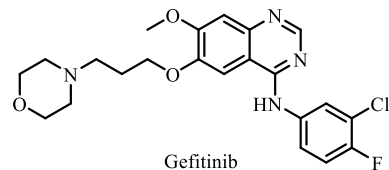
Etoposide



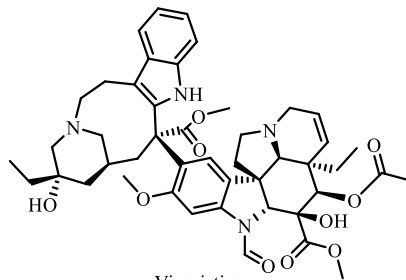
Paclitaxel



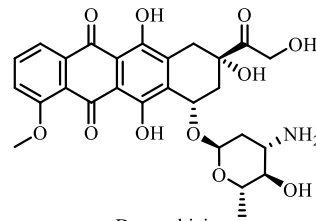
5-Fluorouracil



Gefitinib

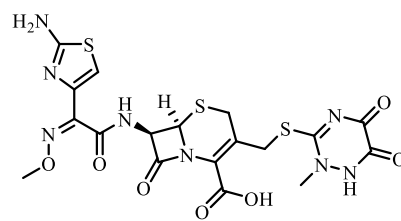


Vincristine

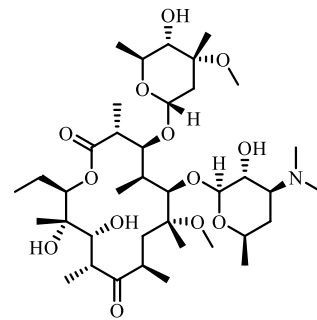


Doxorubicin

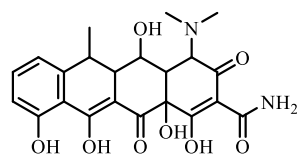
Antibiotics



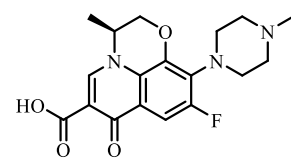
Ceftriaxone



Clarithromycin



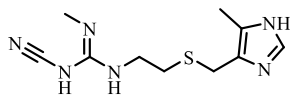
Doxycycline



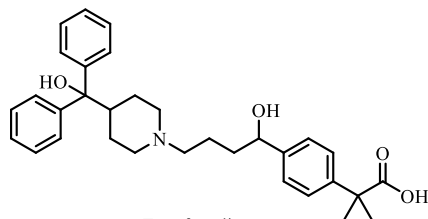
Levofloxacin

Figure 4. The substrates of P-gp (continued)

Antihistamines

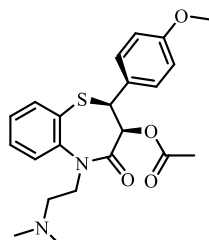


Cimetidine

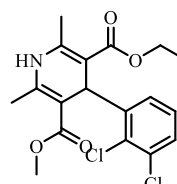


Fexofenadine

Calcium channel blockers

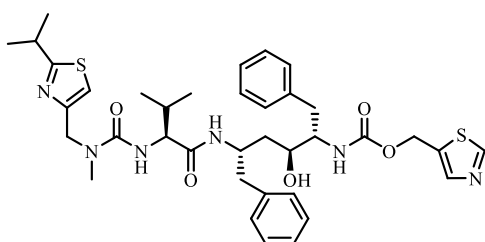


Diltiazem

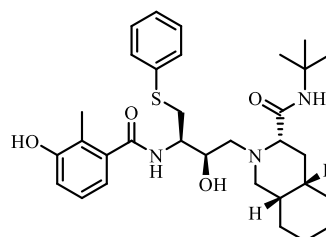


Felodipine

HIV protease inhibitors

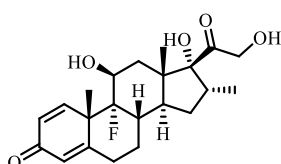


Ritonavir

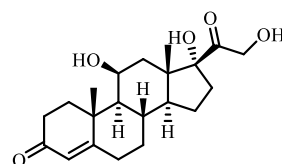


Nelfinavir

Corticosteroids

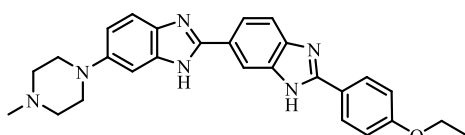


Dexamethasone



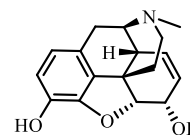
Hydrocortisone

Diagnostic dyes



Hoechst 33342

Analgesics



Morphine

Figure 4. The substrates of P-gp

BCRP can transport hydrophobic substrates such as mitoxantrone, in addition to hydrophilic conjugated organic anions, particularly the sulfated conjugates, while P-gp generally transports hydrophobic compounds.²⁷ It was reported that BCRP substrates imatinib, methotrexate, mitoxantrone, prazosin, and SN-38 are also P-gp substrates.²⁷ The overlap between BCRP and P-gp substrates can lead to a synergistic effect in preventing drugs from crossing tissue barriers such as the blood-brain barrier.^{38,39}

1.2. The Co-expression of BCRP and P-gp in Cancers

Previous reports revealed that cancers with overexpression of multiple transporters may be more resistant to chemotherapy than those with a single transporter expression, thus the coexpression of multiple transporters was associated with worse prognosis. BCRP and P-gp are coexpressed in certain cancers, such as leukemia. Wilson et al.⁴⁰ obtained gene expression profiles of 170 pretreated samples of acute myelogenous leukemia to reveal that the highest levels of drug resistance was associated with increased expression of both BCRP and P-gp. Comparing 380 drug-resistance-related genes from a set of 11 paired samples obtained at diagnosis with those at relapse, increased expression of BCRP and P-gp at relapse was identified in two acute myeloid leukemia patients.⁴¹ Liu et al.⁴² used bone marrow mononuclear cells from 96 *de novo* acute myelogenous leukemia patients to test the expression of several ABC transporters, including BCRP (ABCG2), P-gp (ABCB1), MDR3 (ABCB4), MRP1 (ABCC1), and MRP4 (ABCC4). The results further confirmed that coexpression of multiple transporters was associated with worse prognosis. Another

study showed that the initial response to chemotherapy was strongly associated with the number of overexpressed ABC-transporters in childhood acute myeloid leukemia.⁴³ The patients expressing more ABC-transporters have reduced chance to have less than 5% leukemic cells after the chemotherapy. This can be the reason why some studies involving specific inhibition of P-gp to sensitize leukemic cells were not very effective.⁴⁴

1.3. Mechanisms of Reversing ABC Transporters-mediated MDR

Reversal of MDR can occur through various mechanisms such as direct binding of inhibitors to ABC transporters, inhibiting ATPase activity of ABC transporters, or altered expression level of ABC transporter proteins.

ABC transporters inhibitors can interact with the binding sites of the transporters, thus inhibiting the efflux of anti-cancer drugs, reversing ABC transporter mediated MDR. Previous reports indicated that several tyrosine kinase inhibitors (TKIs), such as gefitinib, imatinib, nilotinib, and erlotinib, inhibited BCRP-mediated MDR. These TKIs themselves are BCRP substrates and may act as competitive BCRP substrates to block the efflux of anticancer drugs.

Compared with TKIs, protein kinase C (PKC) inhibitors suppress the MDR through a different mechanism by inhibiting BCRP or P-gp ATPase activity. It has been reported that PKC inhibitors with bisindolylmaleimide (BIM) or indolocarbazole moiety block BCRP-mediated transport.⁴⁵ In addition, various PKC inhibitors including the pan-PKC inhibitors staurosporine and chelerythrine, the PKC inhibitor enzastaurin⁴⁶ and the bisindolylmaleimide (BIM) PKC inhibitors GF 109203X⁴⁷ and

Ro 32-2241⁴⁸ can directly bind with P-gp transporter to reverse drug resistance.

Certain St. John's Wort constituents, such as quercetin, also decreased P-gp ATPase activity at the blood-brain barrier.⁴⁹

The downregulation of BCRP or P-gp transporters can be another mechanism of modulating the drug resistance. It was reported that BAY-1082439 inhibits the activation of the PI3K 110 α and 110 β catalytic subunits, resulting in the downregulation of ABC transporters BCRP and P-gp, thereby sensitizing human epidermoid carcinoma KB-C2 cells and non-small cell lung cancer (NSCLC) MDR H460/MX20 cells to antitumor drugs.⁵⁰

1.4. BCRP and P-gp Inhibitors

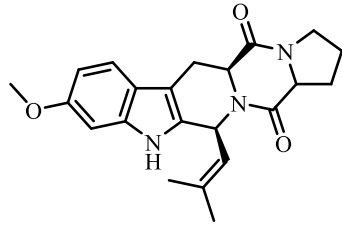
ABC transporters can efflux their substrates including anticancer drugs out of the cancer cells leading to MDR in cancers. Thus, ABC transporter inhibitors can block the efflux function and reverse ABC transporters mediated MDR in cancers. Many ABC transporters are also expressed abundantly in different organs in the human body, and they largely affect drug absorption, distribution and excretion, and exhibit potential effects on the pharmacokinetic properties of drugs. Therefore, ABC transporter inhibitors can affect the pharmacokinetics of substrate drugs of ABC transporters.

1.4.1. Representative BCRP and/or P-gp inhibitors

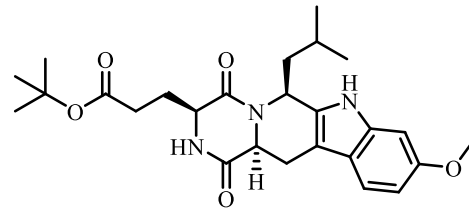
Fumitremorgin C (FTC) (Figure 5) is the first reported BCRP inhibitor⁵¹ which can effectively reverse the drug resistance in cancer. However, FTC exhibited severe neurotoxicity *in vivo*, thus researchers ramped up efforts to discover FTC analogues

with low toxicity. They discovered an **FTC** analogue, Ko143 (**Figure 4**), with potent BCRP inhibitory activity and low toxicity.⁵² It was reported that Ko143 is not only a BCRP inhibitor but also a weak P-gp inhibitor.⁵³ Nevertheless, Ko143 can be metabolized rapidly in rats and transformed into an inactive metabolite, which hinders its clinical use. A wide variety of other compounds, such as anti-HIV protease inhibitors (nelfinavir and ritonavir),⁵⁴ and the dietary flavonoids (chrysin and biochanin A)⁵⁵ (**Figure 5**) have been identified as BCRP inhibitors.

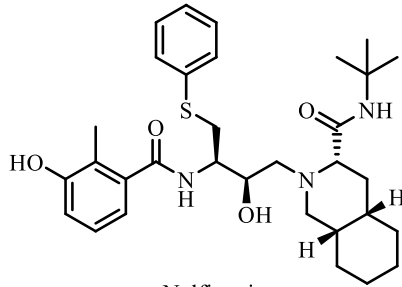
Three generations of P-gp inhibitors have been developed to date. The first generation of P-gp inhibitors include verapamil and cyclosporine A, while the second generation of P-gp inhibitors include (R)-verapamil and valsopodar. The newly developed P-gp inhibitors comprise compounds such as tariquidar, mitotane, and ONT-093 (**Figure 6**).²⁷ Various reports have revealed that some drugs including elacridar, reserpine, cyclosporin A, tariquidar, and valsopodar (**Figure 7**) are effective BCRP and P-gp dual inhibitors. In addition, several TKIs have been found to interact with BCRP and P-gp as both substrates and inhibitors. TKIs imatinib, nilotinib and pazopanib were potent BCRP inhibitors with IC₅₀ values of 0.94, 2.50, and 10.4 μM, while inhibiting P-gp activities with IC₅₀ values of 2.42, 6.11 and 8.06 μM.⁵⁶



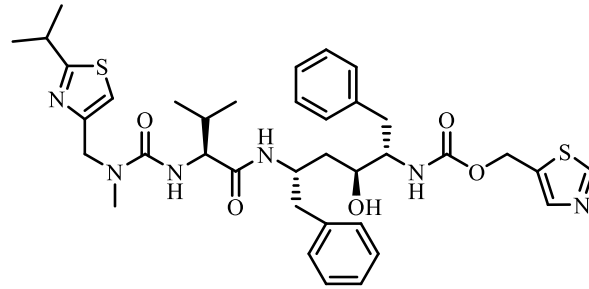
Fumitremogin C



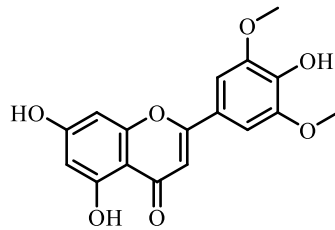
Ko143



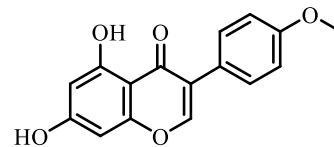
Nelfinavir



Ritonavir



Chrysin



Biochanin A

Figure 5. Structures of representative BCRP inhibitors.

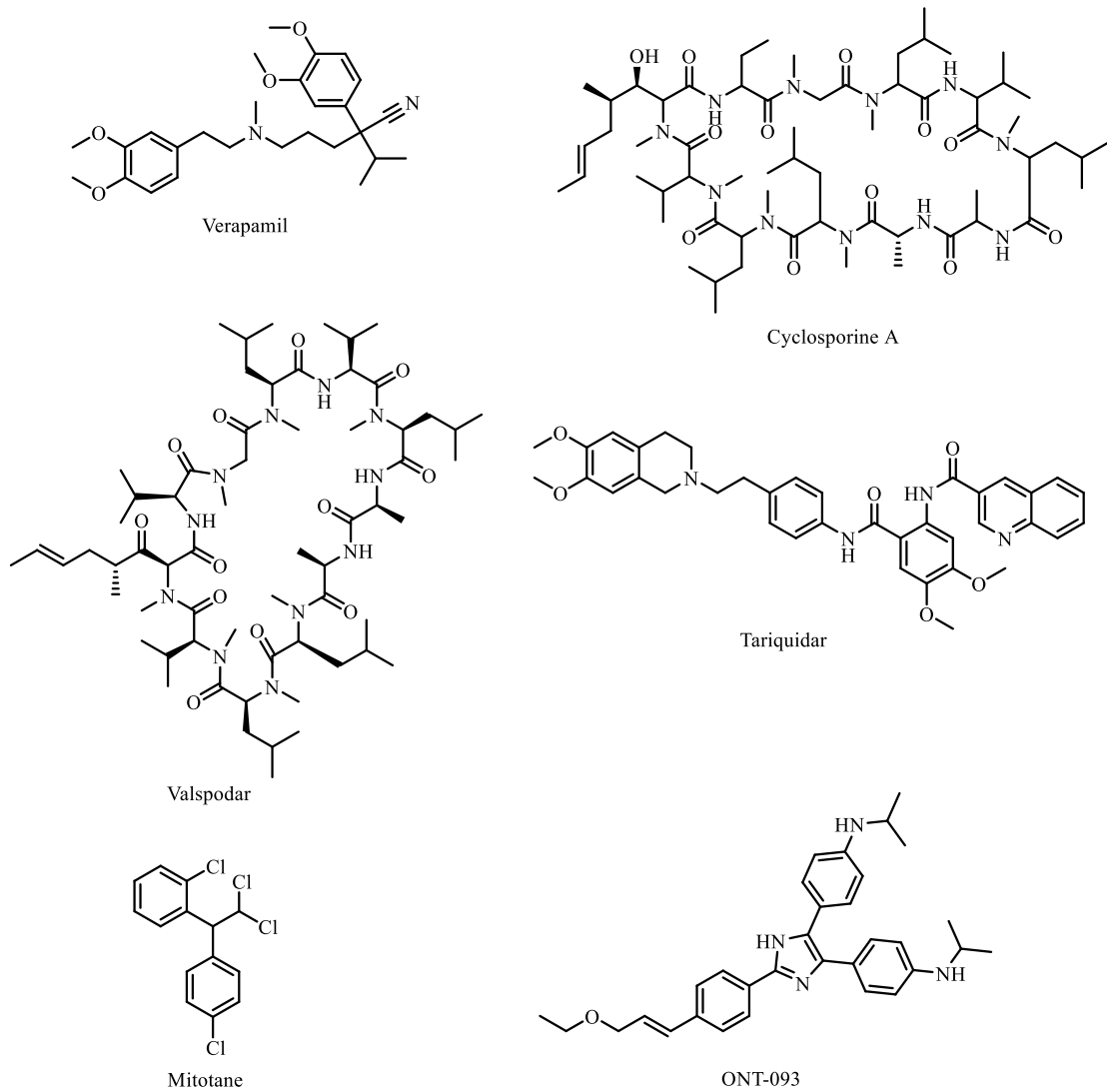


Figure 6. Structures of representative P-gp inhibitors.

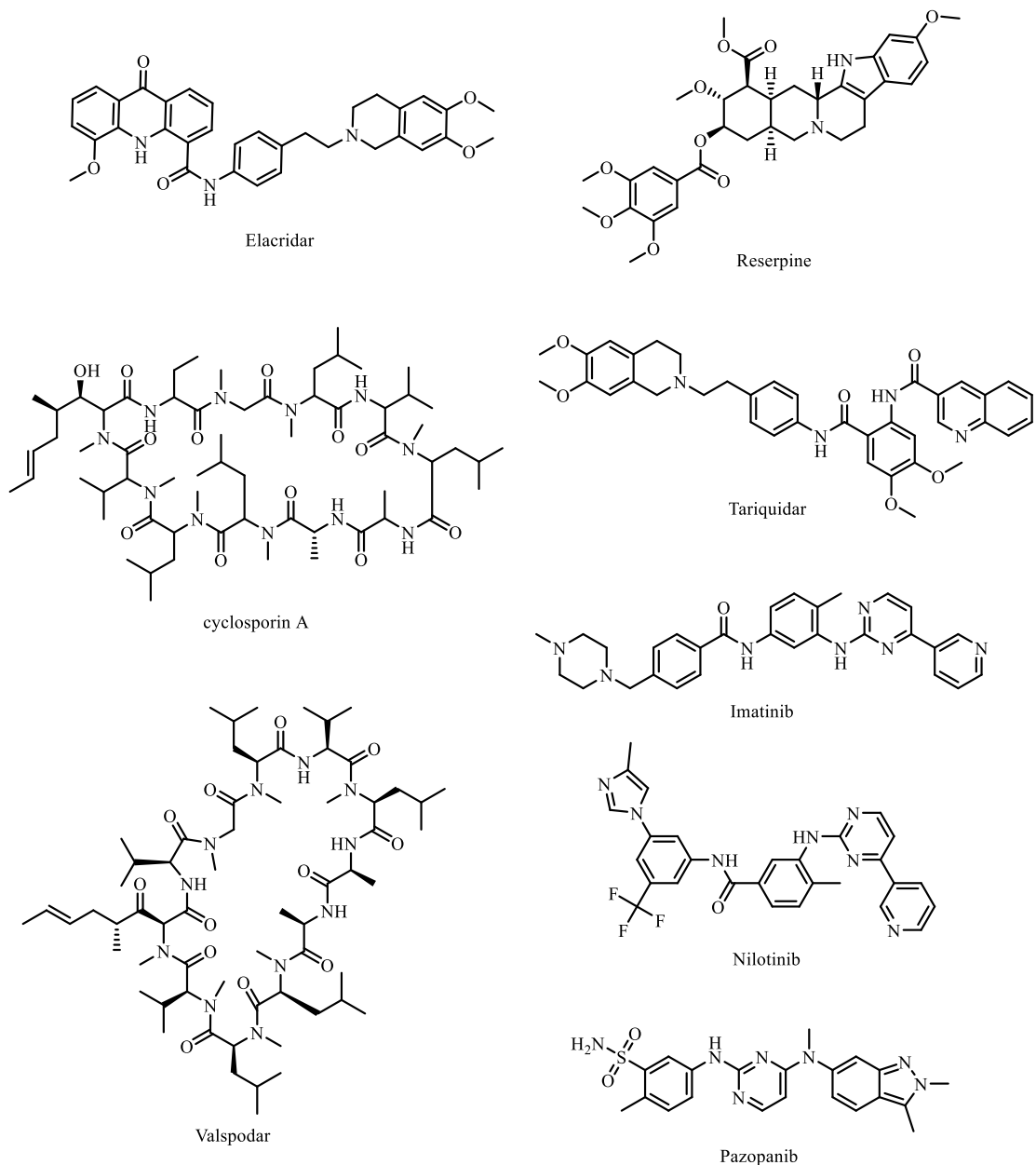


Figure 7. Structures of BCRP and P-gp dual inhibitors

1.4.2. Gefitinib as a BCRP and P-gp Dual Inhibitor

Gefitinib, an EGFR inhibitor with quinazolinamine moiety, is used for the treatment of certain breast, lung and other cancers. It has been reported that gefitinib can inhibit BCRP⁵⁷ and reverse 2.7-fold of drug resistance on P-gp overexpressed PC-6/PTX cells.²⁹ Wiese et al. synthesized a series of quinazolinamines derived from

gefitinib as BCRP inhibitors. They discovered that some quinazolinamines can also inhibit P-gp (**Figure 8**).^{58,59} The IC₅₀ values of compounds **1-3** for BCRP inhibition varied from 202 to 652 nM while the IC₅₀ values for P-gp inhibition were in the range of 1.04 to 1.88 μM. The reports showed that the quinazolinamine derivatives exhibit promising inhibitory activities on BCRP and P-gp transporters. Further investigation of the structure-activity relationship of the quinazolinamine derivatives can help discover potent BCRP and P-gp dual inhibitors for reversing MDR.

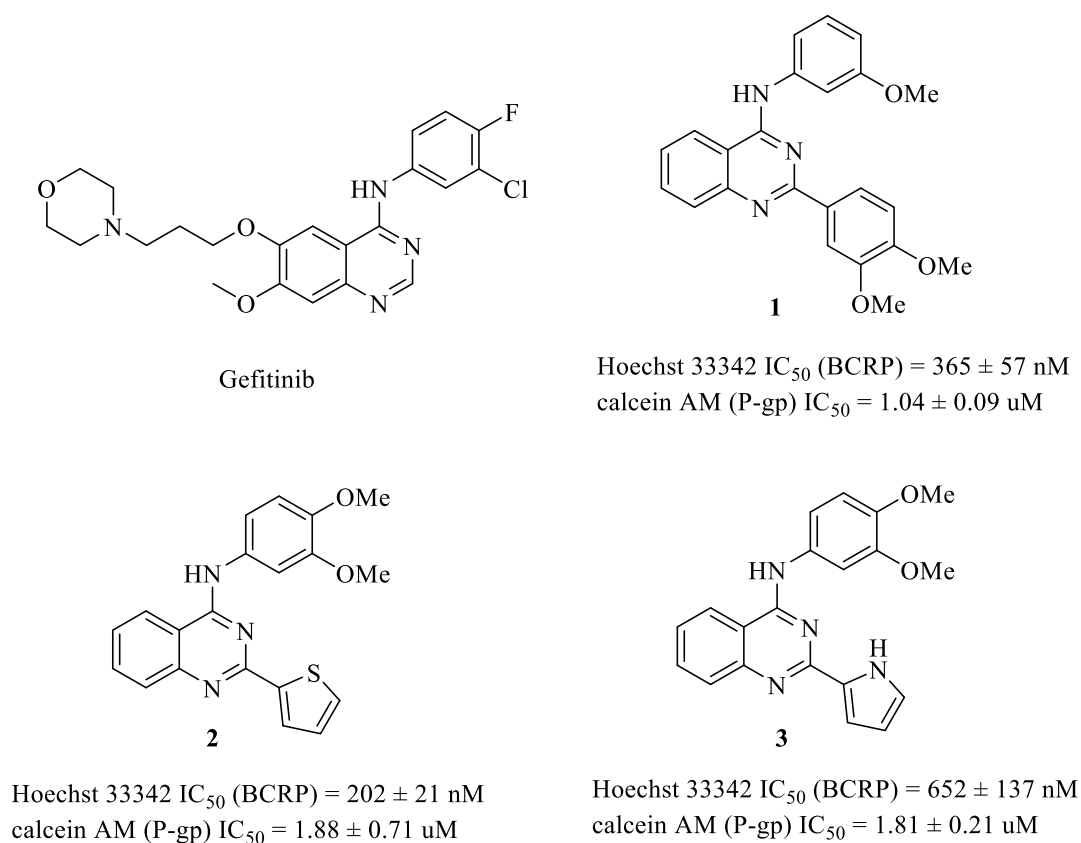


Figure 8. Quinazolinamine analogues as BCRP and P-gp inhibitors

1.5. Electrophilic and Photoaffinity Probes

Covalent drugs and probes are widely used as clinical agents and research tools for the identification and localization of targets. One of the strategies to discover the

covalent probes and drugs is using a non-covalent probe equipped with a reactive group and thus converting it into a covalent probe. Chemical probes with various reactive groups, both electrophilic (e.g., isothiocyanate,⁶⁰ bromoacetamide,⁶¹ and benzophenone⁶²) and photoactivatable (aliphatic/aromatic azides, and trifluoromethyl diazine) type, can react in a chemically defined manner with a distinct amino acid. The method of photoaffinity labeling to identify a target was originally introduced by Westheimer et al. in 1962.⁶³ Afterwards, photoaffinity labeling has served as a powerful tool to covalently bind with its target under UV irradiation to identify targets and interaction sites,⁶⁴ especially for mapping low-abundance protein modifications and low-affinity interactions.⁶⁵ Covalent probes or drugs exhibit various benefits for their clinical use,⁶² including the improvement of the efficiencies for rapidly metabolized and excreted drugs, improved pharmacokinetic properties such as fast clearance and binding to serum proteins, minimizing the side effects, overcoming drug resistance especially when targeting residues of a target protein that are essential for its proper function, avoiding off-target effects. The quinazolinamines with electrophilic groups or photoaffinity label can help serve as probes to investigate the binding of quinazolinamines to ABC transporters.

Chapter 2. Design Rationale

Quinazolinamine derivatives, which share structural similarity with the BCRP and P-gp dual inhibitor gefitinib, have the potential to inhibit both BCRP and P-gp activities. Both BCRP and P-gp are known to transport hydrophobic compounds,²⁷ suggesting that hydrophobicity plays an important role in the binding affinity of target compounds for these transporters.

Nitrogen as a hydrogen bond acceptor can play an important role in the interaction of the quinazolinamine derivatives with ABC transporters. Therefore, a nitrogen atom was incorporated, and its position in the aromatic rings varied to investigate the importance of the nitrogen atom and its location. Target compounds with scaffolds A, B, and C (**Figure 9**) contain a nitrogen atom in rings A, B, or C, respectively. A series of quinazolinamine derivatives with methyl, ethyl and n-propyl groups on rings A or B, in scaffolds A (**6-8**), B (**19-21**), and C (**25-27**), were designed to evaluate the role of hydrophobicity on the binding affinity of the target compounds to BCRP and P-gp transporters (**Table 1a**).

Based on the MTT assay results, quinazolinamine derivatives **7** and **8** with scaffold A showed higher potency as BCRP inhibitors than those compounds with scaffolds B or C, decreasing the IC₅₀ values of mitoxantrone from 5.66 μM to 0.27 and 0.23 μM, respectively. Based on these preliminary results, additional quinazolinamine derivatives with scaffold A (**Table 1b**) were designed to discover more potent BCRP inhibitors with a potential to also inhibit P-gp. BCRP and P-gp inhibitory activities of all quinazolinamine derivatives were determined to investigate

the structure-activity relationship. Compound **28** with no substitution on ring A was designed for comparison. It was reported that quinazolinamines with substitutions at *meta* and *para* positions are more potent than those with substitutions at *ortho* position. Two and three carbon substitutions were made at *meta* and *para* positions to obtain target compounds **29-32**. The inhibitory activities of these compounds were compared with that of the ethyl and propyl substituted compounds **7** and **8**. 3-NO₂-4-OH substituted quinazolinamine has been previously shown to exhibit potent inhibition toward BCRP transporter.⁵⁹ To further investigate the structure-activity relationship of the quinazolinamine series with scaffold A, the 3-NO₂-4-OH moiety was introduced in target compound **33** to probe the effects of the hydrophobic and hydrophilic groups on the reversal activities of quinazolinamines towards BCRP and P-gp transporters. Methoxy quinazolinamine **34** with oxygen as the hydrogen bond acceptor was designed to determine how it affects the inhibitory activity of the quinazolinamine derivative compared to the more hydrophobic ethyl derivative **7**. Compounds **35** and **36** with amine and pyridine groups were included to explore the effect of polarity on the inhibitory activities.

The quinazolinamine derivatives **37-40** with electrophilic or photoaffinity label were designed for the investigation of potential covalent binding between quinazolinamines and ABC transporters (**Table 1b**). Compounds **37** with isothiocyanate group and **38** with bromoacetamide group are electrophilic, while non-electrophilic acetamide **39** can be used as a control. Compound **40** with photoaffinity group azide can covalently bind with the protein upon UV irradiation and can be used

as the probe for investigating the binding site.

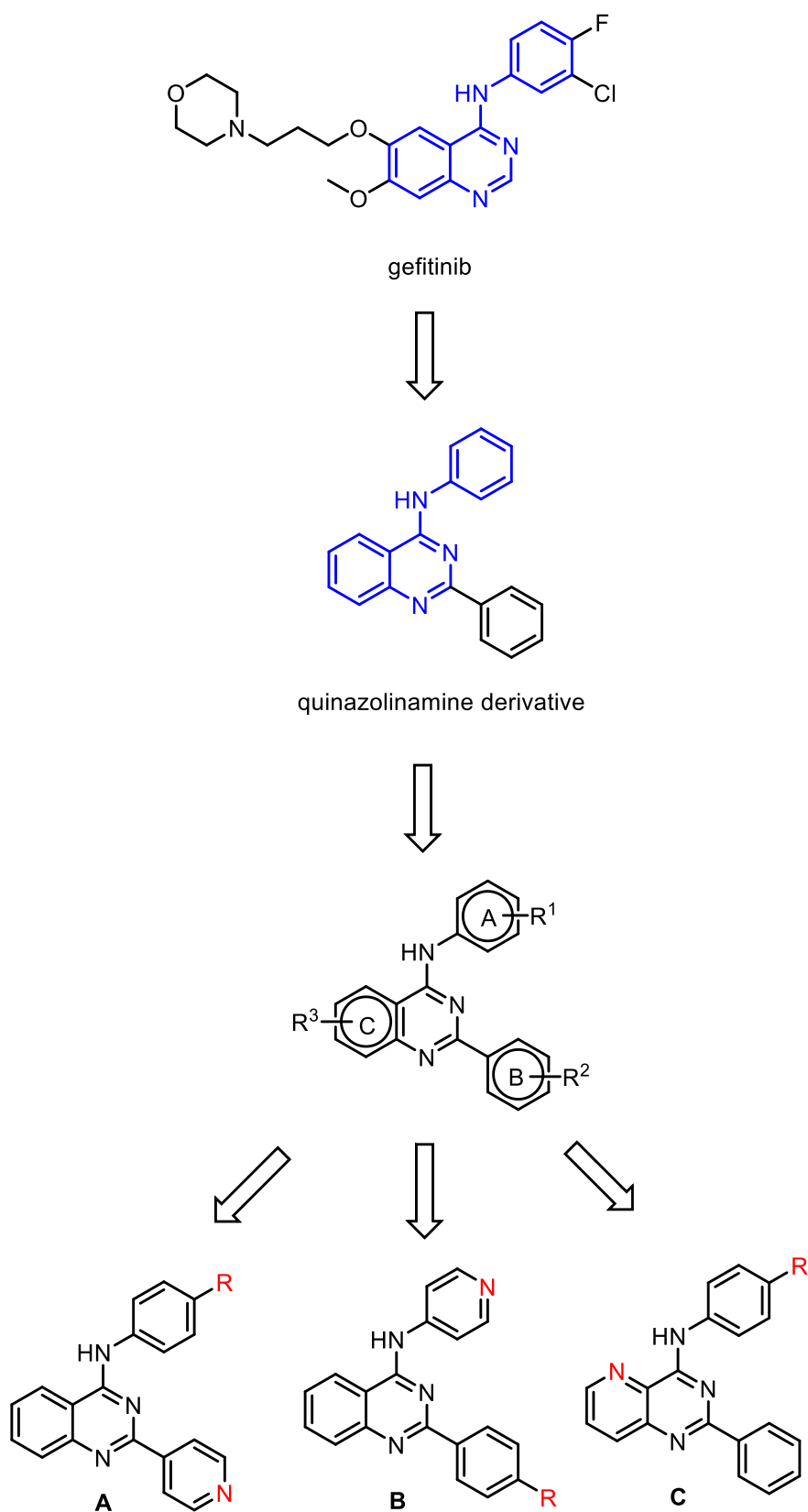


Figure 9. Design Rationale

Table 1a. The list of target compounds 6-8, 19-21, 25-27.

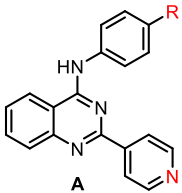
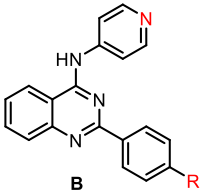
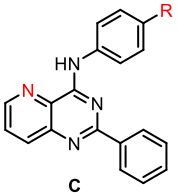
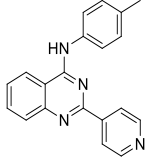
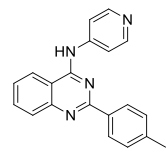
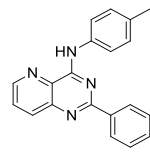
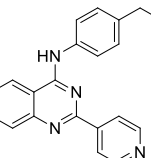
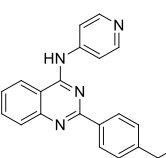
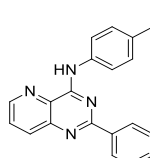
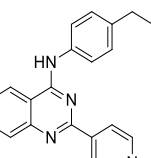
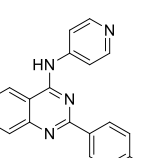
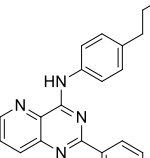
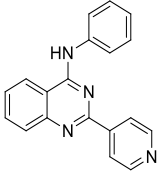
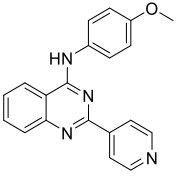
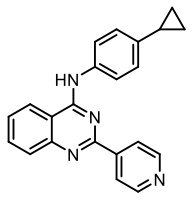
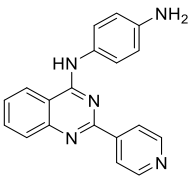
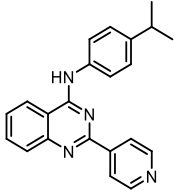
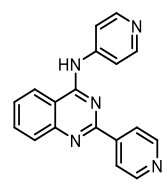
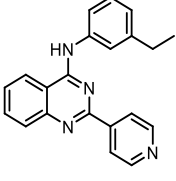
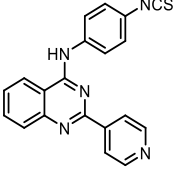
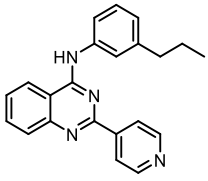
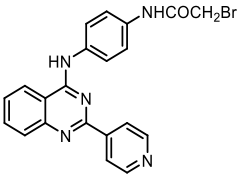
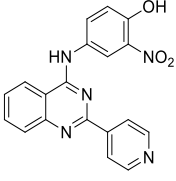
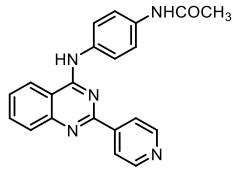
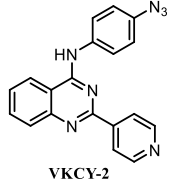
Compd.	Structure	Compd.	Structure	Compd.	Structure
					
6		19		25	
7		20		26	
8		21		27	

Table 1b. The list of target compounds 28-40.

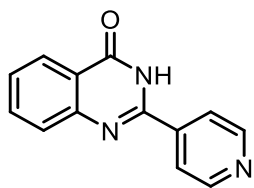
Compd.	Structure	Compd.	Structure
28		34	
29	 VKCY-1	35	
30		36	
31		37	
32		38	
33		39	
		40	 VKCY-2

Chapter 3. Experimental Section

3.1. Chemistry

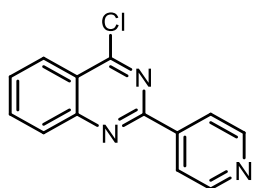
^1H NMR and ^{13}C NMR spectra were acquired with a Bruker 400 UltrashieldTM spectrophotometer (400 MHz). Infrared spectra (IR) were acquired with PerkinElmer Spectrum 100 FT-IR Spectrometers. High resolution mass spectra (HRMS) were obtained for all target compounds on a Waters Xevo G2-XS QToF mass spectrometer equipped with H-Class UPLC inlet and a LockSpray electrospray ionization (ESI) source. Reactions were monitored by thin layer chromatography (TLC) and visualized using UV light at 254 nm. TLC was performed using Analtech UniplateTM Silica Gel GF 250 Micron plates. Purification of reaction mixtures was conducted using silica gel column chromatography or Reveleris[®] X2 flash chromatography system by BÜCHI Labortechnik AG. Melting points were determined on a Thomas-Hoover Capillary Melting Point Apparatus. The purity of all target compounds was determined by high-performance liquid chromatography (HPLC), (LC, Agilent 1200 Infinity; column, Agilent HC-C18(2), 170Å, 4.6 x 250 mm, 5 µm; column temperature, 25°C; mobile phase, solvent A, methanol, solvent B, water, gradient elution, 30-99% solvent A; flow rate, 1 mL/min; UV signals were recorded at 254 nm). All tested compounds were shown to have >95% purity according to HPLC. Chemicals were purchased from Acros Organics or Alfa Aesar Chemical Company and used without further purification.

2-(Pyridin-4-yl)quinazolin-4(3H)-one (4)



A mixture of anthranilamide (681 mg, 5 mmol), 4-pyridinecarboxaldehyde (536 mg, 5 mmol), iodine (1.40 g, 5.5 mmol), and anhydrous potassium carbonate (690 mg, 5 mmol) in DMF (10 mL) was stirred at reflux for 4-8 h. Completion of the reaction was monitored by TLC and the mixture poured into crushed ice to obtain a precipitate. The pH of the mixture was adjusted to 7.0 with concentrated HCl to optimize the precipitation of the desired product. After filtering off the precipitate, it was thoroughly washed with a 20% sodium thiosulfate solution (50 mL) followed by 50 mL of hot distilled water (50 mL). Purification was performed by recrystallization from ethanol to yield **4** as a white solid in 65% yield. $^1\text{H NMR}$ (400 MHz, DMSO) δ 12.83 (s, 1H), 8.80 (dd, $J = 4.6, 1.5$ Hz, 2H), 8.19 (dd, $J = 7.9, 1.1$ Hz, 1H), 8.14 – 8.09 (m, 2H), 7.93 – 7.85 (m, 1H), 7.80 (d, $J = 7.8$ Hz, 1H), 7.63 – 7.55 (m, 1H).

4-Chloro-2-(pyridin-4-yl)quinazolinamine (5)



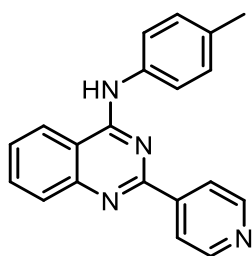
Compound **4** (446 mg, 2 mmol) was added to DMF (5 mL) containing phosphorus oxychloride (0.47 mL, 5 mmol) and stirred for 10 min at room temperature. The mixture was then refluxed for 2 h and the reaction monitored by TLC. After completion of the reaction, excess phosphorus oxychloride was removed

under reduced pressure and the residue poured into ice water (20 mL). Subsequently, the pH of the mixture was adjusted slowly to 7.0 with 25% NaOH solution and extracted three times with dichloromethane (3×20 mL). The organic phase was collected, washed with brine (50 mL) and dried over magnesium sulfate. The solvent was removed under reduced pressure to obtain compound **5** as a white solid which was recrystallized from isopropanol in 96% yield. ¹H NMR (400 MHz, DMSO) δ 8.84 (dd, $J = 4.6, 1.5$ Hz, 2H), 8.37 (dd, $J = 4.5, 1.6$ Hz, 3H), 8.28 – 8.16 (m, 2H), 7.95 (ddd, $J = 8.2, 6.5, 1.6$ Hz, 1H).

General Procedure for the Preparation of the Substituted 4-Anilinoquinazolinamines 6-8.

4-Chloroquinazolinamine derivative **5** (241 mg, 1 mmol) was added to a solution of a *para* substituted aniline derivative (1 mmol) in isopropanol and the mixture was refluxed for a period of 2 h until completion of the reaction as indicated by TLC. The precipitate that was formed was filtered off, washed with isopropanol (10 mL) and recrystallized from ethanol.

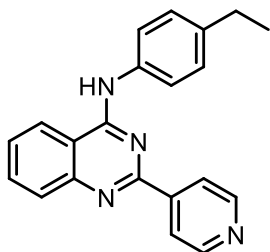
2-(Pyridin-4-yl)-*N*-(*p*-tolyl)quinazolin-4-amine (**6**)



Compound **6** was synthesized from compound **5** as described in the general procedure. It was obtained as a yellow solid in 56% yield, mp. 269-270°C; IR: 3058,

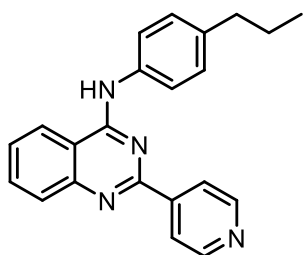
1562, 1500, 1422, 815, 786 cm^{-1} ; ^1H NMR (400 MHz, DMSO) δ 10.36 (s, 1H), 9.00 (dd, $J = 5.3, 1.3$ Hz, 2H), 8.72 (d, $J = 8.3$ Hz, 1H), 8.66 (d, $J = 6.5$ Hz, 2H), 8.04 – 7.95 (m, 2H), 7.82 – 7.71 (m, 3H), 7.31 (d, $J = 8.2$ Hz, 2H), 2.37 (s, 3H). ^{13}C NMR (101 MHz, DMSO) δ 158.79, 155.65, 151.17, 149.24, 145.06, 136.26, 134.50, 134.15, 129.52, 128.34, 128.17, 124.34, 123.89, 123.39, 114.84, 21.09. HRMS (ESI) m/z calcd for $[\text{C}_{20}\text{H}_{16}\text{N}_4 + \text{H}]^+$ 313.1453, found 313.1463.

***N*-(4-Ethylphenyl)-2-(pyridin-4-yl)quinazolin-4-amine (7)**



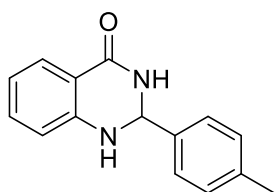
Compound 7 was synthesized from compound 5 as described in the general procedure. It was obtained as a yellow solid in 77% yield, mp. 228-230°C; IR: 2969, 1589, 1614, 1366, 798, 776 cm^{-1} ; ^1H NMR (400 MHz, DMSO) δ 9.96 (s, 1H), 8.76 (d, $J = 5.8$ Hz, 2H), 8.62 (d, $J = 8.3$ Hz, 1H), 8.28 (dd, $J = 4.5, 1.5$ Hz, 2H), 7.92 (d, $J = 3.8$ Hz, 2H), 7.87 (d, $J = 8.5$ Hz, 2H), 7.72 – 7.65 (m, 1H), 7.33 (d, $J = 8.5$ Hz, 2H), 2.67 (q, $J = 7.6$ Hz, 2H), 1.25 (t, $J = 7.6$ Hz, 3H). ^{13}C NMR (101 MHz, DMSO) δ 158.63, 157.11, 150.15, 148.96, 148.85, 147.75, 140.12, 136.85, 134.12, 128.59, 128.27, 127.65, 123.59, 123.01, 114.85, 28.15, 16.09. HRMS (ESI) m/z calcd for $[\text{C}_{21}\text{H}_{18}\text{N}_4 + \text{H}]^+$ 327.1610, found 327.1611.

***N*-(4-Propylphenyl)-2-(pyridin-4-yl)quinazolin-4-amine (8)**



Compound **8** was synthesized from compound **5** as described in the general procedure as a yellow solid in 71% yield, mp. 212-214 °C; IR: 2931, 1513, 1366, 797, 766 cm^{-1} ; ^1H NMR (400 MHz, DMSO) δ 9.96 (s, 1H), 8.75 (d, J = 5.9 Hz, 2H), 8.62 (d, J = 8.4 Hz, 1H), 8.28 (d, J = 5.9 Hz, 2H), 7.92 (d, J = 3.9 Hz, 2H), 7.87 (d, J = 8.4 Hz, 2H), 7.69 (dt, J = 8.4, 4.1 Hz, 1H), 7.31 (d, J = 8.4 Hz, 2H), 2.65 – 2.57 (m, 2H), 1.65 (dd, J = 15.0, 7.5 Hz, 2H), 0.95 (t, J = 7.3 Hz, 3H). ^{13}C NMR (101 MHz, DMSO) δ 158.61, 157.77, 150.65, 150.53, 146.10, 138.35, 137.06, 133.97, 128.85, 128.76, 127.33, 123.52, 122.84, 122.28, 114.87, 37.22, 24.58, 14.13. HRMS (ESI) m/z calcd for $[\text{C}_{22}\text{H}_{20}\text{N}_4 + \text{H}]^+$ 341.1766, found 341.1780.

2-(*p*-Tolyl)-2,3-dihydroquinazolin-4(1*H*)-one (9)



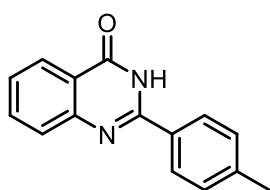
A mixture of anthranilamide (680 mg, 5 mmol), the 4-methylbenzaldehyde (600 mg, 5 mmol), iodine (1.40g, 5.5 mmol), and anhydrous potassium carbonate (690 mg, 5 mmol) in DMF (10 mL) was stirred at reflux for 6 h. Completion of the reaction was monitored by TLC and the mixture poured into crushed ice to obtain a precipitate. The pH of the mixture was adjusted to 7.0 with concentrated HCl to optimize the

precipitation of the desired product. After filtering, the precipitate was thoroughly washed with of 20% sodium thiosulfate solution (50 mL) followed by hot distilled water (50 mL). Purification was performed by recrystallization from ethanol to obtain compound **9** as a white solid in 10% yield. ^1H NMR (400 MHz, DMSO) δ 8.25 (s, 1H), 7.61 (d, $J = 7.6$ Hz, 1H), 7.38 (d, $J = 8.0$ Hz, 2H), 7.27 – 7.16 (m, 3H), 7.07 (s, 1H), 6.74 (d, $J = 8.1$ Hz, 1H), 6.67 (t, $J = 7.4$ Hz, 1H), 5.71 (s, 1H), 2.30 (s, 3H).

General Procedure for the Preparation of the Quinazolinamine Derivatives 13-15.

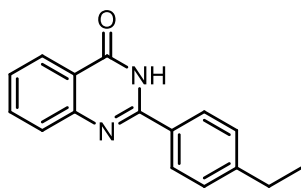
A mixture of anthranilamide (1.36 g, 10 mmol), the corresponding aldehyde (10 mmol), iodine (6.3 g, 25 mmol) in ethanol (20 mL) was stirred at 80°C for 6 h. During the reaction, air was pushed into the mixture. Completion of the reaction was monitored by TLC and the mixture poured into 20% sodium thiosulfate (50 mL) solution followed by hot distilled water (50 mL). Purification was performed by recrystallization from ethanol.

2-(*p*-Tolyl)quinazolin-4(3*H*)-one (**13**)



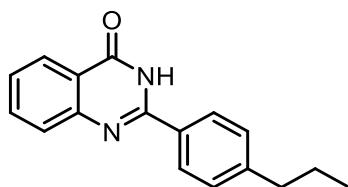
Compound **13** was synthesized as described in the general procedure as a white solid in 83% yield. ^1H NMR (400 MHz, DMSO) δ 12.49 (s, 1H), 8.15 (d, $J = 7.9$ Hz, 1H), 8.11 (d, $J = 8.2$ Hz, 2H), 7.83 (d, $J = 7.0$ Hz, 1H), 7.74 (d, $J = 8.1$ Hz, 1H), 7.52 (t, $J = 7.6$ Hz, 1H), 7.37 (d, $J = 8.4$ Hz, 2H), 2.40 (s, 3H).

2-(4-Ethylphenyl)quinazolin-4(3H)-one (14)



Compound **14** was synthesized as described in the general procedure as a white solid in 84% yield. ^1H NMR (400 MHz, DMSO) δ 12.50 (s, 1H), 8.15 (dd, $J = 14.0$, 4.8 Hz, 3H), 7.87 – 7.81 (m, 1H), 7.74 (d, $J = 8.1$ Hz, 1H), 7.55 – 7.48 (m, 1H), 7.40 (d, $J = 8.2$ Hz, 2H), 2.70 (q, $J = 7.6$ Hz, 2H), 1.23 (t, $J = 7.6$ Hz, 3H).

2-(4-Propylphenyl)quinazolin-4(3H)-one (15)



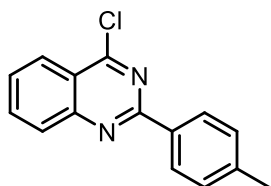
Compound **15** was synthesized as described in the general procedure as a white solid in 98% yield. ^1H NMR (400 MHz, DMSO) δ 12.49 (s, 1H), 8.18 – 8.09 (m, 3H), 7.84 (ddd, $J = 8.6$, 7.1, 1.6 Hz, 1H), 7.73 (dd, $J = 8.2$, 0.6 Hz, 1H), 7.55 – 7.49 (m, 1H), 7.38 (d, $J = 8.4$ Hz, 2H), 2.69 – 2.62 (m, 2H), 1.72 – 1.57 (m, 2H), 0.92 (dd, $J = 8.5$, 6.2 Hz, 3H).

General Procedure for the Preparation of the 4-Chloro-quinazolinamine Derivatives 16-18.

Quinazolinamine derivative **13**, **14** or **15** (2 mmol) was added to DMF (5 mL) containing phosphorus oxychloride (0.47 mL, 5 mmol) and stirred for 10 min at room temperature. The mixture was then refluxed for 2 h and the reaction monitored by TLC. After completion of the reaction, excess phosphorus oxychloride was removed

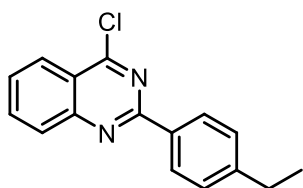
under reduced pressure and the residue poured into ice water (20 mL). Subsequently, the pH of the mixture was adjusted slowly to 7.0 with 25% NaOH solution and was extracted three times with dichloromethane (3×20 mL). With a separatory funnel, the organic phase was collected, washed with 50 mL brine and dried over magnesium sulfate. The solvent was removed under reduced pressure to obtain a white solid which was recrystallized from isopropanol.

4-Chloro-2-(*p*-tolyl)quinazolinamine (16)



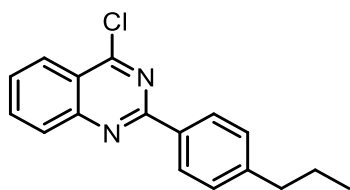
Compound **16** was synthesized from compound **13** as described in the general procedure as a white solid in 85% yield. ¹H NMR (400 MHz, DMO) δ 8.17 (dd, *J* = 7.9, 1.3 Hz, 1H), 8.09 (d, *J* = 8.3 Hz, 2H), 7.87 (ddd, *J* = 8.5, 7.1, 1.5 Hz, 1H), 7.79 (d, *J* = 7.7 Hz, 1H), 7.59 – 7.52 (m, 1H), 7.39 (d, *J* = 8.0 Hz, 2H), 2.41 (s, 3H).

4-Chloro-2-(4-ethylphenyl)quinazolinamine (17)



Compound **17** was synthesized with compound **14** as described in the general procedure as a white solid in 97% yield. ¹H NMR (400 MHz, DMSO) δ 8.18 (dd, *J* = 7.9, 1.4 Hz, 1H), 8.14 – 8.08 (m, 2H), 7.92 – 7.83 (m, 2H), 7.58 (ddd, *J* = 8.1, 6.7, 1.6 Hz, 1H), 7.44 (d, *J* = 8.5 Hz, 2H), 2.72 (q, *J* = 7.6 Hz, 2H), 1.24 (t, *J* = 7.6 Hz, 3H).

4-Chloro-2-(4-propylphenyl)quinazolinamine (18)



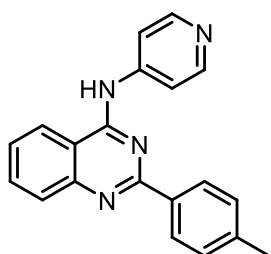
Compound **18** was synthesized with compound **15** as described in the general procedure as a white solid in 91% yield. ^1H NMR (400 MHz, DMSO) δ 8.42 (d, $J = 8.3$ Hz, 2H), 8.31 – 8.27 (m, 1H), 8.16 – 8.09 (m, 2H), 7.84 (ddd, $J = 8.2, 4.8, 3.3$ Hz, 1H), 7.42 (d, $J = 8.4$ Hz, 2H), 2.71 – 2.63 (m, 2H), 1.73 – 1.60 (m, 2H), 0.94 (t, $J = 7.3$ Hz, 3H).

General Procedure for the Preparation of the Substituted 4-

Anilinoquinazolinamines 19-21.

4-Chloroquinazolinamine derivative **16**, **17** or **18** (1 mmol), *p*-aminopyridine (94 mg, 1 mmol) and triethylamine (0.14 mL, 1 mmol) were taken into isopropanol (5 mL). The mixture was refluxed for a period of 3 h until completion of the reaction as indicated by TLC. The solvent was removed under reduced pressure and the remaining solid was purified using flash column chromatography.

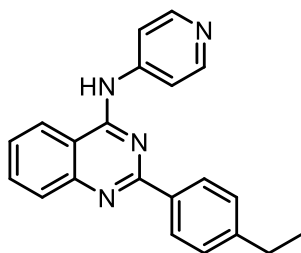
N-(Pyridin-4-yl)-2-(*p*-tolyl)quinazolin-4-amine (19)



Compound **19** was synthesized as described in the general procedure and obtained as a white solid in 53% yield, mp. 278-279 °C; IR: 2997, 1642, 1542, 1370,

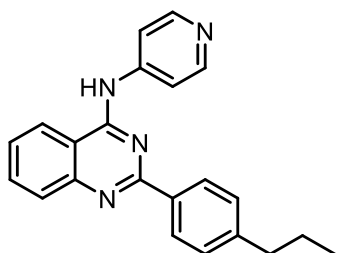
1321, 1160, 732 cm^{-1} ; ^1H NMR (400 MHz, DMSO) δ 9.03 (s, 1H), 8.76 (d, $J = 7.2$ Hz, 2H), 8.47 (d, $J = 8.2$ Hz, 2H), 8.27 (d, $J = 8.0$ Hz, 1H), 8.19 (t, $J = 7.0$ Hz, 1H), 8.01 (d, $J = 8.2$ Hz, 1H), 7.84 (t, $J = 7.1$ Hz, 1H), 7.43 (d, $J = 8.1$ Hz, 2H), 7.13 (d, $J = 7.1$ Hz, 2H), 2.43 (s, 3H). ^{13}C NMR (101 MHz, DMSO) δ 160.97, 159.50, 159.47, 153.81, 142.80, 142.24, 136.53, 133.79, 130.09, 129.71, 129.11, 128.75, 124.59, 116.78, 109.88, 21.56. HRMS (ESI) m/z calcd for $[\text{C}_{20}\text{H}_{16}\text{N}_4 + \text{H}]^+$ 313.1453, found 313.1455.

2-(4-Ethylphenyl)-*N*-(pyridin-4-yl)quinazolin-4-amine (20)



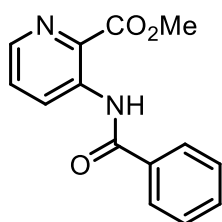
Compound **20** was synthesized as described in the general procedure and obtained as a yellow solid in 65% yield, mp. 234-236 $^{\circ}\text{C}$; IR: 3294, 2967, 1569, 1503, 826, 755 cm^{-1} ; ^1H NMR (400 MHz, DMSO) δ 10.11 (s, 1H), 8.59 (dd, $J = 14.2, 7.3$ Hz, 3H), 8.41 (d, $J = 8.3$ Hz, 2H), 8.10 (dd, $J = 4.9, 1.5$ Hz, 2H), 7.93 (d, $J = 3.8$ Hz, 2H), 7.67 (dt, $J = 8.3, 4.1$ Hz, 1H), 7.41 (d, $J = 8.3$ Hz, 2H), 2.71 (q, $J = 7.6$ Hz, 2H), 1.25 (t, $J = 7.6$ Hz, 4H). ^{13}C NMR (101 MHz, DMSO) δ 159.44, 158.27, 151.17, 150.52, 147.03, 146.98, 136.00, 134.19, 128.68, 128.53, 126.75, 123.55, 115.55, 114.53, 28.55, 15.84. HRMS (ESI) m/z calcd for $[\text{C}_{21}\text{H}_{18}\text{N}_4 + \text{H}]^+$ 327.1610, found 327.1619.

2-(4-Propylphenyl)-N-(pyridin-4-yl)quinazolin-4-amine (21)



Compound **21** was synthesized as described in the general procedure and obtained as a yellow solid in 63% yield, mp. 218-220 °C; IR: 2962, 1569, 1504, 822, 754 cm^{-1} ; ^1H NMR (400 MHz, DMSO) δ 10.12 (s, 1H), 8.60 (dd, $J = 14.2, 7.3$ Hz, 3H), 8.41 (d, $J = 8.1$ Hz, 2H), 8.10 (d, $J = 6.3$ Hz, 2H), 7.93 (d, $J = 4.3$ Hz, 2H), 7.68 (dt, $J = 8.2, 4.2$ Hz, 1H), 7.39 (d, $J = 8.0$ Hz, 2H), 2.70 – 2.61 (m, 2H), 1.72 – 1.59 (m, 2H), 0.94 (t, $J = 7.3$ Hz, 3H). ^{13}C NMR (101 MHz, DMSO) δ 159.45, 158.28, 151.18, 150.53, 146.98, 145.42, 136.03, 134.20, 129.12, 128.68, 128.45, 126.75, 123.56, 115.55, 114.53, 37.58, 24.35, 14.11. HRMS (ESI) m/z calcd for $[\text{C}_{22}\text{H}_{20}\text{N}_4 + \text{H}]^+$ 341.1766, found 341.1773.

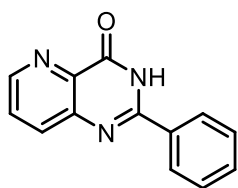
Methyl 3-benzamidopicolinate (22)



To a mixture of methyl 3-aminopicolinate (2.09 g, 5 mmol), and triethylamine (0.7 mL, 5 mmol) in chloroform (10 mL) was added acyl chloride (428 mg, 5.5 mmol) dropwise at 5 °C. After stirring at room temperature for 2.5 h, the reaction mixture was diluted with chloroform and washed with saturated sodium bicarbonate

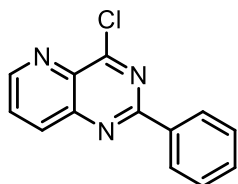
(30 mL) and brine (30 mL). The organic layer was dried over sodium sulfate and concentrated *in vacuo*. The resulting solid was recrystallized from ethyl acetate to obtain compound **22** as a white solid in 86% yield. ^1H NMR (400 MHz, DMSO) δ 11.32 (s, 1H), 8.74 (dd, $J = 8.5, 1.5$ Hz, 1H), 8.46 (dd, $J = 4.5, 1.5$ Hz, 1H), 8.01 – 7.95 (m, 2H), 7.75 – 7.57 (m, 4H), 3.89 (s, 3H).

2-Phenylpyrido[3,2-d]pyrimidin-4(3H)-one (**23**)



To a solution of **22** (256 mg, 1 mmol) in methanol (20 mL) was added 28% aqueous ammonia (20 mL). After stirring at room temperature for 2 h, the reaction mixture was filtered to obtain a mixture of uncyclized benzamide. Isopropanol (5 mL) and 2 N sodium hydroxide (2 mL) were added and the crude mixture was heated at reflux for 3 h. The mixture was cooled, neutralized with 2 N HCl, and the solution was evaporated to obtain a precipitate which was collected to obtain **23** as a white solid in 60% yield. ^1H NMR (400 MHz, DMSO) δ 12.83 (s, 1H), 8.79 (dd, $J = 4.3, 1.5$ Hz, 1H), 8.23 – 8.13 (m, 3H), 7.84 (dd, $J = 8.3, 4.3$ Hz, 1H), 7.66 – 7.54 (m, 3H).

4-Chloro-2-phenylpyrido[3,2-d]pyrimidine (**24**)



Compound **23** (2 mmol) was added to DMF (5 mL) containing phosphorus oxychloride (0.47 mL, 5 mmol) and stirred for 10 min at room temperature. The

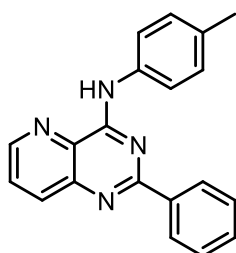
mixture was then refluxed for 2 h and the reaction was monitored by TLC. After completion of the reaction, excess phosphorus oxychloride was removed under reduced pressure and the residue poured into ice water (20 mL). Subsequently, the pH of the mixture was adjusted slowly to 7.0 with 25% NaOH solution and was extracted three times with dichloromethane (3×20 mL). The organic phase was collected, washed with brine (50 mL) and dried over magnesium sulfate. The solvent was removed under reduced pressure to obtain a white solid which was recrystallized from isopropanol in 94% yield. ¹H NMR (400 MHz, DMSO) δ 9.17 (dd, *J* = 4.1, 1.5 Hz, 1H), 8.60 – 8.47 (m, 3H), 8.13 (dd, *J* = 8.6, 4.1 Hz, 1H), 7.67 – 7.57 (m, 3H).

General Procedure for the Preparation of the Substituted 4-

Anilinoquinazolinamines 25-36.

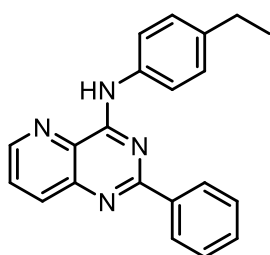
4-Chloroquinazolinamine derivative **5** (48 mg, 0.2 mmol) or **24** (48 mg, 0.2 mmol) was added to a solution of a *para* substituted aniline derivative (0.2 mmol) and triethylamine (0.2 mmol) in isopropanol (3 mL) to synthesize **25-27**, **29-32**, **34-36**. 4- In the case of compounds **28** and **33**, 4-dimethylaminopyridine was used in place of triethylamine. The mixture was refluxed for a period of 3 h until completion of the reaction as indicated by TLC. The solvent was removed under reduced pressure and the remaining solid was purified with flash column.

2-Phenyl-*N*-(*p*-tolyl)pyrido[3,2-*d*]pyrimidin-4-amine (25)



Compound **25** was synthesized as described in the general procedure as a yellow solid in 73% yield. mp. 161-162 °C; IR: 3333, 1597, 1563, 1409, 802 cm⁻¹; ¹H NMR (400 MHz, DMSO) δ 10.11 (s, 1H), 8.59 (dd, $J = 14.2, 7.3$ Hz, 3H), 8.41 (d, $J = 8.3$ Hz, 2H), 8.10 (dd, $J = 4.9, 1.5$ Hz, 2H), 7.93 (d, $J = 3.8$ Hz, 2H), 7.67 (dt, $J = 8.3, 4.1$ Hz, 1H), 7.41 (d, $J = 8.3$ Hz, 2H), 2.71 (q, $J = 7.6$ Hz, 2H), 1.25 (t, $J = 7.6$ Hz, 4H). ¹³C NMR (101 MHz, DMSO) δ 160.29, 157.77, 149.06, 145.60, 138.40, 136.72, 136.41, 133.21, 131.19, 131.12, 129.49, 129.13, 129.00, 128.60, 122.02, 21.03. HRMS (ESI) m/z calcd for [C₂₀H₁₆N₄ + H]⁺ 313.1453, found 313.1465.

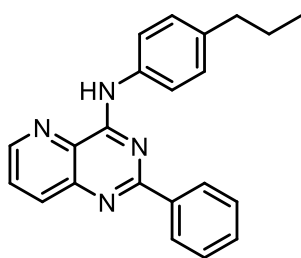
N-(4-Ethylphenyl)-2-phenylpyrido[3,2-*d*]pyrimidin-4-amine (26)



Compound **26** was synthesized as described in the general procedure as a yellow solid (65%), mp. 137-138 °C; IR: 3330, 2962, 1595, 1564, 823, 707 cm⁻¹; ¹H NMR (400 MHz, DMSO) δ 10.28 (s, 1H), 8.91 (dd, $J = 4.2, 1.5$ Hz, 1H), 8.55 – 8.45 (m, 2H), 8.28 (dd, $J = 8.5, 1.5$ Hz, 1H), 8.07 (d, $J = 8.5$ Hz, 2H), 7.93 (dd, $J = 8.5, 4.2$ Hz, 1H), 7.61 – 7.51 (m, 3H), 7.32 (d, $J = 8.5$ Hz, 2H), 2.65 (q, $J = 7.5$ Hz, 2H), 1.23 (t, J

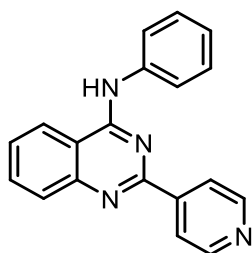
= 7.6 Hz, 3H). ^{13}C NMR (101 MHz, DMSO) δ 160.35, 157.72, 149.11, 145.53, 139.69, 138.36, 136.87, 136.36, 131.15, 131.11, 129.14, 129.01, 128.60, 128.33, 121.92, 28.14, 16.16. HRMS (ESI) m/z calcd for $[\text{C}_{21}\text{H}_{18}\text{N}_4 + \text{H}]^+$ 327.1610, found 327.1620.

2-Phenyl-*N*-(4-propylphenyl)pyrido[3,2-*d*]pyrimidin-4-amine (27)



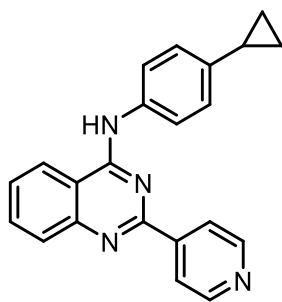
Compound **27** was synthesized as described in the general procedure as a yellow solid in 68% yield, mp. 117-119 °C; IR:3342, 2929, 1594, 1565, 803, 707 cm^{-1} ; ^1H NMR (400 MHz, DMSO) δ 10.28 (s, 1H), 8.91 (dd, $J = 4.2, 1.5$ Hz, 1H), 8.49 (dd, $J = 6.6, 3.2$ Hz, 2H), 8.29 (dd, $J = 8.5, 1.5$ Hz, 1H), 8.07 (d, $J = 8.5$ Hz, 2H), 7.93 (dd, $J = 8.5, 4.2$ Hz, 1H), 7.56 (dd, $J = 5.2, 1.8$ Hz, 3H), 7.30 (d, $J = 8.5$ Hz, 2H), 2.64 – 2.56 (m, 2H), 1.70 – 1.58 (m, 2H), 0.94 (t, $J = 7.3$ Hz, 3H). ^{13}C NMR (101 MHz, DMSO) δ 160.33, 157.69, 149.06, 145.53, 138.37, 138.00, 136.93, 136.36, 131.12, 129.10, 128.99, 128.89, 128.61, 121.80, 37.22, 24.60, 14.13. HRMS (ESI) m/z calcd for $[\text{C}_{22}\text{H}_{20}\text{N}_4 + \text{H}]^+$ 341.1766, found 341.1775.

N-Phenyl-2-(pyridin-4-yl)quinazolin-4-amine (28)



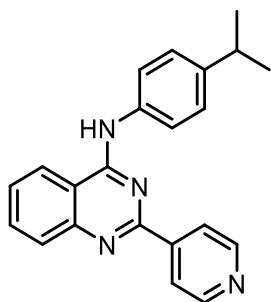
Compound **28** was synthesized as described in the general procedure as a white solid in 85% yield, mp. 282-284 °C; IR: 3261, 3043, 1554, 1523, 1411, 745 cm⁻¹; ¹H NMR (400 MHz, DMSO) δ 10.02 (s, 1H), 8.75 (d, *J* = 6.0 Hz, 2H), 8.63 (d, *J* = 8.4 Hz, 1H), 8.28 (d, *J* = 6.0 Hz, 2H), 7.95 (dd, *J* = 9.9, 5.9 Hz, 4H), 7.74 – 7.66 (m, 1H), 7.50 (t, *J* = 7.9 Hz, 2H), 7.21 (t, *J* = 7.4 Hz, 1H). ¹³C NMR (101 MHz, DMSO) δ 158.67, 157.73, 150.72, 150.62, 145.99, 139.44, 134.01, 129.05, 128.82, 127.35, 124.48, 123.62, 122.98, 122.23, 114.91. HRMS (ESI) *m/z* calcd for [C₁₉H₁₄N₄ + H]⁺ 299.1297, found 299.1303.

***N*-(4-Cyclopropylphenyl)-2-(pyridin-4-yl)quinazolin-4-amine (29)**



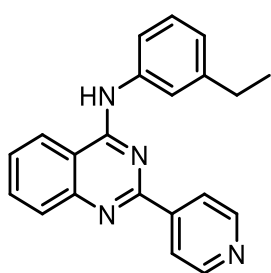
Compound **29** was synthesized as described in the general procedure, yellow solid in 50% yield, mp. 231-232 °C; IR: 3003, 1515, 1409, 1363, 765 cm⁻¹; ¹H NMR (400 MHz, DMSO) δ 9.93 (s, 1H), 8.75 (d, *J* = 5.8 Hz, 2H), 8.60 (d, *J* = 8.4 Hz, 1H), 8.34 – 8.21 (m, 2H), 7.91 (d, *J* = 3.7 Hz, 2H), 7.83 (d, *J* = 8.5 Hz, 2H), 7.74 – 7.61 (m, 1H), 7.20 (d, *J* = 8.5 Hz, 2H), 2.03 – 1.92 (m, 1H), 1.03 – 0.92 (m, 2H), 0.79 – 0.67 (m, 2H). ¹³C NMR (101 MHz, DMSO) δ 158.56, 157.79, 150.72, 150.58, 146.05, 139.78, 136.80, 133.90, 128.79, 127.24, 125.89, 123.58, 122.89, 122.23, 114.92, 15.26, 9.74. HRMS (ESI) *m/z* calcd for [C₂₂H₁₈N₄ + H]⁺ 339.1610, found 339.1617.

***N*-(4-Isopropylphenyl)-2-(pyridin-4-yl)quinazolin-4-amine (30)**



Compound **30** was synthesized as described in the general procedure as a yellow solid in 76% yield, mp. 225-226°C; IR: 2958, 1563, 1513, 1415, 764 cm⁻¹; ¹H NMR (400 MHz, DMSO) δ 9.95 (s, 1H), 8.84 – 8.70 (m, 2H), 8.63 (d, *J* = 8.3 Hz, 1H), 8.37 – 8.20 (m, 2H), 7.91 (t, *J* = 5.7 Hz, 4H), 7.69 (dt, *J* = 8.3, 4.2 Hz, 1H), 7.36 (d, *J* = 8.5 Hz, 2H), 2.95 (dt, *J* = 13.5, 6.7 Hz, 1H), 1.27 (s, 3H), 1.26 (s, 3H). ¹³C NMR (101 MHz, DMSO) δ 158.55, 157.81, 150.73, 150.57, 146.05, 144.48, 137.24, 133.91, 128.81, 127.25, 126.77, 123.60, 122.68, 122.24, 114.92, 33.46, 24.49. HRMS (ESI) *m/z* calcd for [C₂₂H₂₀N₄ + H]⁺ 341.1766, found 341.1780.

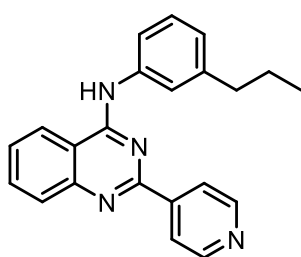
***N*-(3-Ethylphenyl)-2-(pyridin-4-yl)quinazolin-4-amine (31)**



Compound **31** was synthesized as described in the general procedure as a yellow solid in 78% yield, mp. 236-238°C; IR: 2963, 2440, 1568, 1378, 767 cm⁻¹; ¹H NMR (400 MHz, DMSO) δ 10.20 (s, 1H), 8.94 (d, *J* = 4.8 Hz, 2H), 8.68 (d, *J* = 8.1 Hz, 1H), 8.58 (s, 2H), 7.99 (s, 2H), 7.81 – 7.69 (m, 3H), 7.40 (t, *J* = 7.9 Hz, 1H), 7.09 (d, *J* =

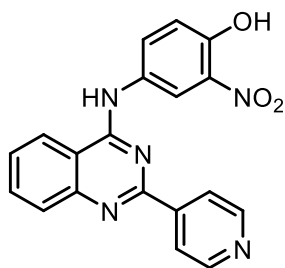
8.0 Hz, 1H), 2.71 (q, $J = 7.4$ Hz, 2H), 1.28 (t, $J = 7.6$ Hz, 3H). ^{13}C NMR (101 MHz, DMSO) δ 158.95, 155.71, 145.11, 144.67, 138.93, 134.57, 128.99, 128.41, 124.62, 124.36, 124.00, 122.84, 120.86, 114.99, 40.63, 40.42, 40.21, 40.00, 39.80, 39.59, 39.38, 28.77, 16.10. HRMS (ESI) m/z calcd for $[\text{C}_{21}\text{H}_{18}\text{N}_4 + \text{H}]^+$ 327.1610, found 327.1620.

***N*-(3-Propylphenyl)-2-(pyridin-4-yl)quinazolin-4-amine (32)**



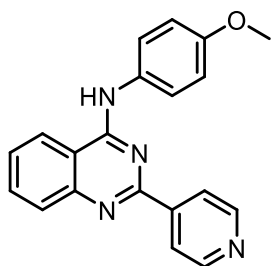
Compound **32** was synthesized as described in the general procedure as a yellow solid in 72% yield, mp. 205-207°C; IR: 2955, 1524, 1365, 787, 757 cm^{-1} ; ^1H NMR (400 MHz, DMSO) δ 9.97 (s, 1H), 8.74 (d, $J = 6.0$ Hz, 2H), 8.63 (d, $J = 8.3$ Hz, 1H), 8.29 (d, $J = 6.0$ Hz, 2H), 7.92 (d, $J = 3.6$ Hz, 2H), 7.84 (s, 1H), 7.74 (d, $J = 8.9$ Hz, 1H), 7.72 – 7.65 (m, 1H), 7.39 (t, $J = 7.8$ Hz, 1H), 7.04 (d, $J = 7.5$ Hz, 1H), 2.68 – 2.61 (m, 2H), 1.70 (dt, $J = 14.5, 7.2$ Hz, 2H), 0.98 (t, $J = 7.3$ Hz, 3H). ^{13}C NMR (101 MHz, DMSO) δ 158.65, 157.69, 150.65, 146.05, 142.90, 139.36, 133.97, 128.84, 127.32, 124.65, 123.62, 123.00, 122.23, 120.36, 114.94, 37.94, 24.65, 14.19. HRMS (ESI) m/z calcd for $[\text{C}_{22}\text{H}_{20}\text{N}_4 + \text{H}]^+$ 341.1766, found 341.1779.

2-Nitro-4-((2-(pyridin-4-yl)quinazolin-4-yl)amino)phenol (33)



Compound **33** was synthesized as described in the general procedure as a yellow solid in 83% yield, mp. 267-268°C; IR: 3427, 3194, 1527, 1487, 1224, 769 cm^{-1} ; ^1H NMR (400 MHz, DMSO) δ 8.83 – 8.69 (m, 2H), 8.43 (d, $J = 8.3$ Hz, 1H), 8.14 (s, 2H), 8.09 – 7.99 (m, 2H), 7.87 (s, 1H), 7.40 (d, $J = 5.8$ Hz, 2H), 7.06 (d, $J = 8.9$ Hz, 1H), 5.91 (s, 2H). ^{13}C NMR (101 MHz, DMSO) δ 167.04, 157.17, 152.03, 150.95, 148.30, 144.29, 142.53, 135.93, 134.08, 129.37, 128.50, 126.09, 124.13, 121.88, 120.28, 115.02, 108.96. HRMS (ESI) m/z calcd for $[\text{C}_{19}\text{H}_{13}\text{N}_5\text{O}_3 + \text{H}]^+$ 360.1097, found 360.1103.

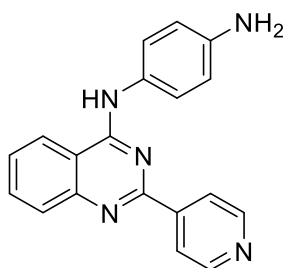
N-(4-Methoxyphenyl)-2-(pyridin-4-yl)quinazolin-4-amine (34)



Compound **34** was synthesized as described in the general procedure as a yellow solid in 85% yield. mp. 219-221 °C; IR: 3291, 1510, 1242, 823, 767 cm^{-1} ; ^1H NMR (400 MHz, DMSO) δ 9.94 (s, 1H), 8.74 (d, $J = 5.4$ Hz, 2H), 8.58 (d, $J = 8.3$ Hz, 1H), 8.26 (d, $J = 5.4$ Hz, 2H), 7.90 (d, $J = 3.8$ Hz, 2H), 7.82 (d, $J = 8.8$ Hz, 2H), 7.67 (dt, $J = 8.0, 4.1$ Hz, 1H), 7.07 (d, $J = 8.8$ Hz, 2H), 3.79 (d, $J = 22.1$ Hz, 3H). ^{13}C NMR (101

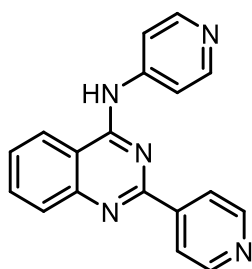
MHz, DMSO) δ 158.64, 157.78, 156.38, 150.64, 150.51, 146.08, 133.75, 132.30, 128.74, 127.10, 124.69, 123.51, 122.21, 114.85, 114.18, 55.72. HRMS (ESI) m/z calcd for $[C_{20}H_{16}N_4O + H]^+$ 329.1402, found 329.1411.

***N*'-(2-(Pyridin-4-yl)quinazolin-4-yl)benzene-1,4-diamine (35)**



Compound **35** was synthesized as described in the general procedure as a pale white solid in 80% yield. mp. 301-303 °C; IR: 3445, 3363, 1556, 1512, 1411, 761 cm^{-1} ; 1H NMR (400 MHz, DMSO) δ 9.78 (s, 1H), 8.73 (d, $J = 5.0$ Hz, 2H), 8.54 (d, $J = 8.3$ Hz, 1H), 8.24 (d, $J = 5.6$ Hz, 2H), 7.86 (d, $J = 3.8$ Hz, 2H), 7.62 (dt, $J = 8.1, 4.0$ Hz, 1H), 7.49 (d, $J = 8.6$ Hz, 2H), 6.69 (d, $J = 8.6$ Hz, 2H), 5.34 (s, 2H). ^{13}C NMR (101 MHz, DMSO) δ 158.72, 157.86, 150.57, 150.47, 146.28, 145.79, 133.59, 128.64, 128.13, 126.94, 124.98, 123.45, 122.20, 114.91, 114.34, 40.64, 40.43, 40.22, 40.01, 39.80, 39.59, 39.38. HRMS (ESI) m/z calcd for $[C_{19}H_{15}N_5 + H]^+$ 314.1406, found 314.1417.

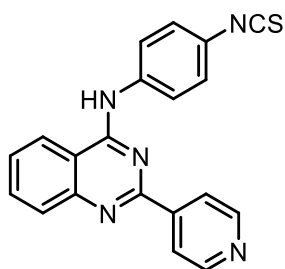
***N*,2-Di(pyridin-4-yl)quinazolin-4-amine (36)**



Compound **36** was synthesized as described in the general procedure as a yellow

solid in 80% yield. mp. 277-279 °C; IR: 2941, 1645, 1544, 1384, 1171, 776, 745 cm⁻¹; ¹H NMR (400 MHz, DMSO) δ 9.07 (s, 1H), 8.87 (d, *J* = 5.9 Hz, 2H), 8.77 (d, *J* = 7.4 Hz, 2H), 8.44 (d, *J* = 6.0 Hz, 2H), 8.36 (d, *J* = 8.4 Hz, 1H), 8.26 (t, *J* = 7.7 Hz, 1H), 8.10 (d, *J* = 8.3 Hz, 1H), 7.95 (t, *J* = 7.6 Hz, 1H), 7.15 (d, *J* = 7.5 Hz, 2H). ¹³C NMR (101 MHz, DMSO) δ 161.10, 159.91, 157.58, 153.59, 151.26, 143.73, 142.83, 136.86, 130.84, 129.49, 124.93, 122.36, 117.73, 109.92, 40.63, 40.42, 40.22, 40.01, 39.80, 39.59, 39.38. HRMS (ESI) *m/z* calcd for [C₁₈H₁₃N₅ + H]⁺ 300.1249, found 300.1285.

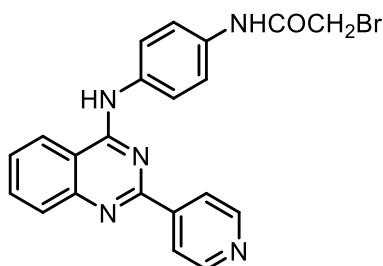
***N*-(4-Isothiocyanatophenyl)-2-(pyridin-4-yl)quinazolin-4-amine (37)**



A solution of amine **35** (31 mg, 0.1 mmol) in dichloromethane (10 mL) was treated dropwise with a solution of di-2-pyridyl thionocarbonate (23 mg, 0.11 mmol) in dichloromethane (1 mL) over a period of 1 min with vigorous stirring at room temperature. The precipitates were filtered and recrystallized from ethyl acetate to obtain a white solid in 73% yield, mp. 307-309 °C; IR: 3279, 3039, 2053, 1491, 1410, 749 cm⁻¹; ¹H NMR (400 MHz, DMSO) δ 10.15 (s, 1H), 8.77 (d, *J* = 5.0 Hz, 2H), 8.61 (d, *J* = 8.4 Hz, 1H), 8.29 (d, *J* = 4.9 Hz, 2H), 8.15 – 8.02 (m, 2H), 7.95 (d, *J* = 3.4 Hz, 2H), 7.79 – 7.67 (m, 1H), 7.57 (d, *J* = 8.6 Hz, 2H). ¹³C NMR (101 MHz, DMSO) δ 158.39, 157.61, 150.81, 150.71, 145.78, 139.21, 134.24, 133.50, 128.91, 127.56, 126.84, 125.29, 123.65, 123.56, 122.26, 114.94. HRMS (ESI) *m/z* calcd for

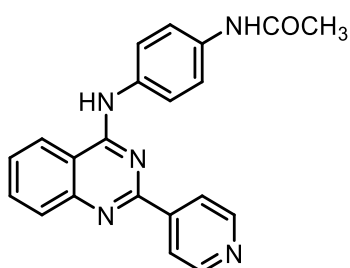
$[\text{C}_{20}\text{H}_{13}\text{N}_5\text{S} + \text{H}]^+$ 356.0970, found 356.0985.

2-Bromo-*N*-(4-((2-(pyridin-4-yl)quinazolin-4-yl)amino)phenyl)acetamide (38)



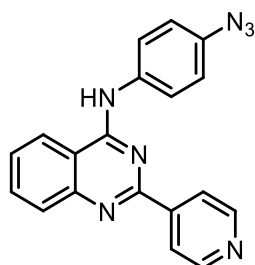
A solution of amine **35** (62 mg, 0.2 mmol) in dichloromethane (2 mL) was treated dropwise with a solution of bromoacetyl bromide (25 mg, 0.2 mmol) in dichloromethane (1 mL) over a period of 1 min with vigorous stirring at 0 °C. The reaction was stirred at room temperature for 24 h. Then water (10 mL) was added into the mixture, and the precipitates were filtered and recrystallized from ethyl acetate to obtain a yellow solid in 72% yield, mp. 336-338 °C; IR: 3033, 1566, 1510, 763 cm^{-1} ; ^1H NMR (400 MHz, DMSO) δ 10.49 (s, 1H), 10.15 (s, 1H), 8.87 (d, $J = 5.2$ Hz, 2H), 8.63 (d, $J = 8.2$ Hz, 1H), 8.46 (d, $J = 4.8$ Hz, 2H), 7.95 (d, $J = 3.8$ Hz, 2H), 7.88 (d, $J = 8.8$ Hz, 2H), 7.72 (d, $J = 8.7$ Hz, 3H), 4.08 (s, 2H). ^{13}C NMR (101 MHz, TFA) δ 169.70, 159.95, 151.90, 147.91, 142.88, 138.31, 138.12, 135.44, 132.91, 131.48, 126.93, 125.42, 123.09, 122.84, 120.14, 112.46, 25.86. HRMS (ESI) m/z calcd for $[\text{C}_{21}\text{H}_{16}\text{BrN}_5\text{O} + \text{H}]^+$ 434.0616, found 434.0627.

N-(4-((2-(pyridin-4-yl)quinazolin-4-yl)amino)phenyl)acetamide (39)



To a solution of amine **35** (62 mg, 0.2 mmol) and triethylamine (0.28 mL, 2 mmol) in dichloromethane (5 mL), acetic anhydride (0.02 mL, 0.2 mmol) was added. The reaction mixture was stirred at room temperature for 1 h. The precipitates were filtered and recrystallized from ethyl acetate to obtain a white solid in 85% yield, mp. 367-369 °C; IR: 3341, 3038, 1670, 1560, 1510, 760 cm⁻¹; ¹H NMR (400 MHz, DMSO) δ 9.98 (d, *J* = 8.7 Hz, 2H), 8.75 (d, *J* = 5.1 Hz, 2H), 8.60 (d, *J* = 8.2 Hz, 1H), 8.27 (d, *J* = 4.9 Hz, 2H), 7.91 (d, *J* = 3.8 Hz, 2H), 7.84 (d, *J* = 8.6 Hz, 2H), 7.69 (d, *J* = 8.8 Hz, 3H), 2.05 (d, *J* = 27.1 Hz, 3H). ¹³C NMR (101 MHz, DMSO) δ 168.74, 158.61, 157.78, 150.68, 150.54, 146.06, 136.01, 134.43, 133.95, 128.76, 127.30, 123.56, 123.50, 122.24, 119.60, 114.84, 24.40. HRMS (ESI) *m/z* calcd for [C₂₁H₁₇N₅O + H]⁺ 356.1511, found 356.1521.

***N*-(4-Azidophenyl)-2-(pyridin-4-yl)quinazolin-4-amine (40)**



A solution of amine **35** (62 mg, 0.2 mmol) in water (2 mL) was treated dropwise with conc. hydrochloric acid (0.2 mL) and stirred at 0 °C, followed by dropwise addition of sodium nitrite (14 mg, 0.2 mmol) dissolved in water (1 mL) at 0 °C. A solution of sodium azide (13 mg, 0.2 mmol) in water (1 mL) was then added to the reaction mixture at 0 °C and the reaction mixture was stirred for 2 h at room temperature. After the reaction was stirred at room temperature for 2 h, 5 mL of water

was added, and the precipitates were filtered and recrystallized from ethyl acetate to obtain a yellow solid in 59% yield, mp. 304-305 °C; IR: 3324, 3033, 2114, 1505, 1410, 761 cm^{-1} ; ^1H NMR (400 MHz, DMSO) δ 10.06 (s, 1H), 8.77 (s, 2H), 8.61 (d, J = 8.4 Hz, 1H), 8.30 (s, 2H), 8.09 – 7.97 (m, 2H), 7.94 (d, J = 3.5 Hz, 2H), 7.76 – 7.65 (m, 1H), 7.27 (d, J = 8.6 Hz, 2H). ^{13}C NMR (101 MHz, DMSO) δ 158.55, 157.69, 150.67, 150.60, 145.99, 136.69, 135.02, 134.06, 128.84, 127.41, 124.41, 123.59, 119.76, 114.89. HRMS (ESI) m/z calcd for $[\text{C}_{19}\text{H}_{13}\text{N}_7 + \text{H}]^+$ 340.1311, found 340.1319.

3.2. Cell Lines and Cell Culture

The human lung cancer cell line H460, and its MX-selected derivative BCRP-overexpressing cell line, H460/MX20, were used in this study. The KB-C2 cell line was selected by colchicine (Alfa Aesar, Haverhill, MA) (2 $\mu\text{g}/\text{mL}$) with human cervical carcinoma cell line KB-3-1. All the cell lines were maintained in Dulbecco's Modified Eagle Medium (Corning Inc.) containing 10% fetal bovine serum (Gibco Inc.) and 1% penicillin/streptomycin (Gibco Inc.) at 37 °C with 5% CO_2 .

3.3. MTT Assay

Cytotoxicity tests and reversal experiments were performed using the MTT colorimetric assay.⁶⁶ Cells were seeded evenly into 96-well plates. To determine the cytotoxicity of the quinazolinamine derivatives, incremental concentrations of each drug were added into the well after 24 h of incubation. To determine the MDR reversal efficacy of the quinazolinamine derivatives, an anticancer drug (mitoxantrone, colchicine, paclitaxel or cisplatin) was added into the designated wells

after 2 h pre-incubation with a quinazolinamine derivative or a positive control inhibitor at non-toxic concentrations. After 72 h of drug incubation, the MTT reagent (4 mg/mL) was added into the wells, and then the plates were incubated for an additional 4 h. Subsequently, the supernatant was discarded and 100 μ L of DMSO was added to dissolve the formazan crystals. Cell viability was determined by measuring the absorbance at a wavelength of 570 nm.

3.4. Metabolic Stability Study

Human liver microsome (20 mg/mL) 6.25 μ L, nicotinamide adenine dinucleotide phosphate (NADPH) (0.75 μ mol), $MgCl_2$ (0.75 μ mol), and the test compound (0.05 μ mol) were added into potassium phosphate buffer (pH 7.4) with 250 μ L of final volume.⁶⁷ The incubation was carried out aerobically at 37 °C. The mixture was pre-incubated without NADPH for 10 min at 37 °C and NADPH was added to start the reaction. At 1 h after the start of reaction, an aliquot (50 μ L) of the incubation mixture was taken from each incubation and mixed with 150 μ L of ice-cold acetonitrile to terminate the reaction. Subsequently, the sample was centrifuged (12,000 rpm) at room temperature. The resulting supernatant was filtered and analyzed using HPLC (LC, Agilent 1200; column, HC-C18(2); column temperature, 25 °C; mobile phase, solvent A, methanol, solvent B, water; gradient elution, 30-99% solvent A; flow rate, 1 mL/min; UV signals were recorded at 254 nm).

3.5. Drug Accumulation Assay

To determine the accumulation of drugs on H460, H460/MX20, KB-3-1, and KB-C2 cells, the cells (2.5×10^6 cells/well) were seeded in the 24-well plates and incubated

at 37 °C with 5% CO₂.⁶⁸ After 12 h of incubation, a test compound (5 μM) was added and the plates were incubated at 37°C for 2 h. Cells were then incubated with 0.01 μM [³H]-MX or [³H]-paclitaxel-containing medium for an additional 2 h at 37°C, with or without a test compound. The cells were washed twice with ice-cold PBS, trypsinized and lysed at the end of incubation. The radioactivity was measured using the Packard TRICARB1 1900A liquid scintillation analyzer.

3.6. Western Blot Analysis

Cells in T25 flask were washed with ice-cold PBS. Lysis buffer (100 μL) was added into T25 flask. Using a cell scraper, scrape adherent cells were scraped off the flask and the cell suspension was transferred into a microcentrifuge tube (1.5 mL). Cells were agitated for 20 min at 4°C and cell lysate was centrifuged mixture at 4°C for 20 min at 12,000 rpm. The supernatant (lysate) was used for the gel electrophoresis. Equal amounts of total cell lysates (20 μg protein) were resolved by sodium dodecyl sulfate polyacrylamide gel electrophoresis (SDS-PAGE) and electrophoretically transferred onto polyvinylidene fluoride (PVDF) membranes.⁶⁹ After incubation in a blocking solution (5% milk) for 2 h at room temperature, the membranes were incubated overnight with primary monoclonal antibodies against GAPDH (GA1R) (Invitrogen, Carlsbad, CA) at 1:1000 dilution of BCRP protein (BXP 21) (Sigma-Aldrich, Inc., St. Louis, MO) (1:1000) or P-gp (F4) (Sigma-Aldrich, Inc., St. Louis, MO) at 4 °C, and were further incubated with horseradish peroxidase (HRP)-conjugated secondary antibody (Thermo Fisher Scientific Inc.) at 1:1000 dilution for 2 h at room temperature. The protein antibody complex was detected

using an enhanced chemiluminescence detection system. The Grayscale ratio was analyzed by ImageJ and normalized by the grayscale of the ABC protein divided by that of GAPDH.

3.7. Immunofluorescence Assay

For immunofluorescence analysis, parental and drug-resistant cells were seeded in 24-well plates at 10,000-20,000 cells/well and incubated for 24 h.⁷⁰ The cells were incubated with or without cyclopropyl quinazolinamine **29** or azide quinazolinamine **40** for 24 h, 48 h, and 72 h. Thereafter, cells were washed with PBS and fixed with 4% paraformaldehyde for 10 min at room temperature and then rinsed with PBS twice, followed by permeabilization with 1% Triton X-100 for 10 min at 4 °C. The cells were again washed twice with PBS, and then blocked with 6% BSA for 1 h at 37 °C. Fixed cells were incubated with monoclonal antibody against the BCRP protein (BXP 21) (Sigma-Aldrich, Inc., St. Louis, MO) (1:1000) or P-gp (F4) (Sigma-Aldrich, Inc., St. Louis, MO) overnight at 4 °C, followed by two washes with PBS. The cells were then further incubated with Alexa flour 488 goat anti-mouse IgG (1:1000) (Abcam plc.) for 2 h at 37 °C. After the cells were washed twice with PBS, 4',6-diamidino-2-phenylindole (DAPI) (2 µg/mL) was used for nuclear counterstaining. The immunofluorescence images were generated using a Nikon TE-2000S fluorescence microscope (Nikon Instruments Inc, Melville, NY).

3.8. ATPase Assay

The Vi-sensitive ATPase activities were determined as previously described, using the PREDEASY ATPase assay kit.⁷¹ The results were presented as vanadate-

sensitive ATPase activities by determining the difference in inorganic phosphate liberation measured in the presence and absence of sodium orthovanadate.

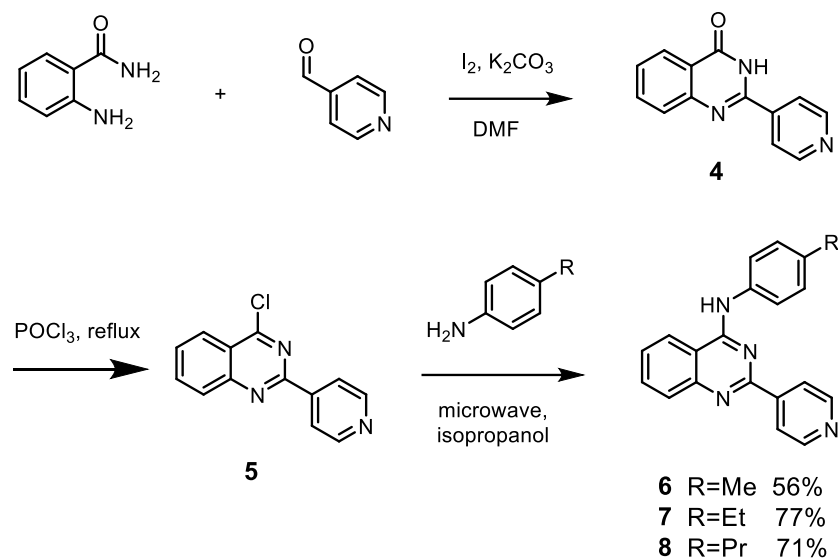
3.9. Molecular Modeling

Molecular modeling was performed in Maestro v11.1 (Schrodinger, LLC, New York, NY, 2020) software as described previously.⁷² The protein preparation of the wild-type human BCRP (PDB ID: 6FFC)⁷³ or human P-gp (PDB ID: 6FN1)⁷⁴ was performed and the grid was generated by selecting residues in the binding pocket of the proteins. The ligands were essentially prepared through LigPrep module. The best-scored ligands were obtained through Glide XP docking and used for graphical analysis.

Chapter 4. Results and Discussion

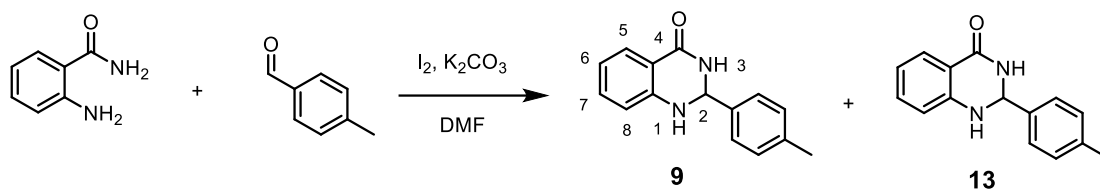
4.1. Chemistry

The quinazolinamines **6-8** were synthesized via the following reactions (**Scheme 1**): cyclic condensation reaction of amide and aldehyde; chlorination of quinazolinone; and then nucleophilic aromatic substitution. As shown in **Scheme 1**, 2-substituted quinazolinone **4** was synthesized⁵⁸ by a cyclic condensation reaction of anthranilamide with 4-pyridinecarboxaldehyde. Subsequently, the quinazolinone derivative was refluxed with phosphorus oxychloride to obtain 4-chloroquinazolinamine derivative **5**. Nucleophilic aromatic substitution of the 4-chloroquinazolinamine derivative with *para*-substituted aniline derivatives was carried out under microwave irradiation to obtain methyl, ethyl, and propyl quinazolinamines **6-8** in 56-77% yields, respectively. We found that the quinazolinamines **6-8** can also be synthesized by the catalysis of triethylamine with traditional heating. In addition, the results showed that microwave irradiation did not shorten the reaction time significantly. Therefore, the other target compounds were synthesized with traditional heating instead of the microwave method.



Scheme 1. The synthesis of **6-8**.

Attempted synthesis of **13** using the same method as the synthesis of quinazolinone derivative **4**, led to compound **13** (29%) and a byproduct dihydroquinazolinone derivative **9** (10%) (**Scheme 2**). ^1H NMR spectrum of compound **9** exhibited a singlet at 5.7 ppm for the proton at position 2 of the dihydroquinazolinone ring (**Figure 10**), a singlet for the amine proton at 7.1 ppm, and a singlet for the amide proton at 8.3 ppm. ^1H NMR spectrum of compound **13** exhibited a singlet for the amide proton at 12.5 ppm and no proton peak in the range of 5.7 ppm or 7.1 ppm (**Figure 11**). The reaction mechanism of the synthesis of quinazolinones is shown in **Scheme 3**. 2-Aminobenzamides and aldehyde reacted to produce the intermediate **10**, followed by cyclization to form the intermediate **11** under the catalysis of molecular iodine. Intermediate **11** is then transformed to 4-quinazolinone **12** by oxidation with molecular iodine and molecular oxygen. In addition, hydrogen iodide generated by the oxidation of intermediate **11**, is reoxidized to molecular iodine.⁷⁵



Scheme 2. The synthesis of **9**.

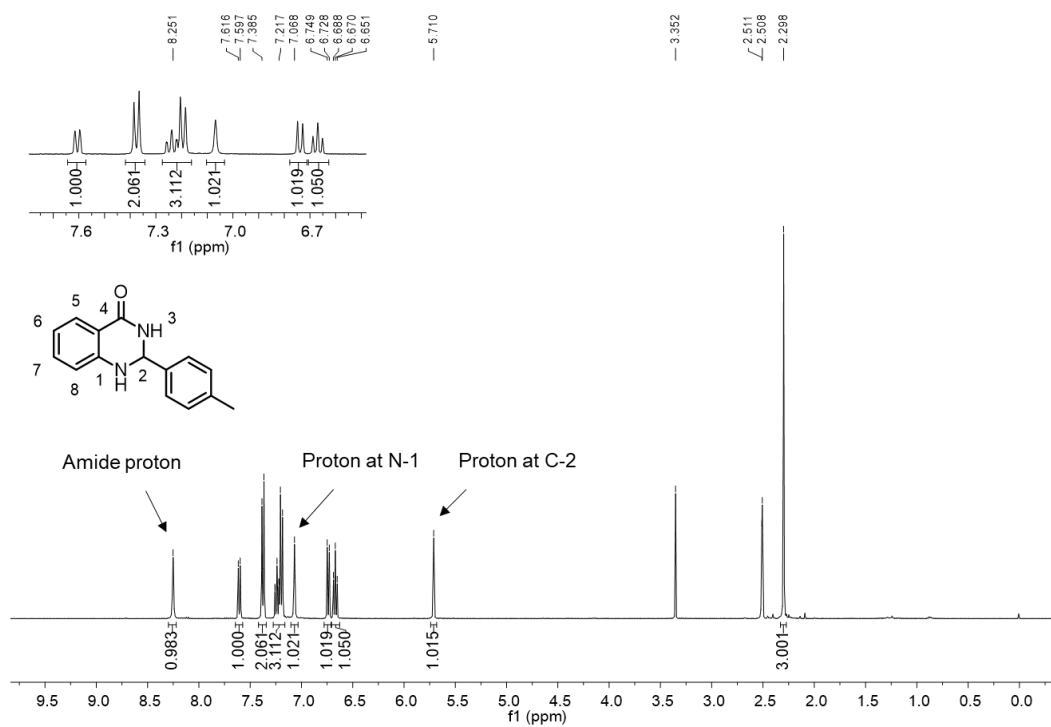


Figure 10. ^1H NMR (400 MHz, d_6 -DMSO) of **9**.

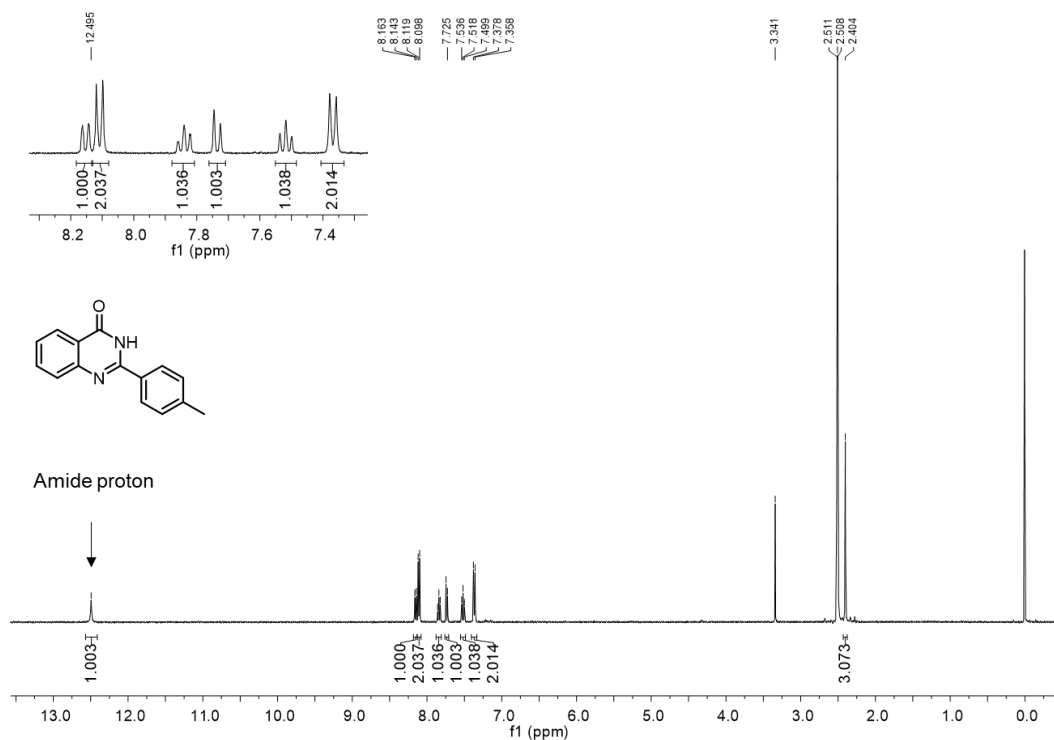
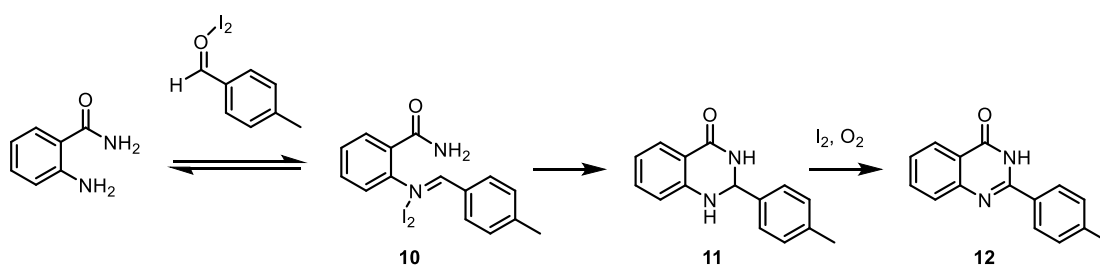


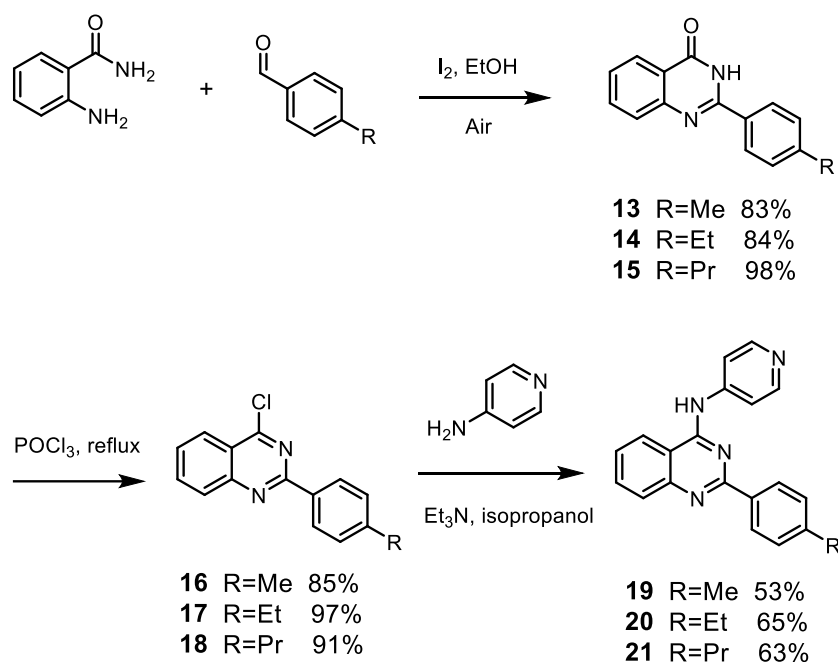
Figure 11. ^1H NMR (400 MHz, d_6 -DMSO) of **13**.



Scheme 3. Plausible pathway of synthesis of 2-aryl-4-quinazolinones.

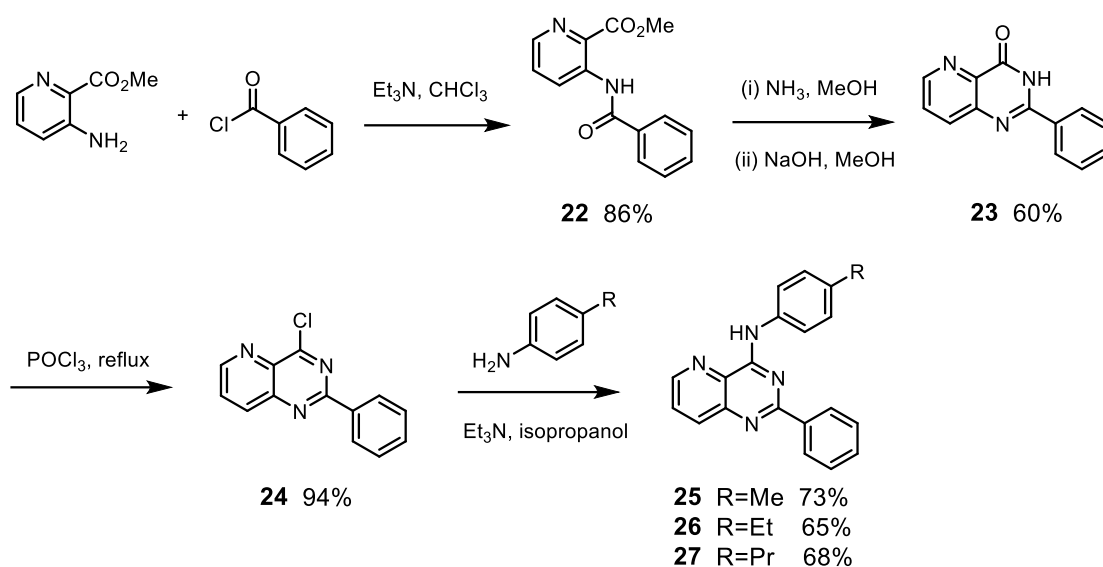
Synthesis of compounds **13-15** via the catalysis of iodine and oxidation by oxygen in EtOH (**Scheme 4**) led to 83%, 84%, and 98% yields, respectively.

Compounds **16-18** were obtained through chlorination of corresponding quinazolinones **13-15**, followed by nucleophilic aromatic substitution to produce the desired target quinazolinamine derivatives **19-21**.



Scheme 4. The synthesis of **19-21**.

Compound **23** could not be obtained successfully from 3-aminopicolinamide by the catalysis of iodine. Therefore, a two-step synthesis starting with methyl-3-aminopicolinate was used to obtain compound **23** via compound **22** as shown in **Scheme 5**. Acylation of the amino group of methyl 3-aminopicolinate with phenyl acyl chloride provided benzamidopicolinate **22**. Treatment of compound **22** with aqueous ammonium hydroxide followed by cyclization with aqueous sodium hydroxide provided quinazolinone **23** in 60% yield.⁷⁶ Chloroquinazolinamine derivative **24** was synthesized using phosphorus oxychloride as described previously. Quinazolinamine derivatives **25-27** were obtained by reacting compound **24** with substituted anilines in presence of triethylamine in 65-73% yields.

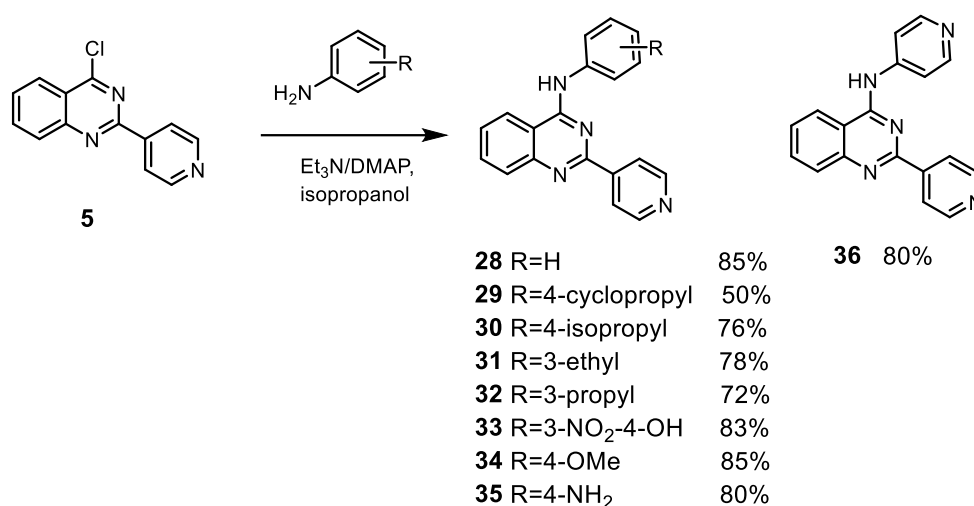


Scheme 5. The synthesis of **25-27**.

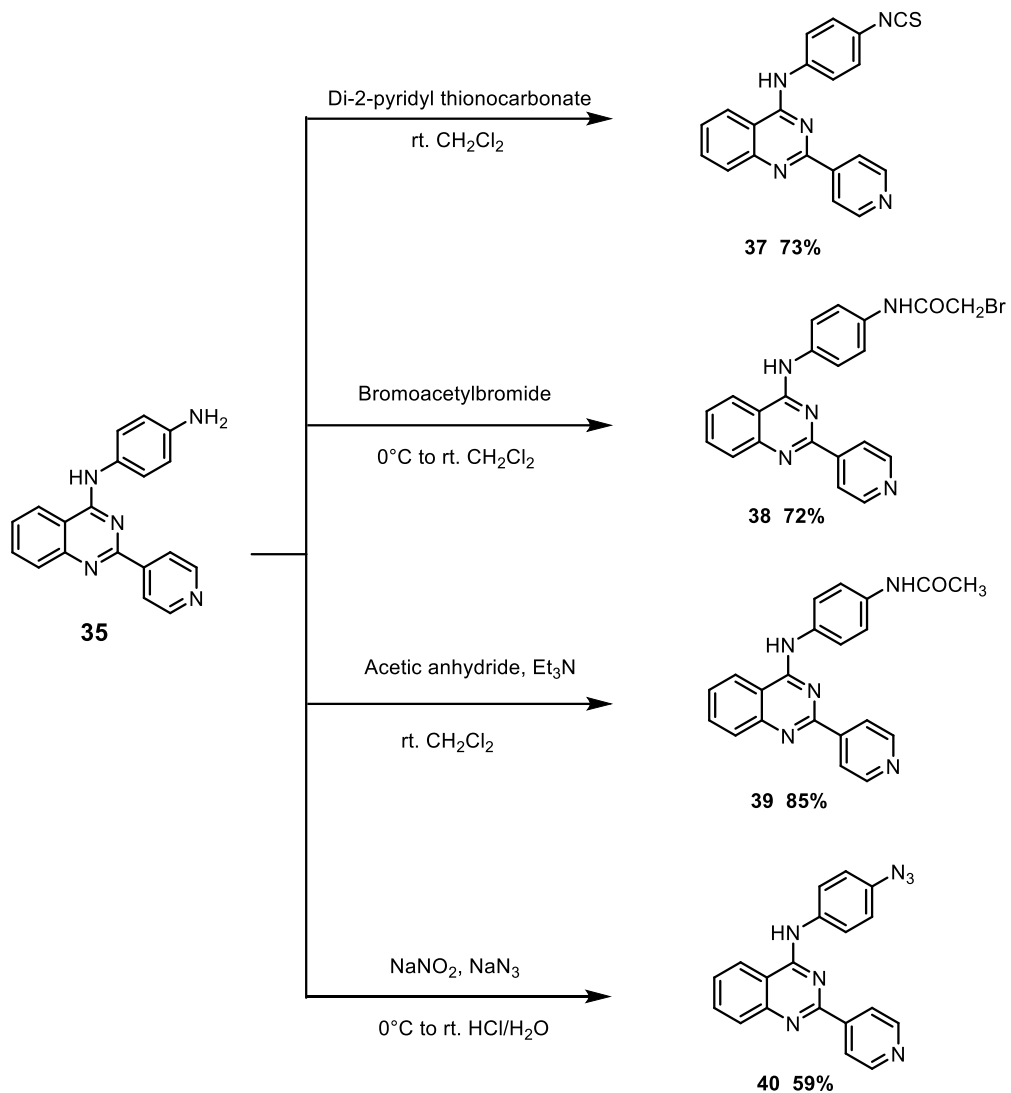
Based on the MTT assay results, quinazolinamine derivatives **7** and **8** with scaffold A showed higher potency as BCRP inhibitors than those compounds with scaffolds B or C, decreasing the IC_{50} values of mitoxantrone from 5.66 μM to 0.27 and 0.23 μM , respectively. Thus, additional quinazolinamine derivatives with scaffold A were synthesized in an effort to discover more potent reversal agents of BCRP and to further investigate the structure-activity relationship of the quinazolinamines as reversal agents of P-gp. Synthesis of target compounds **28-40** is shown in **Schemes 6** and **7**. Target compounds **28-36** were synthesized from compound **5** in a similar fashion as compounds **6-8**. Nucleophilic aromatic substitution of the 4-chloroquinazolinamine derivatives with various substituted aniline derivatives was carried out to obtain the desired quinazolinamines **28-36**. It should be noted that the synthesis of compounds **28** and **33** required 4-dimethylaminopyridine as a base instead of triethylamine.

Isothiocyanate derivative **37** was obtained by treating amino derivative **35**

dropwise with a solution of di-2-pyridyl thionocarbonate in dichloromethane. The IR spectrum of target compound **37** exhibited a peak characteristic of the isothiocyanate group at 2053 cm^{-1} (**Figure 12**). A solution of amine **35** was reacted with a solution of bromoacetyl bromide in dichloromethane to obtain the bromoacetamide derivative **38**. Bending band of $\text{C}(=\text{O})\text{N-H}$ at 1510 cm^{-1} , and comb bands C-N & N-H at 1566 cm^{-1} show the formation of bromoacetamide group in the infrared spectrum of compound **38** (**Figure 13**). Acetamide **39** was synthesized by the reaction of amine **35** and acetic anhydride in the presence of triethylamine. Bending band of $\text{C}(=\text{O})\text{N-H}$ at 1510 cm^{-1} , and comb bands C-N & N-H at 1560 cm^{-1} in the infrared spectrum reflect the formation of acetamide derivative **39** (**Figure 14**). Treatment of amine **35** dropwise with conc. HCl at $0\text{ }^\circ\text{C}$, followed by the reaction with sodium nitrite to produce diazonium salt, and subsequent reaction with sodium azide led to azide quinazolinamine derivative **40**. A stretching band at 2115 cm^{-1} in the infrared spectrum is observed confirming the formation of the azide derivative **40** (**Figure 15**).



Scheme 6. The synthesis of **28-36**.



Scheme 7. The synthesis of 37-40.

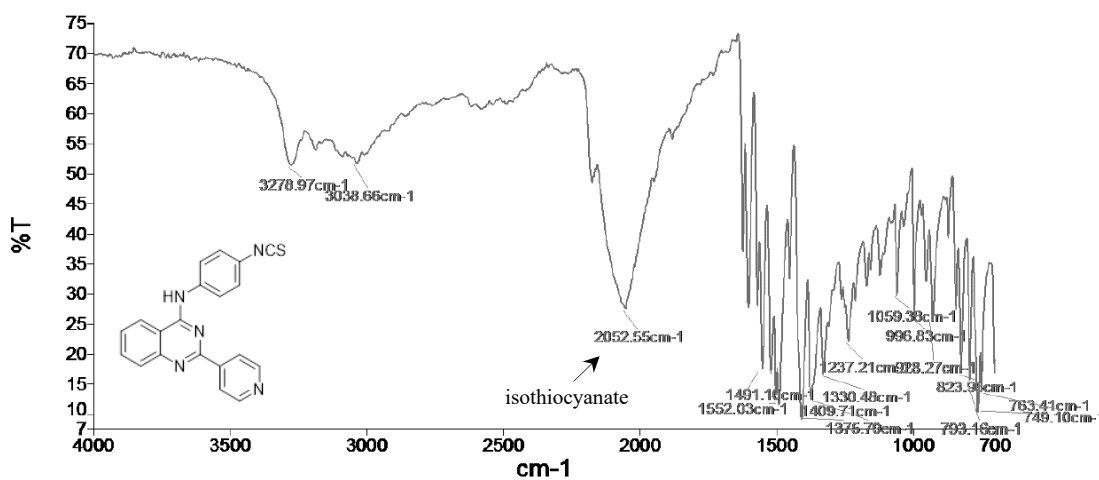


Figure 12. IR spectrum of 37

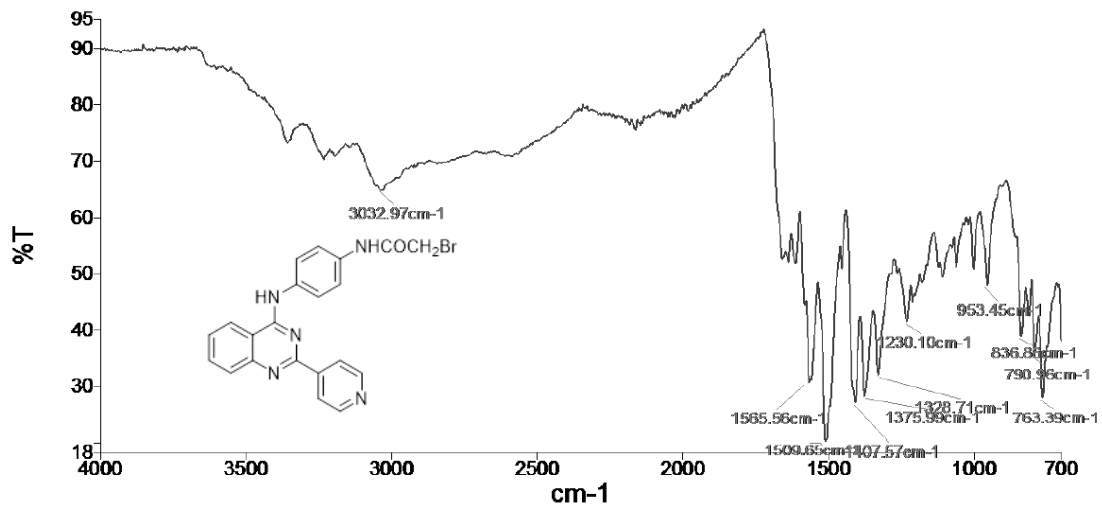


Figure 13. IR spectrum of 38

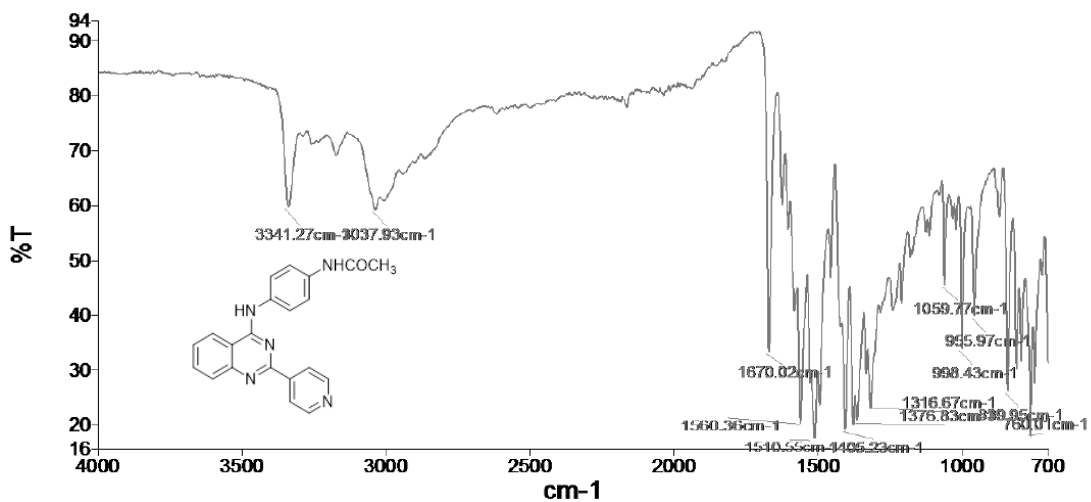


Figure 14. IR spectrum of 39

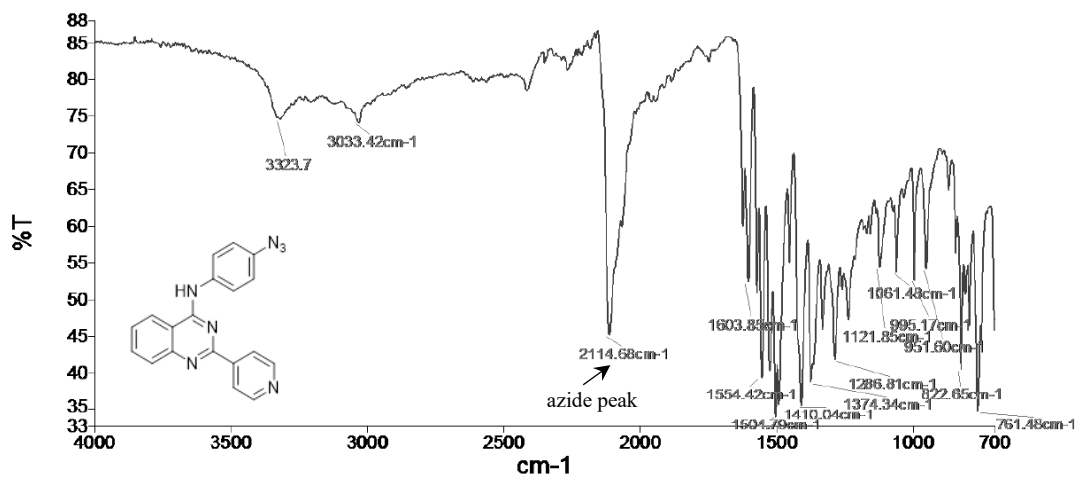


Figure 15. IR spectrum of 40

4.2. Cytotoxicity and Reversal Study on BCRP

The cytotoxicities of quinazolinamine derivatives were tested to determine the concentrations of quinazolinamines needed for reversal study. Quinazolinamine derivatives **6-8**, **19-21**, and **25-27** exhibited low cytotoxicity toward the parental H460 and BCRP-overexpressing H460/MX20 cell lines at which the compounds decreased the viability of H460 and H460/MX20 cell lines by less than 20%. (**Table 2**). Next, the reversal assays were conducted on drug-resistant H460/MX20 cell line at 5 μM concentration of the quinazolinamine derivatives **6-8**, **19-21**, and **25-27**. Based on the MTT assay (**Table 3**), ethyl and propyl substituted derivatives **7** and **8** exhibit the strongest reversal activities on BCRP-mediated MDR. Mitoxantrone is a known BCRP substrate. The IC_{50} value of MX on H460 and H460/MX20 are 0.072 μM and 5.66 μM , respectively. In combination with most of the quinazolinamine derivatives, the IC_{50} value of MX on H460/MX20 decreased. Ko 143, a known BCRP inhibitor, can effectively decrease the IC_{50} value of MX on H460/MX20 to 0.18 μM . The efficacies of compounds **7** and **8** with scaffold A are comparable to Ko143, decreasing the IC_{50} values of MX on H460/MX20 to 0.27 μM and 0.23 μM , respectively.

Table 2. The cytotoxicities of quinazolinamine derivatives 6-8, 19-21, and 25-27 on H460 and H460/MX20 cell lines.

Treatments	$\text{IC}_{50} \pm \text{SD} (\mu\text{M})$	
	H460	H460/MX20
6	>100	>100
7	>100	>100

8	>100	>100
19	24.8 ± 1.8	>100
20	38.3 ± 0.2	27.4 ± 0.9
21	59.7 ± 2.8	39.6 ± 6.6
25	>100	>100
26	>100	>100
27	>100	>100

Table 3. The reversal effects of quinazolinamine derivatives 6-8, 19-21, and 25-27 on BCRP-mediated MDR cell line H460/MX20.

Treatments	IC ₅₀ ± SD (μM)	
	H460	H460/MX20
Mitoxantrone	0.072 ± 0.009	5.66 ± 0.29
+ 6 (5 μM)	0.052 ± 0.005	0.47 ± 0.02
+ 7 (5 μM)	0.054 ± 0.003	0.27 ± 0.01
+ 8 (5 μM)	0.045 ± 0.006	0.23 ± 0.02
+ 19 (5 μM)	0.059 ± 0.001	4.82 ± 0.22
+ 20 (5 μM)	0.048 ± 0.003	0.32 ± 0.02
+ 21 (5 μM)	0.054 ± 0.001	0.41 ± 0.07
+ 25 (5 μM)	0.063 ± 0.014	0.65 ± 0.06
+ 26 (5 μM)	0.064 ± 0.006	0.88 ± 0.08
+ 27 (5 μM)	0.053 ± 0.006	1.04 ± 0.12
+ Ko143 (5 μM)	0.029 ± 0.004	0.18 ± 0.02

MTT assays on target compounds **28-40** were conducted to determine whether these quinazolinamine derivatives at the concentration of 5 μM are non-toxic to H460 and H460/MX20 cell lines (**Table 4**). The results showed that the derivatives

exhibited low cytotoxicities on the H460 and H460/MX20 cell lines and did not decrease the viability of the cells by more than 20%. Thus, the reversal activities of quinazolinamine derivatives were determined at 5 μM . Target compounds **29-32** and **34** were found to be most potent with potencies similar to those of **7** or **8** (Table 5). The IC_{50} value of mitoxantrone was found to be 0.42 μM when combined with azide **40** (5 μM), but upon UV activation at 254 nm, its IC_{50} value decreased to 0.19 μM . It is hypothesized that the covalent binding of azide **40** with BCRP may have reduced the off-target effect. Gefitinib showed the most potent inhibition on BCRP, decreasing the IC_{50} value of mitoxantrone to 0.13 μM .

Table 4. The cytotoxicities of quinazolinamine derivatives 28-40 on H460 and H460/MX20 cell lines.

Compd.	$\text{IC}_{50} \pm \text{SD} (\mu\text{M})$	
	H460	H460/MX20
28	>100	>100
29	31.0 \pm 2.7	31.0 \pm 0.8
30	51.2 \pm 3.3	16.9 \pm 3.2
31	>100	>100
32	>100	>100
33	>100	>100
34	>100	>100
35	>100	>100
36	>100	>100
37	>100	31.1 \pm 5.5
38	>100	>100
39	>100	>100

40	>100	>100
Gefitinib	65.5 ± 3.2	36.5 ± 1.1

Table 5. The reversal effects of quinazolinamine compounds 28-40 on BCRP-mediated MDR cell line H460/MX20.

Treatments	IC ₅₀ ± SD (μM)	
	H460	H460/MX20
Mitoxantrone	0.154 ± 0.051	6.50 ± 0.14
+ 28 (5 μM)	0.073 ± 0.007	0.44 ± 0.02
+ 29 (5 μM)	0.103 ± 0.003	0.30 ± 0.01
+ 30 (5 μM)	0.070 ± 0.006	0.24 ± 0.02
+ 31 (5 μM)	0.078 ± 0.023	0.29 ± 0.02
+ 32 (5 μM)	0.075 ± 0.004	0.30 ± 0.01
+ 33 (5 μM)	0.052 ± 0.004	0.61 ± 0.04
+ 34 (5 μM)	0.081 ± 0.008	0.32 ± 0.04
+ 35 (5 μM)	0.076 ± 0.002	0.54 ± 0.08
+ 36 (5 μM)	0.082 ± 0.013	4.11 ± 0.29
+ 37 (5 μM)	0.091 ± 0.004	4.58 ± 0.41
+ 38 (5 μM)	0.083 ± 0.019	5.41 ± 0.55
+ 39 (5 μM)	0.110 ± 0.011	1.92 ± 0.47
+ 40 (5 μM)	0.074 ± 0.013	0.42 ± 0.04
+ 7 (5 μM)	0.102 ± 0.007	0.34 ± 0.02
+ 8 (5 μM)	0.081 ± 0.002	0.35 ± 0.01
+ 40 (5 μM) + UV	0.065 ± 0.013	0.19 ± 0.01
+ Ko143 (5 μM)	0.070 ± 0.008	0.25 ± 0.05
+ gefitinib (5 μM)	0.029 ± 0.005	0.13 ± 0.02

4.3. Cytotoxicities and Reversal Effects on P-gp

Inhibitory activities of the quinazolinamines derivatives **6-8**, **19-21**, and **25-40** on P-gp were studied to investigate the selectivity of these compounds. As shown in **Table 6**, the quinazolinamine derivatives exhibit low cytotoxicity at 5 μM concentration toward the parental KB-3-1 and P-gp-overexpressing KB-C2 cell lines. Hence, the reversal assays were conducted on drug-resistant KB-C2 cell line with the quinazolinamine derivatives at the concentration of 5 μM . The results indicated that compounds **7-8**, **20**, **29-32**, and **34** exhibit potent P-gp inhibitory effect (**Figure 16**). When these quinazolinamines were combined with a P-gp substrate, colchicine (0.5 μM), the survival rate of KB-C2 cells dramatically decreased, compared to the colchicine alone. Therefore, these eight compounds were further investigated, and it was found that compounds **7-8**, **29-31**, **34** exhibited higher potency than verapamil and gefitinib (**Figure 17**). The results indicated that, in combination with compounds **7-8**, **29-31**, **34**, the IC_{50} value of colchicine on KB-C2 cells were decreased dramatically from 7.34 μM to lower than 0.30 μM , while verapamil and gefitinib decreased the IC_{50} value of colchicine to 0.43 and 0.55 μM , respectively. In addition, azide derivative **40** did not show potent inhibition on the P-gp with IC_{50} value of 6.05 μM for colchicine after the combination.

Table 6. The cytotoxicities of quinazolinamine derivatives 6-8, 19-21, and 25-40 on KB-3-1 and KB-C2 cell lines.

Compd.	IC ₅₀ ± SD (μM)	
	KB-3-1	KB-C2
6	>100	>100
7	>100	>100
8	>100	>100
19	24.4 ± 3.4	26.9 ± 0.5
20	16.3 ± 1.5	37.7 ± 0.2
21	36.8 ± 3.7	55.7 ± 7.7
25	>100	>100
26	>100	>100
27	>100	>100
28	>100	>100
29	>100	>100
30	12.7 ± 2.3	72.0 ± 11.2
31	60.9 ± 11.6	>100
32	>100	>100
33	>100	>100
34	>100	>100
35	14.5 ± 3.1	>100
36	>100	>100
37	33.2 ± 4.1	>100
38	50.6 ± 2.9	>100
39	>100	>100
40	>100	>100
Gefitinib	56.1 ± 13.8	41.7 ± 4.0

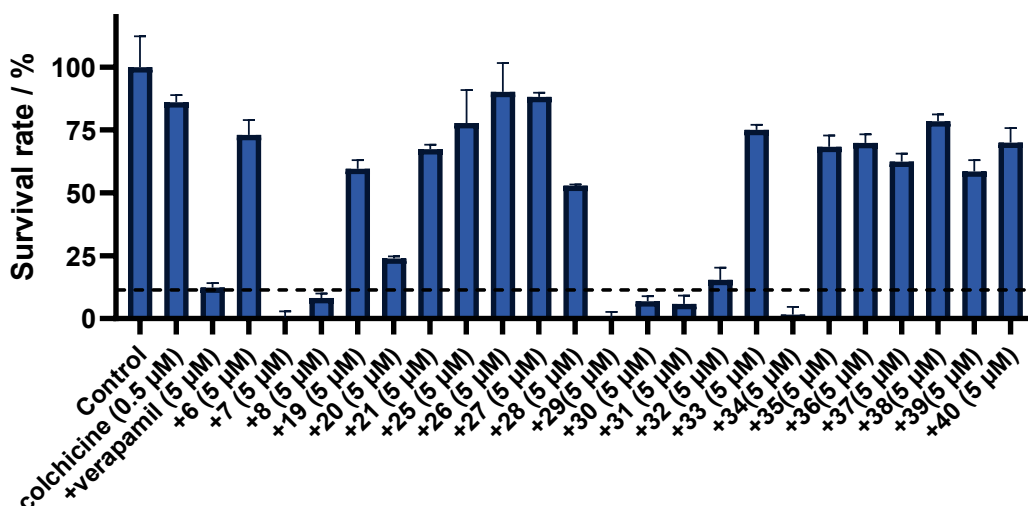


Figure 16. The reversal effects of quinazolinamine derivatives 6-8, 19-21, and 25-40 on P-gp-mediated MDR cell line KB-C2.

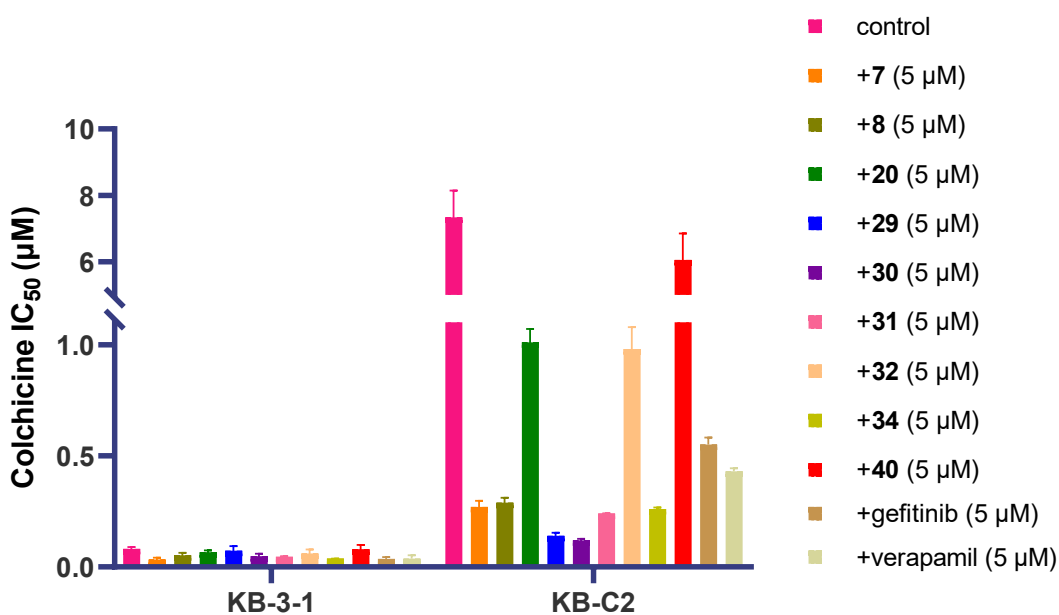


Figure 17. The reversal effects of quinazolinamine derivatives on P-gp-mediated MDR cell line KB-C2.

4.4. Metabolic Stability Study

Ko 143, as a potent BCRP inhibitor, is widely used as a positive control BCRP inhibitor in the scientific research. However, Ko 143 has limitation for clinical use due to the low metabolic stability *in vivo*.⁷⁷ Therefore, the design of metabolically

more stable reversal agents for BCRP-mediated MDR is highly desired.

Human liver microsomes contain a wide variety of membrane bound drug metabolizing CYP450 enzymes,⁷⁸ derived from human liver where the drugs are mainly metabolized. Thus, *in vitro* metabolic stability testing with human liver microsomes has been commonly used to predict the *in vivo* hepatic metabolism of the drugs in the human body.⁷⁹ The potent BCRP and P-gp inhibitors **7-8**, **29-31**, **34**, and potent BCRP inhibitor azide **40** were selected for metabolic stability study. The results showed that 80-92% of the seven quinazolinamine derivatives remained after 1 h incubation with human liver microsomes, indicating that these compounds have higher metabolic stability than Ko143 (**Table 7**). Thus, these quinazolinamines could be valuable and suitable for clinical application in the future. Significantly, 92% of cyclopropyl derivative **29** remained after incubation with human liver microsomes compared to 41% of Ko143. It has been reported that cyclopropyl group can enhance potency, reduce off-target effects, increase metabolic stability, increase brain permeability, decrease plasma clearance, contribute to an entropically more favorable binding to the receptor, restrict the conformation of peptides/peptidomimetics to prevent proteolytic hydrolysis, and alter drug pKa.⁸⁰ Since the results showed that compound **29** is a potent BCRP and P-gp inhibitor with high metabolic stability, it was selected for investigation of its mechanism in reversing the MDR mediated by BCRP and P-gp. In addition, azide derivative **40** was found to be a potent BCRP inhibitor indicating the strong binding with BCRP. Therefore, compound **40** with a photoaffinity label was also considered to be suitable for further investigation to learn

about the binding mode of quinazolinamines to BCRP protein.

Table 7. Metabolic stability of selected quinazolinamine derivatives with human liver microsomes

Compd.	Metabolic stability ^a /%
7	87 ± 12
8	80 ± 5
29	92 ± 8
30	75 ± 6
31	91 ± 3
34	83 ± 1
40	86 ± 11
Ko143	41 ± 7

^a Metabolic stability was calculated as the % compound remaining after 1 h of incubation with human liver microsomes.

4.5 The Reversal Study of 29 (VKCY-1) and 40 (VKCY-2) in Combination with Anticancer Drugs

Reversal study was conducted to further investigate the effects of compounds **29** and **40** in combination with BCRP substrate -- mitoxantrone, P-gp substrate -- paclitaxel, or a non-substrate of both pumps--cisplatin. The results showed that the reversal effects of compound **29 (VKCY-1)** on P-gp is not limited to one substrate (**Figure 18A**). It can sensitize KB-C2 cells to the anticancer drug, paclitaxel, in addition to colchicine. A non BCRP or P-gp substrate, cisplatin, was used as a negative control (**Figure 18B, 18C**). The results suggested that the sensitizing effects of compounds **29 (VKCY-1)** and **40 (VKCY-2)** is limited to BCRP and/or P-gp substrates for ABC transporter mediated

MDR cancer cell lines.

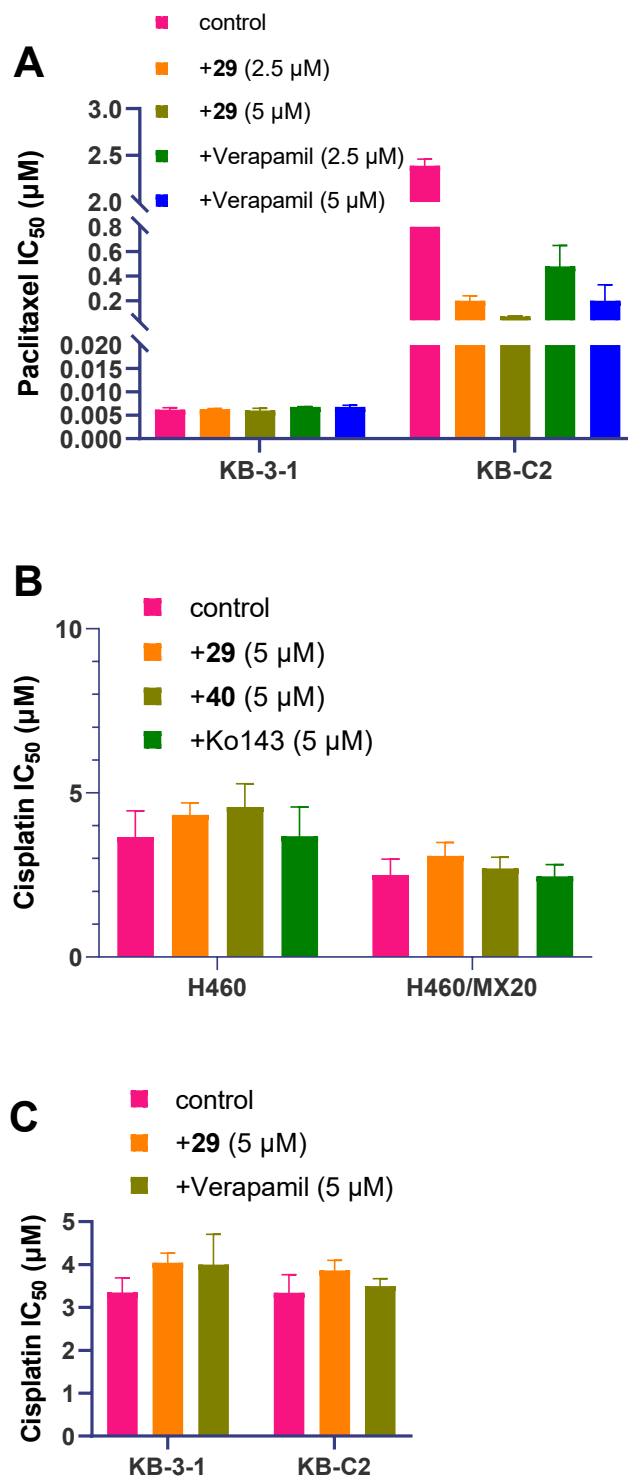


Figure 18. The reversal study of compounds **29** and **40** in combination with anticancer drugs. (A) The reversal study of compound **29** with paclitaxel on P-gp-mediated MDR cell line KB-C2. (B) The reversal study of compounds **29** and **40** with cisplatin on BCRP-mediated MDR cell line H460/MX20. (C) The reversal study of compound **29**

with cisplatin on P-gp-mediated MDR cell line KB-C2.

4.6. Drug Accumulation Assay

Drug accumulation assays were conducted to determine the effects of cyclopropyl derivative **29** and azide derivative **40** on the accumulation of mitoxantrone in H460 or H460/MX20 cells, or paclitaxel in KB-3-1 and KB-C2 cells. The results of accumulation assay showed that both cyclopropyl derivative **29** and azide **40** can slightly increase the accumulation of mitoxantrone in parental H460 cells (**Figure 19A**). Since low level of BCRP transporter is expressed in H460 cells, compounds **29** and **40** can also inhibit the efflux function of BCRP in H460 cell. In addition, the two compounds increased the accumulation of mitoxantrone in resistant H460/MX20 cells which overexpressed BCRP transporter. Treatment of compound **40** followed by UV light activation, showed that accumulation of mitoxantrone was increased compared to the group without activation. It explained the reason why IC_{50} value of mitoxantrone for the activated **40** treatment group (**Table 5**) was lower than that of the unactivated **40** treatment group. In addition, **29** did not increase the accumulation of paclitaxel in the parental cells KB-3-1, while **29** significantly increased the accumulation of paclitaxel in the resistant cell line KB-C2 (**Figure 19B**). When in combination with **29** or **40**, the accumulation of mitoxantrone and paclitaxel in MDR cells were enhanced and viability of cancer cells decreased. It explained why the IC_{50} values of mitoxantrone and paclitaxel decreased when they were combined with **29** or **40**.

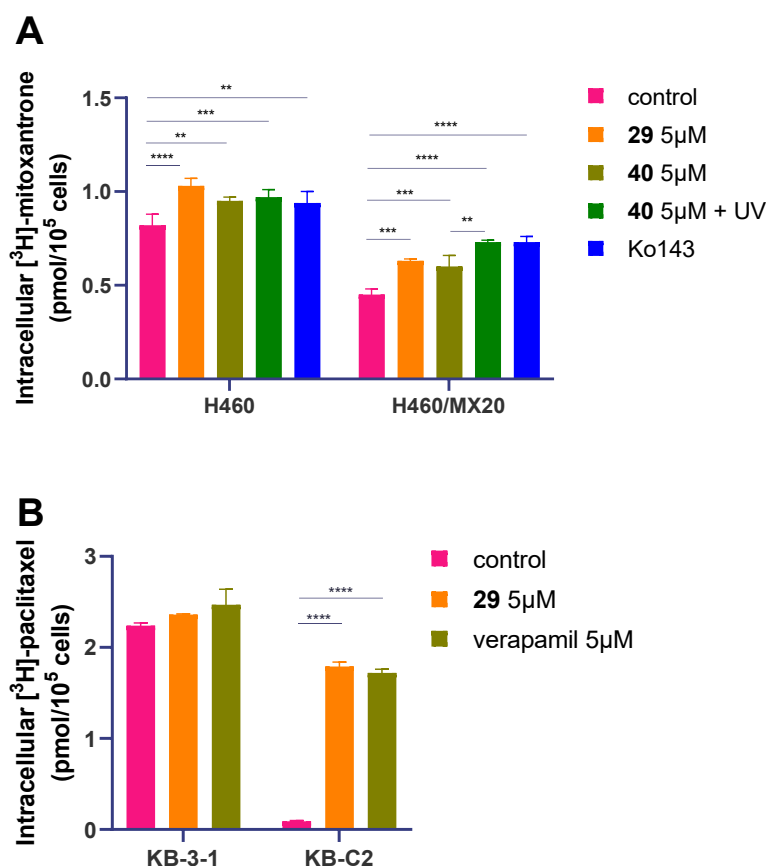


Figure 19. The effect of **29** and **40** on the accumulation of mitoxantrone on H460/MX20 or paclitaxel on KB-C2 cells.

4.7. Western Blot Assay

Western blot assays were conducted to investigate the effects of compounds **29** and **40** on the expression levels of BCRP or P-gp proteins. It was observed that compound **29** did not alter the expression level of BCRP on H460/MX20 cells, nor did it change the P-gp expression on KB-C2 cells (**Figure 20**). The BCRP expression level on H460/MX20 cells was not altered by compound **40** (**Figure 21**). Thus, it was concluded that blocking the efflux function of BCRP or P-gp was not due to the downregulation of expression level.

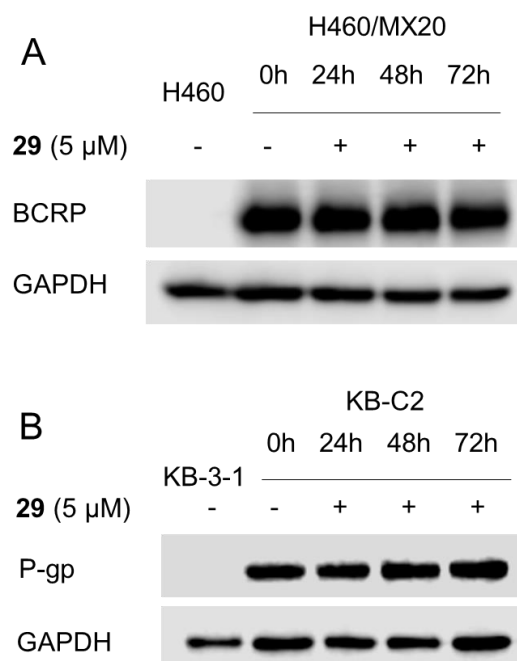


Figure 20. The effect of **29** on BCRP and P-gp expression level in drug resistant cell lines.

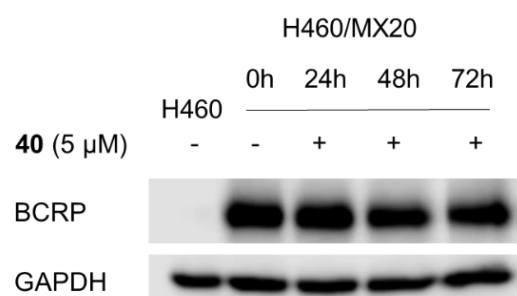


Figure 21. The effect of **40** on BCRP expression level in H460/MX20 cells.

4.8. Immunofluorescence Assay

The immunofluorescence assays were conducted to determine the effects of compounds **29** and **40** on the localization of BCRP or P-gp proteins. BCRP protein is expressed on the membranes of drug resistant cells H460/MX20 and the P-gp protein is expressed on the membranes of KB-C2 cells in the control groups (**Figure 22** and **23**). With the incubation of compound **29** (5 μ M) for 24, 48, and 72 h, the fluorescence on the membranes of H460/MX20 decreased gradually. With the

treatment of compound **29** (5 μ M) for 24 and 48 h, the fluorescence on the membranes of KB-C2 cells did not decrease significantly, while the fluorescence decreased slightly at 72 h. Since compound **29** does not change the expression level of BCRP and P-gp protein based on the Western blot analysis. It is hypothesized that the intracellular localization of the ABC transporters on both H460/MX20 and KB-C2 cells were altered by compound **29**. The alteration of ABC transporters localization can result in the loss of efflux function of ABC transporter mediated MDR cells. Thus, the anticancer drugs can be accumulated in the cells, and effectively kill the cells. Interestingly, compound **40** did not change the intracellular localization of BCRP on H460/MX20 cells (**Figure 24**). The reversal effect of compound **40** on BCRP can be due to other mechanisms instead of the alteration of BCRP localization.

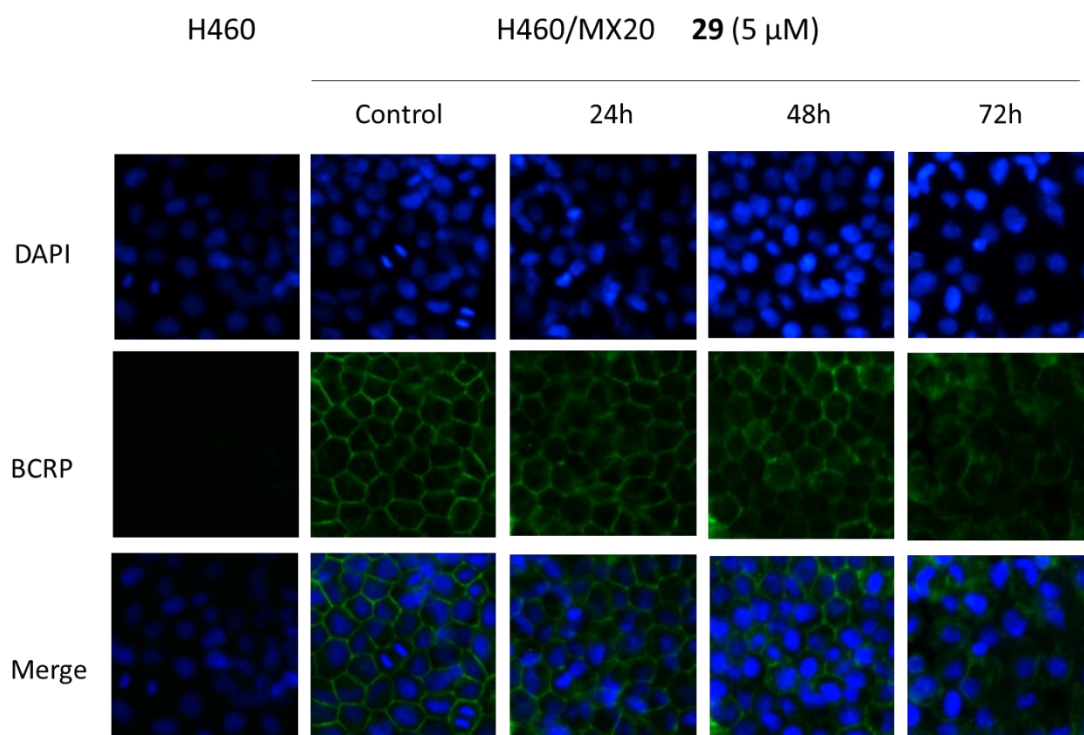


Figure 22. The effect of compound **29** on BCRP localization in H460 and H460/MX20 cells.

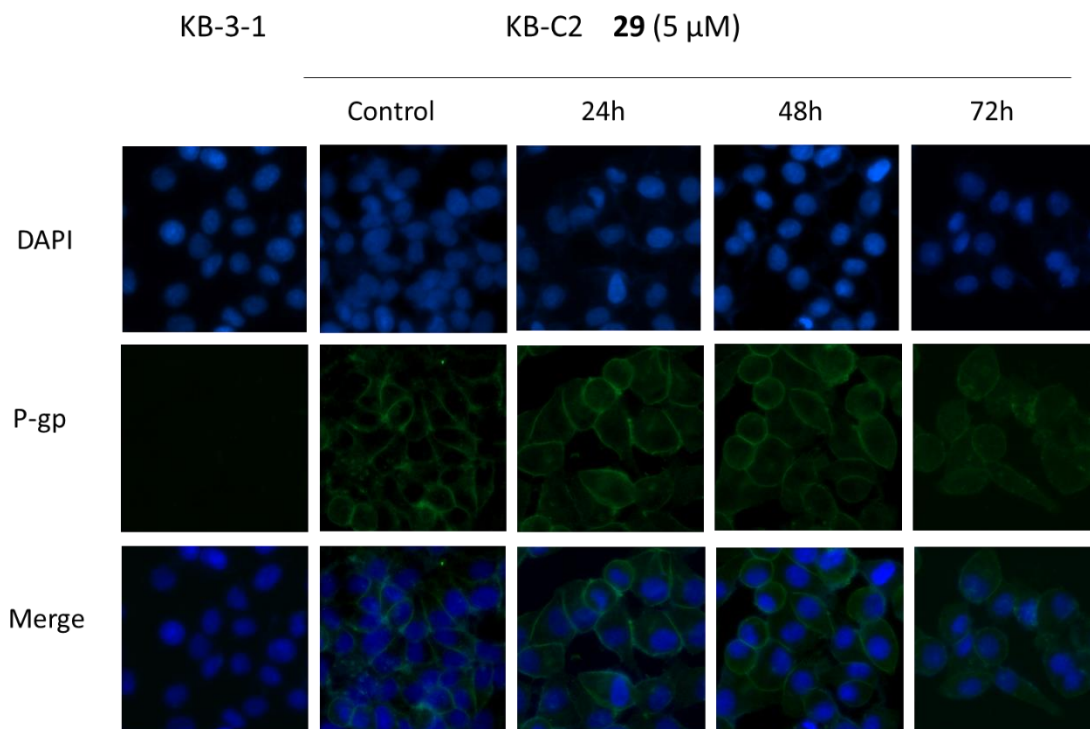


Figure 23. The effect of compound **29** on P-gp localization in KB-C2 cells.

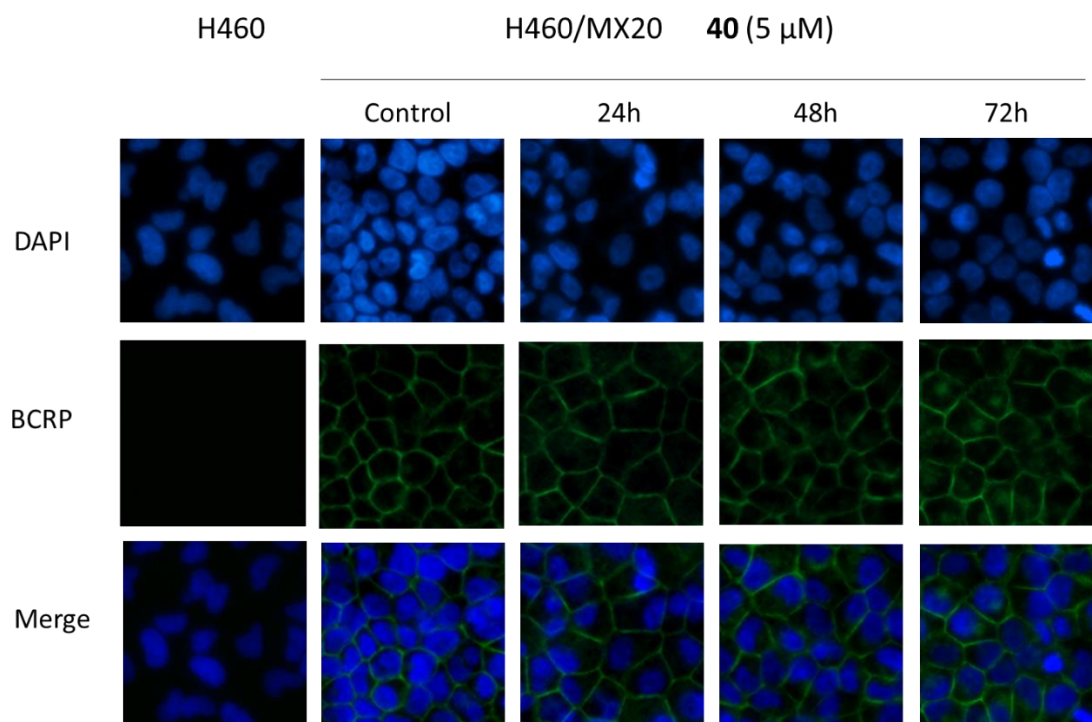


Figure 24. The effect of compound **40** on BCRP localization in H460/MX20 cells.

4.9. The effect of compound 29 on BCRP and P-gp expression levels on membrane and cytoplasm.

Previous reports have shown that the localization of BCRP can be changed with the treatment of LY294002,⁸¹ an inhibitor of the Akt effector protein phosphatidylinositol 3-kinase. In addition, LY294002 can cause the translocation of BCRP from the membrane to the intracellular compartment.⁸¹ To further investigate whether compound **29** affects the localization of BCRP and P-gp, the proteins were extracted from the membrane and cytoplasm of the cells, respectively. It was found that compound **29** decreased the expression level of BCRP protein on the membranes of H460/MX20 cells. On the other hand, BCRP protein expression level in the cytoplasm was increased by target compound **29** (**Figure 25A, 25B**). Compound **29** showed similar effect on the P-gp protein expression of KB-C2 cells (**Figure 26A, 26B**) that the expression level of P-gp protein on the membranes slightly decreased and the cytoplasmic P-gp slightly increased through the quantifications with Image J. These results revealed that compound **29** can translocate BCRP or P-gp protein from the membranes to the cytoplasm.

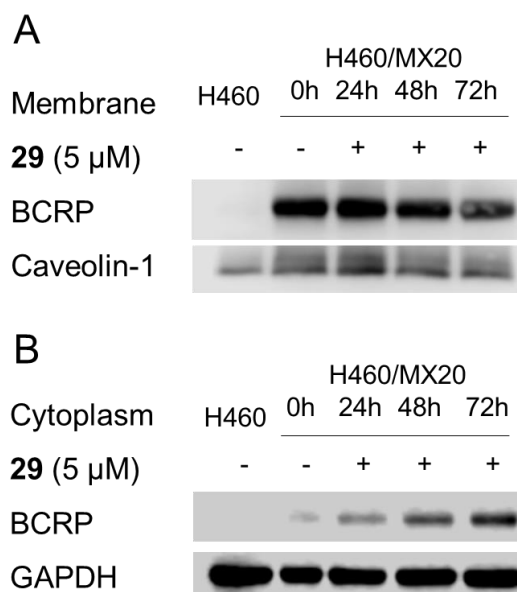


Figure 25. The effect of **29** on BCRP expression level on membrane and cytoplasm. (A) The effect of **29** on BCRP expression level in membrane of H460/MX20 cells. (B) The effect of **29** on BCRP expression level in cytoplasm of H460/MX20 cells.

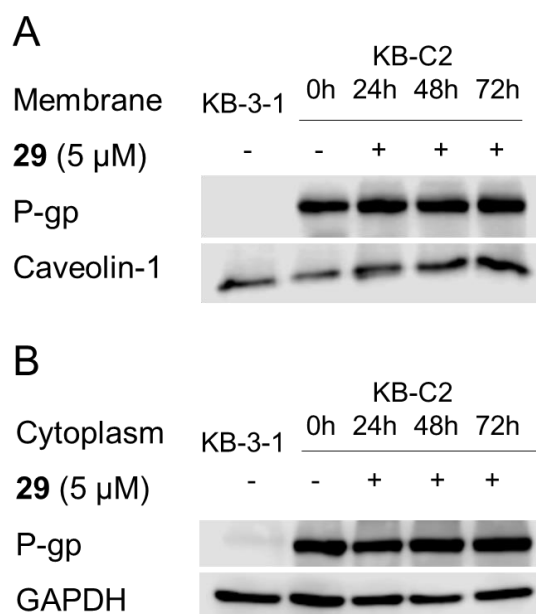


Figure 26. The effect of compound **29** on P-gp expression level on membrane and cytoplasm. (A) The effect of compound **29** on P-gp expression level in membrane of KB-C2 cells. (B) The effect of compound **29** on P-gp expression level in cytoplasm of KB-C2 cells.

4.10. ATPase Assay

ATPase assays were conducted to determine whether compounds **29** and **40** affect

the BCRP or P-gp ATPase activities. The results of ATPase assay showed that both compound **29** (Figure 27) and compound **40** (Figure 28) were the substrates of BCRP transporter. Therefore, they could act as potential competitive substrates, thus blocking the efflux of anticancer drugs and increase the accumulation of anticancer drugs. The results indicated that compound **29** (Figure 29) can neither stimulate or inhibit the P-gp ATPase, thus it is not the substrate or inhibitor of BCRP. From the results of Western blot and ATPase assay, compound **29** did not change the P-gp protein expression level and did not affect the P-gp ATPase activity. Therefore, compound **29** likely reverses the P-gp-mediated MDR through altering the localization of P-gp on MDR cancer cells.

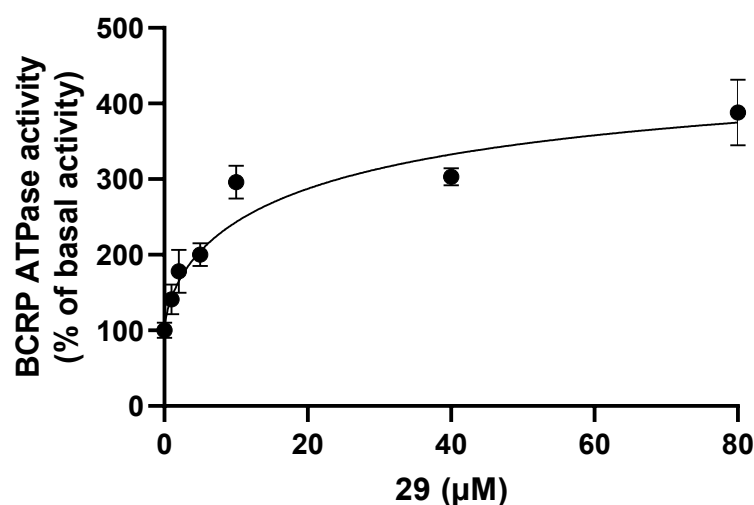


Figure 27. The effect of compound **29** on orthovanadate (Vi)-sensitive BCRP ATPase activity.

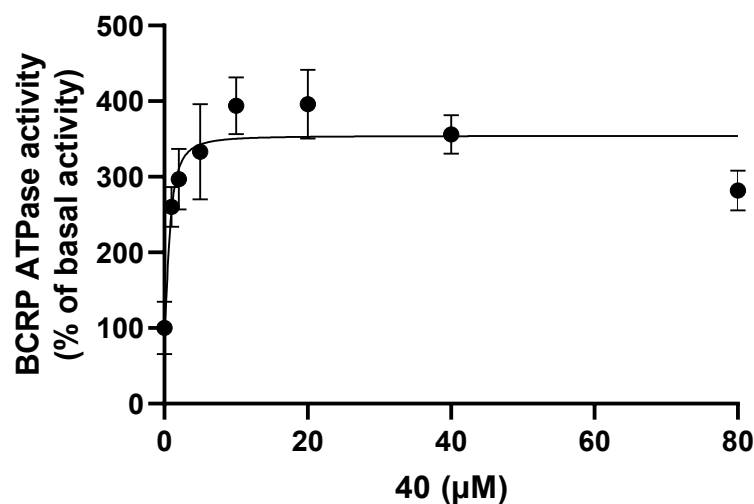


Figure 28. The effect of compound **40** on orthovanadate (Vi)-sensitive BCRP ATPase activity.

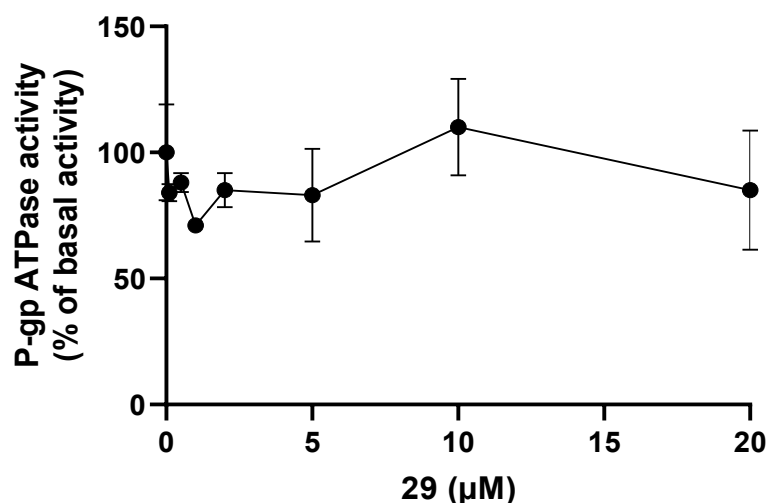


Figure 29. The effect of compound **29** on orthovanadate (Vi)-sensitive P-gp ATPase activity.

4.11. Docking Analysis

The Glide docking scores of **29**, **40**, and Ko143 binding with BCRP (PDB 6FFC) are -11.123, -10.403 and -12.017 kcal/mol, respectively (**Figure 30**). The quinazoline ring and the pyridine ring of **29** interacted with Phe439 of BCRP model through π - π interactions. The amino group of **29** formed a hydrogen bond with the carbonyl group

in the side chain of Asn436 (**Figure 30A, 30D**). The quinazoline ring of **40** interacted with Phe439 of BCRP model through π - π interactions (**Figure 30B, 30E**). The nitrogen in the pyridine ring of **40** formed a hydrogen bond with the amino group in the side chain of Asn436. The amino group of Ko143 interacted with the carbonyl group in the side chain of Asn436 through a hydrogen bond. The carbonyl group of Ko143 forms a hydrogen bond with hydroxyl group of Thr542. (**Figure 30C &F**). Compounds **29** and **40** were stabilized into a pocket formed by residues Phe432, Thr435, Thr542, Val546, and Met549 of BCRP. The Glide docking scores of **29** and verapamil binding with P-gp (PDB 6FN1) are -9.599 and -7.789 kcal/mol, respectively (**Figure 31**). The quinazoline ring and the pyridine ring of **29** interacted with the side chain of Trp231 of P-gp model through π - π interactions. A nitrogen in the quinazoline ring interacted with the amino group in the side chain of Trp231 through a hydrogen bond, while verapamil formed cation- π interaction with the side chain of Phe335 in P-gp. The tertiary amine of verapamil can become a cation in cancers due to the acidic tumor microenvironment¹⁵ and bind with Phe335.

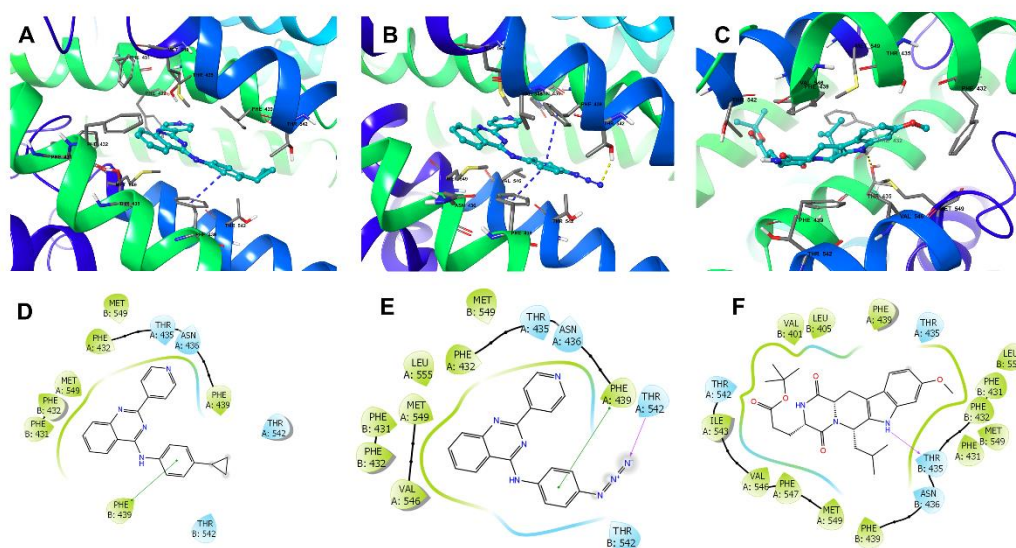


Figure 30. The docking analysis of compound **29**, **40**, and Ko143 binding with BCRP (PDB 6FFC). (A) Docked position of compound **29** within the binding site of the human BCRP transporter protein. Compound **29** is shown as a ball and stick model, with the atoms colored as follows: carbon- cyan, hydrogen-white, nitrogen-blue, and oxygen-red. The important residues are depicted as sticks with the same color scheme as above except that carbons are indicated by the gray color. Ring centroids were represented as dark green dots. Dotted red lines indicate hydrogen bonds. (B) A two-dimensional ligand-receptor interaction diagram shows the important interactions of compound **29** with the binding site residues of human BCRP. The amino acids are shown as colored bubbles, cyan indicates polar residues and green indicates hydrophobic residues. Hydrogen bonds are indicated by the purple dotted arrow, and p-p stacking aromatic interactions are indicated by the green lines. (C) Docked position of compound **40** within the binding site of the human BCRP transporter protein. (D) A two-dimensional ligand-receptor interaction diagram shows the important interactions of compound **40** with the binding site residues of the human BCRP transporter protein. (E) Docked position of Ko143 within the binding site of the human BCRP protein. (F) A two-dimensional diagram shows the important contacts of Ko143 with the binding site residues of the human BCRP transporter protein.

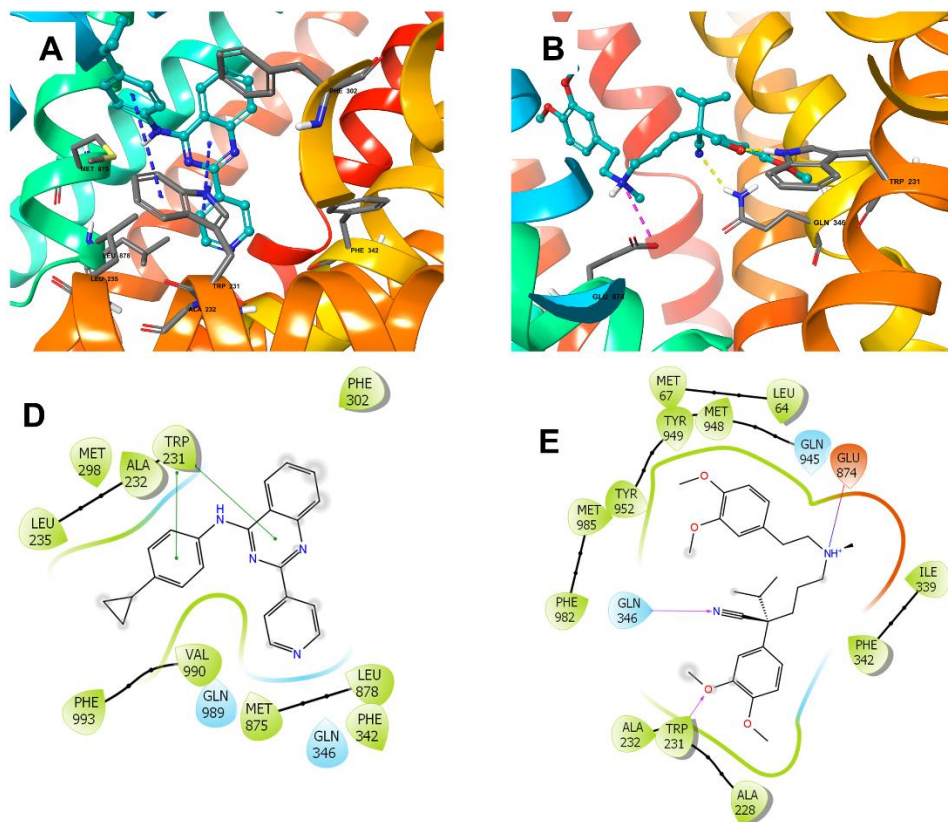


Figure 31. The docking analysis of compound **29** and verapamil binding with human P-gp (PDB 6FN1). The color scheme is consistent with **Figure 30**. (A) Docked position of compound **29** within the binding site of the human P-gp model. (B) A two-dimensional ligand-receptor interaction diagram shows the important interactions of compound **29** with the binding site residues of human P-gp. (C) Docked position of verapamil within the binding site of the human P-gp model. Cation- π interaction is indicated by the green dotted line. (D) A two-dimensional ligand-receptor interaction diagram shows the important interactions of verapamil with the binding site residues of human P-gp. Cation- π interaction is indicated by short red line.

Chapter 5. Conclusions

In this study, we synthesized a series of 22 quinazolinamine derivatives and determined their reversal activities for BCRP- and P-gp-mediated MDR. Based on the structure-activity relationship, quinazolinamines with scaffold A were found to be more potent BCRP inhibitors than those with scaffolds B or C. The results indicated that alkyl quinazolinamine analogues **7-8**, **20**, **29-32**, and methoxy quinazolinamine **34** are potent BCRP and P-gp dual inhibitors with a potential to reverse MDR by blocking the efflux of anticancer drugs. In addition, selected quinazolinamine derivatives (**7-8**, **29-31**, **34**, and **40**) that were investigated for metabolic stability exhibited higher metabolic stability than Ko143. Cyclopropyl quinazolinamine **29** (**VKCY-1**) potently inhibited both BCRP- and P-gp, significantly increased the accumulation of mitoxantrone in BCRP-overexpressing H460/MX20 cells, or paclitaxel in KB-C2 cells with P-gp overexpression. The results indicated that compound **29** (**VKCY-1**) changed the localization of BCRP in H460/MX20 cells and P-gp in KB-C2 cells but did not alter the expression level of BCRP or P-gp, thus blocking the efflux function of ABC transporters. In addition, the stimulation of ATP hydrolysis of BCRP by compound **29** (**VKCY-1**) can be another mechanism for reversing the BCRP-mediated MDR. Interestingly, compared to compound **29** (**VKCY-1**), azide quinazolinamine **40** (**VKCY-2**) is a BCRP inhibitor with different mechanism in that it does not alter the localization of BCRP protein. In addition, compound **40** (**VKCY-2**) did not change the BCRP protein expression level. The ATPase results showed that compound **40** (**VKCY-2**) significantly stimulated the ATP

hydrolysis of BCRP transporter indicating it could be a competitive substrate of BCRP transporter to block the efflux of anticancer drugs. Azide quinazolinamine **40 (VKCY-2)** with photoaffinity label can be activated by the UV light and covalently bind with the BCRP transporter. Thus, it can be a probe to investigate the binding site of quinazolinamine derivatives with the BCRP protein. From the molecular modeling results, quinazolinamines **29 (VKCY-1)** and **40 (VKCY-2)** showed high docking scores when docked with human BCRP and/or P-gp model, indicating the high affinity between compounds **29 (VKCY-1)**, **40 (VKCY-2)** and BCRP and/or P-gp protein. The interactions between compounds **29 (VKCY-1)** and **40 (VKCY-2)** and the important residues can be important clues for the further modification of quinazolinamine derivatives. The results give insight into the rational design of quinazolinamines reversing BCRP and P-gp coexpressing MDR in cancers.

References

- (1) Siegel, R. L.; Miller, K. D.; Jemal, A. Cancer Statistics, 2020. *CA. Cancer J. Clin.* **2020**, *70* (1), 7–30. <https://doi.org/10.3322/caac.21590>.
- (2) Robey, R. W.; Pluchino, K. M.; Hall, M. D.; Fojo, A. T.; Bates, S. E.; Gottesman, M. M. Revisiting the Role of ABC Transporters in Multidrug-Resistant Cancer. *Nat. Rev. Cancer* **2018**, *18* (7), 452–464. <https://doi.org/10.1038/s41568-018-0005-8>.
- (3) Torgovnick, A.; Schumacher, B. DNA Repair Mechanisms in Cancer Development and Therapy. *Front. Genet.* **2015**, *6*, 157. <https://doi.org/10.3389/fgene.2015.00157>.
- (4) Du, B.; Shim, J. S. Targeting Epithelial-Mesenchymal Transition (EMT) to Overcome Drug Resistance in Cancer. *Molecules* **2016**, *21* (7), 965. <https://doi.org/10.3390/molecules21070965>.
- (5) Housman, G.; Byler, S.; Heerboth, S.; Lapinska, K.; Longacre, M.; Snyder, N.; Sarkar, S. Drug Resistance in Cancer: An Overview. *Cancers (Basel)*. **2014**, *6* (3), 1769–1792. <https://doi.org/10.3390/cancers6031769>.
- (6) Filipits, M. Mechanisms of Cancer: Multidrug Resistance. *Drug Discov. Today Dis. Mech.* **2004**, *1* (2), 229–234. <https://doi.org/10.1016/J.DDMEC.2004.10.001>.
- (7) Nakanishi, T.; Ross, D. D. Breast Cancer Resistance Protein (BCRP/ABCG2): Its Role in Multidrug Resistance and Regulation of Its Gene Expression. *Chin. J. Cancer* **2012**, *31* (2), 73–99. <https://doi.org/10.5732/cjc.011.10320>.

- (8) Srikant, S. Evolutionary History of ATP-Binding Cassette Proteins. *FEBS Lett.* **2020**, *594* (23), 3882–3897. [https://doi.org/https://doi.org/10.1002/1873-3468.13985](https://doi.org/10.1002/1873-3468.13985).
- (9) Doyle, L. A.; Yang, W.; Abruzzo, L. V; Krogmann, T.; Gao, Y.; Rishi, A. K.; Ross, D. D. A Multidrug Resistance Transporter from Human MCF-7 Breast Cancer Cells. *Proc. Natl. Acad. Sci. U. S. A.* **1998**, *95* (26), 15665–15670. <https://doi.org/10.1073/pnas.95.26.15665>.
- (10) Eckenstaler, R.; Benndorf, R. A. 3D Structure of the Transporter ABCG2-What's New? *Br. J. Pharmacol.* **2020**, *177* (7), 1485–1496. <https://doi.org/10.1111/bph.14991>.
- (11) Robey, R. W.; To, K. K. K.; Polgar, O.; Dohse, M.; Fetsch, P.; Dean, M.; Bates, S. E. ABCG2: A Perspective. *Adv. Drug Deliv. Rev.* **2009**, *61* (1), 3–13. <https://doi.org/10.1016/j.addr.2008.11.003>.
- (12) Krishnamurthy, P.; Xie, T.; Schuetz, J. D. The Role of Transporters in Cellular Heme and Porphyrin Homeostasis. *Pharmacol. Ther.* **2007**, *114* (3), 345–358. <https://doi.org/10.1016/j.pharmthera.2007.02.001>.
- (13) Grube, M.; Reuther, S.; Meyer Zu Schwabedissen, H.; Köck, K.; Draber, K.; Ritter, C. A.; Fusch, C.; Jedlitschky, G.; Kroemer, H. K. Organic Anion Transporting Polypeptide 2B1 and Breast Cancer Resistance Protein Interact in the Transepithelial Transport of Steroid Sulfates in Human Placenta. *Drug Metab. Dispos.* **2007**, *35* (1), 30–35. <https://doi.org/10.1124/dmd.106.011411>.
- (14) Doyle, L. A.; Ross, D. D. Multidrug Resistance Mediated by the Breast Cancer

- Resistance Protein BCRP (ABCG2). *Oncogene* **2003**, *22* (47), 7340–7358.
<https://doi.org/10.1038/sj.onc.1206938>.
- (15) Ni, Z.; Bikadi, Z.; Rosenberg, M. F.; Mao, Q. Structure and Function of the Human Breast Cancer Resistance Protein (BCRP/ABCG2). *Curr. Drug Metab.* **2010**, *11* (7), 603–617.
- (16) Pan, G.; Giri, N.; Elmquist, W. F. Abcg2/Bcrp1 Mediates the Polarized Transport of Antiretroviral Nucleosides Abacavir and Zidovudine. *Drug Metab. Dispos.* **2007**, *35* (7), 1165–1173. <https://doi.org/10.1124/dmd.106.014274>.
- (17) Robey, R. W.; Honjo, Y.; Morisaki, K.; Nadjem, T. A.; Runge, S.; Risbood, M.; Poruchynsky, M. S.; Bates, S. E. Mutations at Amino-Acid 482 in the ABCG2 Gene Affect Substrate and Antagonist Specificity. *Br. J. Cancer* **2003**, *89* (10), 1971–1978. <https://doi.org/10.1038/sj.bjc.6601370>.
- (18) Zhou, L.; Narahariseti, S. B.; Wang, H.; Unadkat, J. D.; Hebert, M. F.; Mao, Q. The Breast Cancer Resistance Protein (Bcrp1/Abcg2) Limits Fetal Distribution of Glyburide in the Pregnant Mouse: An Obstetric-Fetal Pharmacology Research Unit Network and University of Washington Specialized Center of Research Study. *Mol. Pharmacol.* **2008**, *73* (3), 949–959. <https://doi.org/10.1124/mol.107.041616>.
- (19) Feinshtein, V.; Holcberg, G.; Amash, A.; Erez, N.; Rubin, M.; Sheiner, E.; Polachek, H.; Ben-Zvi, Z. Nitrofurantoin Transport by Placental Choriocarcinoma JAr Cells: Involvement of BCRP, OATP2B1 and Other MDR Transporters. *Arch. Gynecol. Obstet.* **2010**, *281* (6), 1037–1044.

<https://doi.org/10.1007/s00404-009-1286-7>.

- (20) Zhang, Y.; Gupta, A.; Wang, H.; Zhou, L.; Vethanayagam, R. R.; Unadkat, J. D.; Mao, Q. BCRP Transports Dipyridamole and Is Inhibited by Calcium Channel Blockers. *Pharm. Res.* **2005**, *22* (12), 2023–2034. <https://doi.org/10.1007/s11095-005-8384-4>.
- (21) Robey, R. W.; Steadman, K.; Polgar, O.; Bates, S. E. ABCG2-Mediated Transport of Photosensitizers: Potential Impact on Photodynamic Therapy. *Cancer Biol. Ther.* **2005**, *4* (2), 187–194.
- (22) Tan, K. W.; Cooney, J.; Jensen, D.; Li, Y.; Paxton, J. W.; Birch, N. P.; Scheepens, A. Hop-Derived Prenylflavonoids Are Substrates and Inhibitors of the Efflux Transporter Breast Cancer Resistance Protein (BCRP/ABCG2). *Mol. Nutr. Food Res.* **2014**, *58* (11), 2099–2110. <https://doi.org/10.1002/mnfr.201400288>.
- (23) Natarajan, K.; Xie, Y.; Baer, M. R.; Ross, D. D. Role of Breast Cancer Resistance Protein (BCRP/ABCG2) in Cancer Drug Resistance. *Biochem. Pharmacol.* **2012**, *83* (8), 1084–1103. <https://doi.org/10.1016/j.bcp.2012.01.002>.
- (24) Järvinen, E.; Deng, F.; Kidron, H.; Finel, M. Efflux Transport of Estrogen Glucuronides by Human MRP2, MRP3, MRP4 and BCRP. *J. Steroid Biochem. Mol. Biol.* **2018**, *178*, 99–107. <https://doi.org/10.1016/j.jsbmb.2017.11.007>.
- (25) Kim, Y.; Chen, J. Molecular Structure of Human P-Glycoprotein in the ATP-Bound, Outward-Facing Conformation. *Science* (80-.). **2018**. <https://doi.org/10.1126/science.aar7389>.
- (26) Hrycyna, C. A.; Ramachandra, M.; Ambudkar, S. V; Ko, Y. H.; Pedersen, P. L.;

- Pastan, I.; Gottesman, M. M. Mechanism of Action of Human P-Glycoprotein ATPase Activity: PHOTOCHEMICAL CLEAVAGE DURING A CATALYTIC TRANSITION STATE USING ORTHOVANADATE REVEALS CROSS-TALK BETWEEN THE TWO ATP SITES*. *J. Biol. Chem.* **1998**, *273* (27), 16631–16634. <https://doi.org/10.1074/jbc.273.27.16631>.
- (27) Liu, X. ABC Family Transporters. *Adv. Exp. Med. Biol.* **2019**, *1141*, 13–100. https://doi.org/10.1007/978-981-13-7647-4_2.
- (28) Jang, S. H.; Wientjes, M. G.; Au, J. L. Kinetics of P-Glycoprotein-Mediated Efflux of Paclitaxel. *J. Pharmacol. Exp. Ther.* **2001**, *298* (3), 1236–1242.
- (29) Kitazaki, T.; Oka, M.; Nakamura, Y.; Tsurutani, J.; Doi, S.; Yasunaga, M.; Takemura, M.; Yabuuchi, H.; Soda, H.; Kohno, S. Gefitinib, an EGFR Tyrosine Kinase Inhibitor, Directly Inhibits the Function of P-Glycoprotein in Multidrug Resistant Cancer Cells. *Lung Cancer* **2005**, *49* (3), 337–343. <https://doi.org/10.1016/j.lungcan.2005.03.035>.
- (30) Balayssac, D.; Cayre, A.; Authier, N.; Bourdu, S.; Penault-Llorca, F.; Gillet, J. P.; Maublant, J.; Eschalier, A.; Coudore, F. Patterns of P-Glycoprotein Activity in the Nervous System during Vincristine-Induced Neuropathy in Rats. *J. Peripher. Nerv. Syst.* **2005**, *10* (3), 301–310. <https://doi.org/10.1111/j.1085-9489.2005.10308.x>.
- (31) Mechetner, E.; Kyshtoobayeva, A.; Zonis, S.; Kim, H.; Stroup, R.; Garcia, R.; Parker, R. J.; Fruehauf, J. P. Levels of Multidrug Resistance (MDR1) P-Glycoprotein Expression by Human Breast Cancer Correlate with in Vitro

- Resistance to Taxol and Doxorubicin. *Clin. cancer Res. an Off. J. Am. Assoc. Cancer Res.* **1998**, *4* (2), 389–398.
- (32) Elmeliegy, M.; Vourvahis, M.; Guo, C.; Wang, D. D. Effect of P-Glycoprotein (P-Gp) Inducers on Exposure of P-Gp Substrates: Review of Clinical Drug-Drug Interaction Studies. *Clin. Pharmacokinet.* **2020**, *59* (6), 699–714. <https://doi.org/10.1007/s40262-020-00867-1>.
- (33) Wessler, J. D.; Grip, L. T.; Mendell, J.; Giugliano, R. P. The P-Glycoprotein Transport System and Cardiovascular Drugs. *J. Am. Coll. Cardiol.* **2013**, *61* (25), 2495–2502. <https://doi.org/https://doi.org/10.1016/j.jacc.2013.02.058>.
- (34) Washington, C. B.; Duran, G. E.; Man, M. C.; Sikic, B. I.; Blaschke, T. F. Interaction of Anti-HIV Protease Inhibitors with the Multidrug Transporter P-Glycoprotein (P-Gp) in Human Cultured Cells. *J. Acquir. Immune Defic. Syndr. Hum. Retrovirol.* **1998**, *19* (3), 203–209. <https://doi.org/10.1097/00042560-199811010-00001>.
- (35) Crowe, A.; Tan, A. M. Oral and Inhaled Corticosteroids: Differences in P-Glycoprotein (ABCB1) Mediated Efflux. *Toxicol. Appl. Pharmacol.* **2012**, *260* (3), 294–302. <https://doi.org/10.1016/j.taap.2012.03.008>.
- (36) Shapiro, A. B.; Corder, A. B.; Ling, V. P-Glycoprotein-Mediated Hoechst 33342 Transport out of the Lipid Bilayer. *Eur. J. Biochem.* **1997**, *250* (1), 115–121. <https://doi.org/10.1111/j.1432-1033.1997.00115.x>.
- (37) Mercer, S. L.; Coop, A. Opioid Analgesics and P-Glycoprotein Efflux Transporters: A Potential Systems-Level Contribution to Analgesic Tolerance.

Curr. Top. Med. Chem. **2011**, *11* (9), 1157–1164.

<https://doi.org/10.2174/156802611795371288>.

- (38) Kodaira, H.; Kusuhara, H.; Ushiki, J.; Fuse, E.; Sugiyama, Y. Kinetic Analysis of the Cooperation of P-Glycoprotein (P-Gp/Abcb1) and Breast Cancer Resistance Protein (Bcrp/Abcg2) in Limiting the Brain and Testis Penetration of Erlotinib, Flavopiridol, and Mitoxantrone. *J. Pharmacol. Exp. Ther.* **2010**, *333* (3), 788–796. <https://doi.org/10.1124/jpet.109.162321>.
- (39) Polli, J. W.; Olson, K. L.; Chism, J. P.; John-Williams, L. S.; Yeager, R. L.; Woodard, S. M.; Otto, V.; Castellino, S.; Demby, V. E. An Unexpected Synergist Role of P-Glycoprotein and Breast Cancer Resistance Protein on the Central Nervous System Penetration of the Tyrosine Kinase Inhibitor Lapatinib (N-{3-Chloro-4-[(3-Fluorobenzyl)Oxy]Phenyl}-6-[5-({[2-(Methylsulfonyl)Ethyl]Amino}met. *Drug Metab. Dispos.* **2009**, *37* (2), 439–442. <https://doi.org/10.1124/dmd.108.024646>.
- (40) Wilson, C. S.; Davidson, G. S.; Martin, S. B.; Andries, E.; Potter, J.; Harvey, R.; Ar, K.; Xu, Y.; Kopecky, K. J.; Ankerst, D. P.; Gundacker, H.; Slovak, M. L.; Mosquera-Caro, M.; Chen, I.-M.; Stirewalt, D. L.; Murphy, M.; Schultz, F. A.; Kang, H.; Wang, X.; Radich, J. P.; Appelbaum, F. R.; Atlas, S. R.; Godwin, J.; Willman, C. L. Gene Expression Profiling of Adult Acute Myeloid Leukemia Identifies Novel Biologic Clusters for Risk Classification and Outcome Prediction. *Blood* **2006**, *108* (2), 685–696. <https://doi.org/10.1182/blood-2004-12-4633>.

- (41) Patel, C.; Stenke, L.; Varma, S.; Lindberg, M. L.; Björkholm, M.; Sjöberg, J.; Viktorsson, K.; Lewensohn, R.; Landgren, O.; Gottesman, M. M.; Gillet, J.-P. Multidrug Resistance in Relapsed Acute Myeloid Leukemia: Evidence of Biological Heterogeneity. *Cancer* **2013**, *119* (16), 3076–3083. <https://doi.org/10.1002/cncr.28098>.
- (42) Liu, B.; Li, L.-J.; Gong, X.; Zhang, W.; Zhang, H.; Zhao, L. Co-Expression of ATP Binding Cassette Transporters Is Associated with Poor Prognosis in Acute Myeloid Leukemia. *Oncol. Lett.* **2018**, *15* (5), 6671–6677. <https://doi.org/10.3892/ol.2018.8095>.
- (43) Bartholomae, S.; Gruhn, B.; Debatin, K.-M.; Zimmermann, M.; Creutzig, U.; Reinhardt, D.; Steinbach, D. Coexpression of Multiple ABC-Transporters Is Strongly Associated with Treatment Response in Childhood Acute Myeloid Leukemia. *Pediatr. Blood Cancer* **2016**, *63* (2), 242–247. <https://doi.org/10.1002/pbc.25785>.
- (44) Becton, D.; Dahl, G. V.; Ravindranath, Y.; Chang, M. N.; Behm, F. G.; Raimondi, S. C.; Head, D. R.; Stine, K. C.; Lacayo, N. J.; Sikic, B. I.; Arceci, R. J.; Weinstein, H. Randomized Use of Cyclosporin A (CsA) to Modulate P-Glycoprotein in Children with AML in Remission: Pediatric Oncology Group Study 9421. *Blood* **2006**, *107* (4), 1315–1324. <https://doi.org/10.1182/blood-2004-08-3218>.
- (45) Austin Doyle, L.; Ross, D. D. Multidrug Resistance Mediated by the Breast Cancer Resistance Protein BCRP (ABCG2). *Oncogene* **2003**, *22* (47), 7340–

7358. <https://doi.org/10.1038/sj.onc.1206938>.

- (46) Michaelis, M.; Rothweiler, F.; Löschmann, N.; Sharifi, M.; Ghafourian, T.; Cinatl, J. J. Enzastaurin Inhibits ABCB1-Mediated Drug Efflux Independently of Effects on Protein Kinase C Signalling and the Cellular P53 Status. *Oncotarget* **2015**, *6* (19), 17605–17620. <https://doi.org/10.18632/oncotarget.2889>.
- (47) Gekeler, V.; Boer, R.; Uberall, F.; Ise, W.; Schubert, C.; Utz, I.; Hofmann, J.; Sanders, K. H.; Schächtele, C.; Klemm, K.; Grunicke, H. Effects of the Selective Bisindolylmaleimide Protein Kinase C Inhibitor GF 109203X on P-Glycoprotein-Mediated Multidrug Resistance. *Br. J. Cancer* **1996**, *74* (6), 897–905. <https://doi.org/10.1038/bjc.1996.454>.
- (48) Merritt, J. E.; Sullivan, J. A.; Drew, L.; Khan, A.; Wilson, K.; Mulqueen, M.; Harris, W.; Bradshaw, D.; Hill, C. H.; Rumsby, M.; Warr, R. The Bisindolylmaleimide Protein Kinase C Inhibitor, Ro 32-2241, Reverses Multidrug Resistance in KB Tumour Cells. *Cancer Chemother. Pharmacol.* **1999**, *43* (5), 371–378. <https://doi.org/10.1007/s002800050909>.
- (49) Ott, M.; Huls, M.; Cornelius, M. G.; Fricker, G. St. John's Wort Constituents Modulate P-Glycoprotein Transport Activity at the Blood-Brain Barrier. *Pharm. Res.* **2010**, *27* (5), 811–822. <https://doi.org/10.1007/s11095-010-0074-1>.
- (50) Zhang, L.; Li, Y.; Wang, Q.; Chen, Z.; Li, X.; Wu, Z.; Hu, C.; Liao, D.; Zhang, W.; Chen, Z.-S. The PI3K Subunits, P110 α and P110 β Are Potential Targets for Overcoming P-Gp and BCRP-Mediated MDR in Cancer. *Mol. Cancer* **2020**,

19 (1), 10. <https://doi.org/10.1186/s12943-019-1112-1>.

- (51) Rabindran, S. K.; Ross, D. D.; Doyle, L. A.; Yang, W.; Greenberger, L. M. Fumitremorgin C Reverses Multidrug Resistance in Cells Transfected with the Breast Cancer Resistance Protein. *Cancer Res.* **2000**, *60* (1), 47–50.
- (52) Allen, J. D.; van Loevezijn, A.; Lakhai, J. M.; van der Valk, M.; van Tellingen, O.; Reid, G.; Schellens, J. H. M.; Koomen, G.-J.; Schinkel, A. H. Potent and Specific Inhibition of the Breast Cancer Resistance Protein Multidrug Transporter in Vitro and in Mouse Intestine by a Novel Analogue of Fumitremorgin C. *Mol. Cancer Ther.* **2002**, *1* (6), 417–425.
- (53) Weidner, L. D.; Zoghbi, S. S.; Lu, S.; Shukla, S.; Ambudkar, S. V.; Pike, V. W.; Mulder, J.; Gottesman, M. M.; Innis, R. B.; Hall, M. D. The Inhibitor Ko143 Is Not Specific for ABCG2. *J. Pharmacol. Exp. Ther.* **2015**, *354* (3), 384–393. <https://doi.org/10.1124/jpet.115.225482>.
- (54) Gupta, A.; Zhang, Y.; Unadkat, J. D.; Mao, Q. HIV Protease Inhibitors Are Inhibitors but Not Substrates of the Human Breast Cancer Resistance Protein (BCRP/ABCG2). *J. Pharmacol. Exp. Ther.* **2004**, *310* (1), 334–341. <https://doi.org/10.1124/jpet.104.065342>.
- (55) Zhang, S.; Yang, X.; Morris, M. E. Flavonoids Are Inhibitors of Breast Cancer Resistance Protein (ABCG2)-Mediated Transport. *Mol. Pharmacol.* **2004**, *65* (5), 1208–1216. <https://doi.org/10.1124/mol.65.5.1208>.
- (56) D’Cunha, R.; Bae, S.; Murry, D. J.; An, G. TKI Combination Therapy: Strategy to Enhance Dasatinib Uptake by Inhibiting Pgp- and BCRP-Mediated Efflux.

- Biopharm. Drug Dispos.* **2016**, *37* (7), 397–408.
<https://doi.org/10.1002/bdd.2022>.
- (57) Yanase, K.; Tsukahara, S.; Asada, S.; Ishikawa, E.; Imai, Y.; Sugimoto, Y. Gefitinib Reverses Breast Cancer Resistance Protein-Mediated Drug Resistance. *Mol. Cancer Ther.* **2004**, *3* (9), 1119–1125.
- (58) Krapf, M. K.; Gallus, J.; Wiese, M. Synthesis and Biological Investigation of 2,4-Substituted Quinazolines as Highly Potent Inhibitors of Breast Cancer Resistance Protein (ABCG2). *Eur. J. Med. Chem.* **2017**, *139*, 587–611.
<https://doi.org/10.1016/j.ejmech.2017.08.020>.
- (59) Krapf, M. K.; Gallus, J.; Spindler, A.; Wiese, M. Synthesis and Biological Evaluation of Quinazoline Derivatives - A SAR Study of Novel Inhibitors of ABCG2. *Eur. J. Med. Chem.* **2019**, *161*, 506–525.
<https://doi.org/10.1016/j.ejmech.2018.10.026>.
- (60) Kulkarni, P. M.; Kulkarni, A. R.; Korde, A.; Tichkule, R. B.; Laprairie, R. B.; Denovan-Wright, E. M.; Zhou, H.; Janero, D. R.; Zvonok, N.; Makriyannis, A.; Cascio, M. G.; Pertwee, R. G.; Thakur, G. A. Novel Electrophilic and Photoaffinity Covalent Probes for Mapping the Cannabinoid 1 Receptor Allosteric Site(S). *J. Med. Chem.* **2016**, *59* (1), 44–60.
<https://doi.org/10.1021/acs.jmedchem.5b01303>.
- (61) Punthasee, P.; Laciak, A. R.; Cummings, A. H.; Ruddraraju, K. V.; Lewis, S. M.; Hillebrand, R.; Singh, H.; Tanner, J. J.; Gates, K. S. Covalent Allosteric Inactivation of Protein Tyrosine Phosphatase 1B (PTP1B) by an Inhibitor–

- Electrophile Conjugate. *Biochemistry* **2017**, *56* (14), 2051–2060.
<https://doi.org/10.1021/acs.biochem.7b00151>.
- (62) Kathman, S. G.; Statsyuk, A. V. Covalent Tethering of Fragments For Covalent Probe Discovery. *Medchemcomm* **2016**, *7* (4), 576–585.
<https://doi.org/10.1039/c5md00518c>.
- (63) Singh, A.; Thornton, E. R.; Westheimer, F. H. The Photolysis of Diazoacetylchymotrypsin. *J. Biol. Chem.* **1962**, *237*, 3006–3008.
- (64) Herner, A.; Marjanovic, J.; Lewandowski, T. M.; Marin, V.; Patterson, M.; Miesbauer, L.; Ready, D.; Williams, J.; Vasudevan, A.; Lin, Q. 2-Aryl-5-Carboxytetrazole as a New Photoaffinity Label for Drug Target Identification. *J. Am. Chem. Soc.* **2016**, *138* (44), 14609–14615.
<https://doi.org/10.1021/jacs.6b06645>.
- (65) Zacharias, A. O.; Fang, Z.; Rahman, A.; Talukder, A.; Cornelius, S.; Chowdhury, S. M. Affinity and Chemical Enrichment Strategies for Mapping Low-Abundance Protein Modifications and Protein-Interaction Networks. *J. Sep. Sci.* **2021**, *44* (1), 310–322. <https://doi.org/10.1002/jssc.202000930>.
- (66) DeGraff, W. G.; Mitchell, J. B. Evaluation of a Tetrazolium-Based Semiautomated Colorimetric Assay: Assessment of Chemosensitivity Testing. *Cancer Res.* **1987**, *47* (4), 936–942.
- (67) Tung, Y.-S.; Coumar, M. S.; Wu, Y.-S.; Shiao, H.-Y.; Chang, J.-Y.; Liou, J.-P.; Shukla, P.; Chang, C.-W.; Chang, C.-Y.; Kuo, C.-C.; Yeh, T.-K.; Lin, C.-Y.; Wu, J.-S.; Wu, S.-Y.; Liao, C.-C.; Hsieh, H.-P. Scaffold-Hopping Strategy: Synthesis

- and Biological Evaluation of 5,6-Fused Bicyclic Heteroaromatics To Identify Orally Bioavailable Anticancer Agents. *J. Med. Chem.* **2011**, *54* (8), 3076–3080. <https://doi.org/10.1021/jm101027s>.
- (68) Cai, C. Y.; Zhai, H.; Lei, Z. N.; Tan, C. P.; Chen, B. L.; Du, Z. Y.; Wang, J. Q.; Zhang, Y. K.; Wang, Y. J.; Gupta, P.; Wang, B.; Chen, Z. S. Benzoyl Indoles with Metabolic Stability as Reversal Agents for ABCG2-Mediated Multidrug Resistance. *Eur. J. Med. Chem.* **2019**, *179*, 849–862. <https://doi.org/10.1016/j.ejmech.2019.06.066>.
- (69) Ji, N.; Yang, Y.; Cai, C. Y.; Lei, Z. N.; Wang, J. Q.; Gupta, P.; Shukla, S.; Ambudkar, S. V.; Kong, D.; Chen, Z. S. Selonsertib (GS-4997), an ASK1 Inhibitor, Antagonizes Multidrug Resistance in ABCB1- and ABCG2-Overexpressing Cancer Cells. *Cancer Lett.* **2019**, *440–441*, 82–93. <https://doi.org/10.1016/j.canlet.2018.10.007>.
- (70) Fan, Y. F.; Zhang, W.; Zeng, L.; Lei, Z. N.; Cai, C. Y.; Gupta, P.; Yang, D. H.; Cui, Q.; Qin, Z. D.; Chen, Z. S.; Trombetta, L. D. Dacomitinib Antagonizes Multidrug Resistance (MDR) in Cancer Cells by Inhibiting the Efflux Activity of ABCB1 and ABCG2 Transporters. *Cancer Lett.* **2018**, *421*, 186–198. <https://doi.org/10.1016/j.canlet.2018.01.021>.
- (71) Beéry, E.; Rajnai, Z.; Abonyi, T.; Makai, I.; Bánsághi, S.; Erdő, F.; Sziráki, I.; Herédi-Szabó, K.; Kis, E.; Jani, M.; Márki-Zay, J.; Tóth, G. K.; Krajcsi, P. ABCG2 Modulates Chlorothiazide Permeability--in Vitro-Characterization of Its Interactions. *Drug Metab. Pharmacokinet.* **2012**, *27* (3), 349–353.

<https://doi.org/10.2133/dmpk.dmpk-11-nt-068>.

- (72) Cai, C. Y.; Zhang, W.; Wang, J. Q.; Lei, Z. N.; Zhang, Y. K.; Wang, Y. J.; Gupta, P.; Tan, C. P.; Wang, B.; Chen, Z. S. Biological Evaluation of Non-Basic Chalcone CYB-2 as a Dual ABCG2/ABCB1 Inhibitor. *Biochem. Pharmacol.* **2020**, *175*, 113848. <https://doi.org/10.1016/j.bcp.2020.113848>.
- (73) Jackson, S. M.; Manolaridis, I.; Kowal, J.; Zechner, M.; Taylor, N. M. I.; Bause, M.; Bauer, S.; Bartholomaeus, R.; Bernhardt, G.; Koenig, B.; Buschauer, A.; Stahlberg, H.; Altmann, K.-H.; Locher, K. P. Structural Basis of Small-Molecule Inhibition of Human Multidrug Transporter ABCG2. *Nat. Struct. Mol. Biol.* **2018**, *25* (4), 333–340. <https://doi.org/10.1038/s41594-018-0049-1>.
- (74) Alam, A.; Kung, R.; Kowal, J.; McLeod, R. A.; Tremp, N.; Broude, E. V.; Roninson, I. B.; Stahlberg, H.; Locher, K. P. Structure of a Zosuquidar and UIC2-Bound Human-Mouse Chimeric ABCB1. *Proc. Natl. Acad. Sci. U. S. A.* **2018**, *115* (9), 1973–1982. <https://doi.org/10.1073/pnas.1717044115>.
- (75) Nagasawa, Y.; Matsusaki, Y.; Nobuta, T.; Tada, N.; Miura, T.; Itoh, A. Aerobic Photooxidative Synthesis of 2-Aryl-4-Quinazolinones from Aromatic Aldehydes and Aminobenzamide Using Catalytic Amounts of Molecular Iodine. *RSC Adv.* **2015**, *5* (78), 63952–63954. <https://doi.org/10.1039/C5RA07275A>.
- (76) Hayakawa, M.; Kaizawa, H.; Moritomo, H.; Koizumi, T.; Ohishi, T.; Okada, M.; Ohta, M.; Tsukamoto, S.; Parker, P.; Workman, P.; Waterfield, M. Synthesis and Biological Evaluation of 4-Morpholino-2-Phenylquinazolines and Related Derivatives as Novel PI3 Kinase P110alpha Inhibitors. *Bioorg. Med. Chem.* **2006**,

- 14 (20), 6847–6858. <https://doi.org/10.1016/j.bmc.2006.06.046>.
- (77) Liu, K.; Zhu, J.; Huang, Y.; Li, C.; Lu, J.; Sachar, M.; Li, S.; Ma, X. Metabolism of KO143, an ABCG2 Inhibitor. *Drug Metab. Pharmacokinet.* **2017**, *32* (4), 193–200. <https://doi.org/10.1016/j.dmpk.2017.02.003>.
- (78) Asha, S.; Vidyavathi, M. Role of Human Liver Microsomes in in Vitro Metabolism of Drugs-a Review. *Appl. Biochem. Biotechnol.* **2010**, *160* (6), 1699–1722. <https://doi.org/10.1007/s12010-009-8689-6>.
- (79) Baker, J. A.; Altman, M. D.; Martin, I. J. Interpretation of in Vitro Metabolic Stability Studies for Racemic Mixtures. *ACS Med. Chem. Lett.* **2018**, *9* (8), 843–847. <https://doi.org/10.1021/acsmchemlett.8b00259>.
- (80) Talele, T. T. The “Cyclopropyl Fragment” Is a Versatile Player That Frequently Appears in Preclinical/Clinical Drug Molecules. *J. Med. Chem.* **2016**, *59* (19), 8712–8756. <https://doi.org/10.1021/acs.jmedchem.6b00472>.
- (81) Mogi, M.; Yang, J.; Lambert, J.-F.; Colvin, G. A.; Shiojima, I.; Skurk, C.; Summer, R.; Fine, A.; Quesenberry, P. J.; Walsh, K. Akt Signaling Regulates Side Population Cell Phenotype via Bcrp1 Translocation. *J. Biol. Chem.* **2003**, *278* (40), 39068–39075. <https://doi.org/10.1074/jbc.M306362200>.
- (82) Boedtker, E.; Pedersen, S. F. The Acidic Tumor Microenvironment as a Driver of Cancer. *Annu. Rev. Physiol.* **2020**, *82*, 103–126. <https://doi.org/10.1146/annurev-physiol-021119-034627>.

VITA

Name: *Chao-Yun Cai*

Baccalaureate Degree: *Bachelor of Science, Sun Yat-sen University, Guangzhou, Major: Chemistry*

Date Graduated: 2013.06

Master's Degree: *Master of Science, Sun Yat-sen University, Guangzhou, Major: Organic Chemistry*

Date Graduated: 2016.06